EFFECT OF FSP-INSERTED COBALT IN TITANIA-ZIRCONIA SUPPORT
ON FISCHER-TROPSCH SYNTHESIS OVER COBALT CATALYST

By

MR. Krasanai SUKCHOKNAMCHAI

A Thesis Submitted in Partial Fulfillment of the Requirements
for Master of Engineering (CHEMICAL ENGINEERING)
Department of CHEMICAL ENGINEERING
Graduate School, Silpakorn University
Academic Year 2017
Copyright of Graduate School, Silpakorn University

ผลของโคบอลต์ที่ใส่ด้วยวิธีเฟลมสเปรย์ไพโรไลซิสในตัวรองรับไททาเนีย-เซอร์โคเนีย
ต่อการสังเคราะห์ฟิชเชอร์-โทรป บนตัวเร่งปฏิกิริยาโคบอลต์

โดย
นายกรัสนัย สุขโชคนำชัย

วิทยานิพนธ์นี้เป็นส่วนหนึ่งของการศึกษาตามหลักสูตรวิศวกรรมศาสตรมหาบัณฑิต
สาขาวิชาวิศวกรรมเคมี แผน ก แบบ ก 2 ระดับปริญญามหาบัณฑิต
ภาควิชาวิศวกรรมเคมี
บัณฑิตวิทยาลัย มหาวิทยาลัยศิลปากร
ปีการศึกษา 2560

EFFECT OF FSP-INSERTED COBALT IN TITANIA-ZIRCONIA SUPPORT ON FISCHER-TROPSCH SYNTHESIS OVER COBALT CATALYST

By

MR. Krasanai SUKCHOKNAMCHAI

Title	Effect of FSP-inserted cobalt in titania-zirconia support on Fischer-Tropsch synthesis over cobalt catalyst
By	Krasanai SUKCHOKNAMCHAI
Field of Study	(CHEMICAL ENGINEERING)
Advisor	CHOOWONG CHAISUK

Graduate School Silpakorn University in Partial Fulfillment of the Requirements for the Master of Engineering

-- Dean of graduate school
(Associate Professor Jurairat Nunthanid, Ph.D.)

Approved by

-- Chair person
(Assistant Professor TARAWIPA PUANGPETCH , Ph.D.)
-- Advisor
(Assistant Professor CHOOWONG CHAISUK , D.Eng.)
-- Examiner
(NUTCHAPON CHOTIGKRAI , D.Eng.)
-- External Examiner
(Associate Professor KRIANGSAK KRAIWATTHANAWONG , D.Eng.)
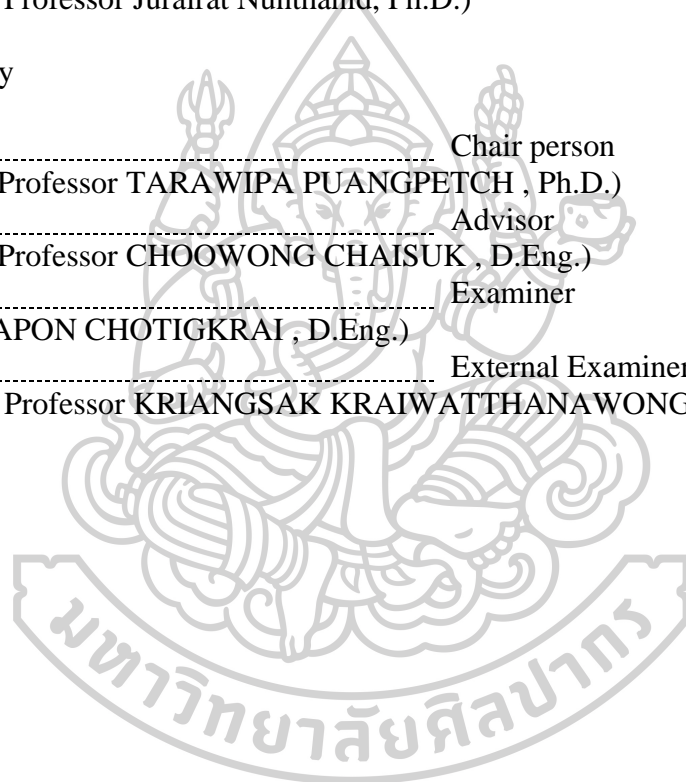
57404201 : Major (CHEMICAL ENGINEERING)

Keyword : Co catalyst, binary support, tertiary support, Flame spray pyrolysis, Fischer-Tropsch synthesis

MR. KRASANAI SUKCHOKNAMCHAI : EFFECT OF FSP-INSERTED COBALT IN TITANIA-ZIRCONIA SUPPORT ON FISCHER-TROPSCH SYNTHESIS OVER COBALT CATALYST THESIS ADVISOR : ASSISTANT PROFESSOR CHOOWONG CHAISUK, D.Eng.

In this research, the Fischer-Tropsch synthesis (FTS) over cobalt catalysts supported on binary (Co-TiO_2 and Co-ZrO_2) and tertiary (Co-TiO_2-ZrO_2) support were studied with various amount of inserted-cobalt and TiO_2-to-ZrO_2 wieght ratio in range of 5 to 30% and 4:1 to 1:4, respectively. The mixed support was prepared by flame spray pyrolysis (FSP). Finally, the 20 wt. % Co was impregnated on these supports. The catalysts were characterized by several technique such as X-ray diffraction (XRD), N_2-physisorption, Temperature programmed reduction (H_2-TPR) and H_2-chemisorption. The catalytic properties were tested by FTS. The support preparation by FSP using mixture liquid precursors can produce the mixture of metallic phases such as cobalt titanate ($CoTiO_3$), titanium zirconate (Ti_2ZrO_6) and zirconium titanate ($ZrTiO_4$). The reduction degree of Co catalysts was decreased with increasing amount of inserted-Co. Because of the addition of inserted-Co induced to strong metal-support interaction in catalysts. Cobalt metallic sites of catalysts decreased due to the increasing of metal-support interaction, except the catalyst supported on zirconia. The addition of 5% inserted-cobalt to TiO_2 and ZrO_2 support improved heavy hydrocarbon selectivity and rate of reaction, respectively. Role of small inserted-cobalt in modified TiO_2 support disturbed the dispersion of impregnated-cobalt led to large cobalt oxide size, reflected to hydrocarbon-chain propagation. On the other hand, cobalt in modified ZrO_2 support dispersed on the surface of catalyst that difference from TiO_2 because of weak metal-support interaction. Increasing of cobalt dispersion enhanced rate of reaction. The addition of small inserted-cobalt in mixed TiO_2-ZrO_2 support with 4:1 weight ratio exhibited the best catalytic activities than other mixed support catalysts.

ACKNOWLEDGEMENTS

TABLE OF CONTENTS

Page

LIST OF TABLES

Page

LIST OF FIGURES

Page

CHAPTER I

INTRODUCTION

1.1 Motivation

In present, the demand of fossil fuel (natural gas, crude oil and coal) in used as major energy source resulting in this source is decreased continuously. The combustion of energy source leaves carbon monoxide and carbon dioxide (CO and CO_2) which is important greenhouse gas. One of the possible ways to decreased fossil fuel is gas to liquids (GTL) process. This process is one of the promising processes to produce environmentally fuels with lower emission of pollutants. Fischer–Tropsch synthesis (FTS) is one of most efficient routes to convert synthesis gas (CO and H_2) to hydrocarbon products. FTS are usually categorized based on operating conditions; high temperature Fischer-Tropsch (HTFT) operates at 300-350°C and low temperature Fischer-Tropsch (LTFT) operates at 200-240°C [1].

The following reactions take place during FTS, with alkanes and alkenes are the desired products.

Alkane production: $(2n + 1) H_2 + nCO \rightarrow C_nH_{2n+2} + nH_2O$ (1-1)

Alkene production: $2nH_2 + nCO \rightarrow C_nH_{2n} + nH_2O$ (1-2)
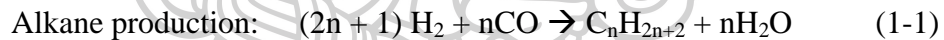
Side reactions such as water-gas shift (WGS) reaction, alcohols production and Boudouard reaction may occur.

WGS reaction: $CO + H_2O \leftrightarrow CO_2 + H_2$ (1-3)

Alcohols production: $2nH_2 + nCO \rightarrow C_nH_{2n+2}O + (n-1) H_2O$ (1-4)

Boudouard reaction: $2CO \rightarrow C + CO_2$ (1-5)
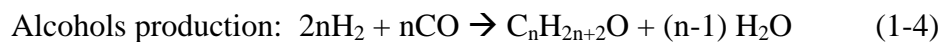
Due to the FTS product is very broad, i.e. light gas, gasoline, kerosene, diesel and lubricant, many researchers interested to improve the catalytic performance which high catalysts activity and product selectivity. Ru, Ni, Fe and Co are commonly accepted to be the best catalysts for FTS [2].

Ru is one of the active catalysts for FTS producing long chain hydrocarbons; however it is very expensive and not suitable for industrial processes. Ni-based catalysts have high methane selectivity, which low price and undesired products [3]. Iron-based catalysts, generally operating at HTFT, have high selectivity to heavy olefins and oxygenate hydrocarbons. But, Fe has a high activity for WGS reaction, which the undesired reaction in FTS process [4]. The cobalt catalysts are prefer due to its high selectivity to long chain paraffins, low activity for the WGS reaction and lower price than noble metals [5].

From the high selectivity for heavy hydrocarbons of catalysts, Fe and Co are widely use as catalysts in Fischer–Tropsch processes. And they are well known that the catalysts activity and product selectivity are depending on the chemical and textural properties of support.

Al_2O_3, SiO_2 and TiO_2 are generally use for the support in FTS process. The influence of the support in FTS has been widely studies in a large number of papers. Alumina supported catalysts have a strong interaction with active phase which promote to a highly metal dispersion cause to the small metal particle. However, one of drawback is poorly reducible active phase, formation of non-reducible species such as cobalt aluminate, that lead to fewer amounts of metal active sites, low FTS activity [6-16]. In case of SiO_2 supported catalysts presents a weak metal-support interaction leading to a high reducibility of cobalt oxides but low Co dispersion on the silica support and easy to sintering of Co metal [17-19]. TiO_2 is the alternative support for FTS catalyst because it has the strength of metal-support interaction in the middle of SiO_2 and Al_2O_3 that cause to medium metal dispersion and reducibility [20-23]. However, TiO_2 is the active oxide cause to the formation of non-reducible, which is inactive phase in FTS.

Many researchers use the noble metals (Pt, Pd and Ru) and transition metal oxides (ZrO_2 and MnO_x) as a promotor for improve the reducibility of catalysts [24]. Moreover, Enache et al. investigate the performance of catalysts which use ZrO_2 as a support and they talk about the catalysts supported on ZrO_2 have high reducibility than Al_2O_3 support and higher CO conversions when operating at low pressure [25].

The support of binary and tertiary mixed oxides was also investigated. Wu et al. [14] reported that the mixed support (Ti and Zr mixed with SiO_2) increased the reducibility and dispersion of cobalt and therefore caused to increase the CO conversion. Many researchers prepared the catalysts by flame spray pyrolysis (FSP) in single-step. It was found that this method can produce new compounds. Examples were the formation of $LaCoO_3$ and $CoAl_2O_4$ reported by Sinchai et al. [26] and the production of $CoTiO_3$ and $Zr_5Ti_7O_{24}$ reported by Meetipkij et al. [27]. The new compound, such as $Zr_5Ti_7O_{24}$, was proved that improved the catalyst activity for CO hydrogenation [27].

However, the catalysts were prepared by FSP have a limited reducibility due to strong metal-support interaction [26, 27]. Some researcher report the addition of high Co loading (>20 wt. %) in catalyst. They found that it show two advantages; easy to activate and high resistant to deactivation [28], which facilitate to high activity in FTS.

In this work, the Co-based catalysts supported on mixed metal oxides were investigated. The support consisting of three precursors (cobalt, titanium and zirconium) was focused. It was prepared by flame spray pyrolysis. These catalysts were characterized by XRD, N_2-physisorption, TPR and H_2 chemisorption. The catalytic performances were evaluated by Fischer-Tropsch synthesis in a fixed bed reactor.

1.2 Objective of research

The aim of this research is to study the effect of FSP-inserted cobalt in TiO_2-ZrO_2 support on Fischer-Tropsch synthesis over Co-based catalyst.

1.3 Scope of research

1.3.1 Catalyst preparation

In this research, the supports containing three metal precursors (cobalt, titanium and zirconium) are prepared by flame spray pyrolysis (FSP) procedure. Both the cobalt loading and the ratio of TiO_2 and ZrO_2 in the support are studied. The amount of cobalt is varied as 5, 10, 20 and 30 wt. % while the ratio of TiO_2 and ZrO_2 is simultaneously adjusted as 80:20, 60:40, 40:60 and 20:80. The pure TiO_2 and ZrO_2 inserted by cobalt are also prepared. Finally, the 20 wt. % Co was impregnated on these supports.
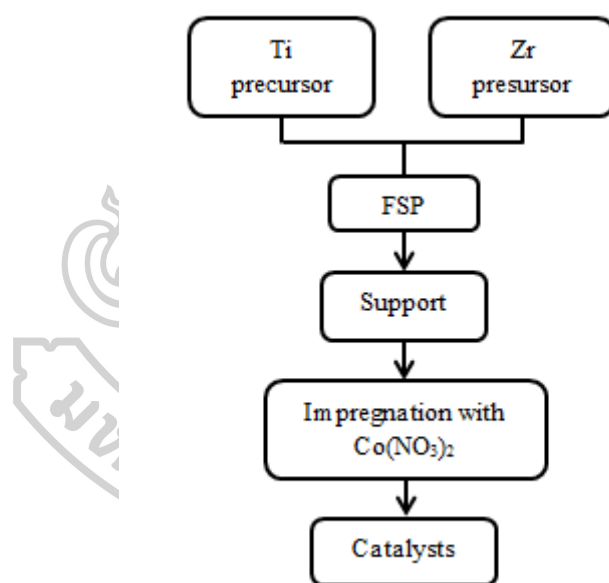
Figure 1 Scheme of the Co catalysts supported on TiO$_2$-ZrO$_2$ supports in this work
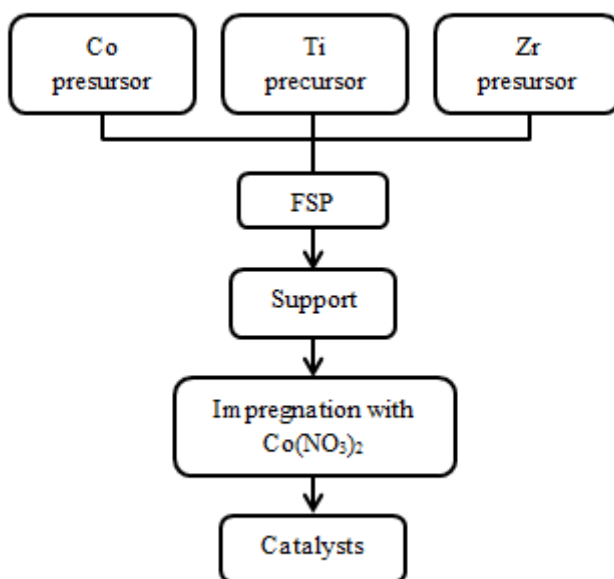
Figure 2 Scheme of the Co catalysts supported on FSP-inserted cobalt in TiO$_2$-ZrO$_2$ supports in this work

1.3.2 Catalyst characterization

The bulk crystal structure and chemical phase composition are determined by X-ray diffraction (XRD). The specific surface area and pore characteristics of catalyst are determined by N$_2$ physisorption. Temperature programmed reduction (TPR) is test to determine the reducibility of catalyst. The cobalt metallic sites on the catalyst samples are determined by H$_2$ chemisorption.

1.3.3 Catalyst performance test

The catalytic properties are test by Fischer-Tropsch synthesis in a fixed-bed reactor. The reaction conditions are maintained at 230°C and atmospheric pressure. The reactant and product are analyzed by two GCs connecting with TCD and FID detectors.

1.4 Contribution of research

The Co-based catalyst supported with tertiary mixtures (Co-TiO$_2$-ZrO$_2$) can be possible to improve the FTS activity and the product selectivity to heavy hydrocarbon.

CHAPTER II

FISCHER–TROPSCH SYNTHESIS

2.1 Fischer–Tropsch Synthesis

The promising alternative pathways are clean, sustainable and renewable fuel is the Fischer-Tropsch synthesis (FTS) process. FTS is the original process by two German scientists, Franz Fischer and Hans Tropsch, in the 1920s. The FTS is a cleaning process which converts synthesis gas (CO and H_2) to hydrocarbon fuels. This process can produce a wide range of hydrocarbons: methane, light gas, gasoline, diesel fuel and wax.

FTS is either high temperature process (HTFT) or low temperature process (LTFT) depending on the product required. High temperature process operates at 300–350 °C on Fe-based catalysts and is mainly used for the production of C_{5+} and linear olefins while the low temperature process operates at 200–240°C on Co-based catalysts and is applied for the production of waxy material.

The FTS has many reactions take place during the process; alkanes and alkenes productions are the desired reactions while water-gas shift and Boudouard reaction are undesired reactions.

2.2 Mechanism of Fischer-Tropsch Synthesis

The three major reaction mechanisms of Fischer-Tropsch synthesis are as follow.

2.2.1 Surface carbide mechanism

The first accepted mechanism for Fischer-Tropsch synthesis is the carbide mechanism. This mechanism is involved the formation and hydrogenation of the metal carbides to give a methylene (CH_2) groups on the metal surface. It starts from CO which adsorbed on the surface of metal and dissociates. The adsorbed oxygen atom can contract with hydrogen to the formation of water, which rapidly desorbs.

Meanwhile, the chemisorbed carbon is hydrogenated to the formation of methylene which oligomerized to produce long-chain hydrocarbon.
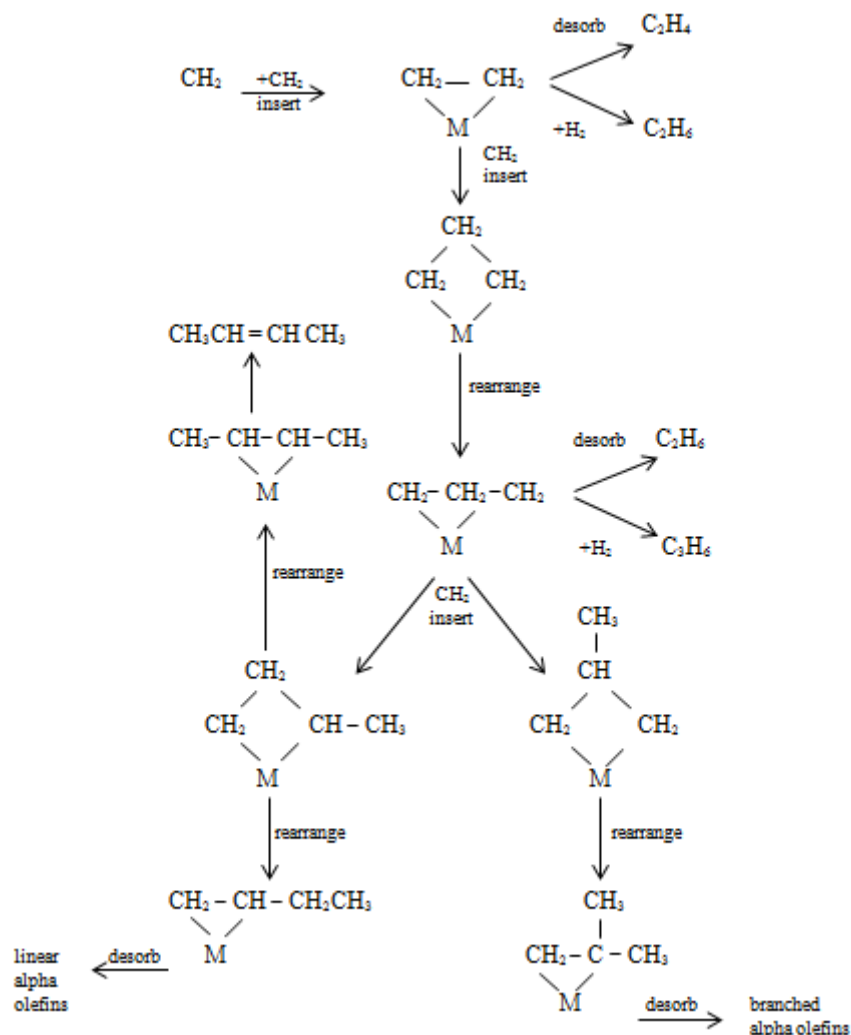
Figure 3 Surface carbide mechanism [29]

2.2.2 The oxygenate (enol) mechanism

The oxygenate (enol) mechanism is the chain growth of the carbon and oxygen which adsorbed on surface of metal reacts with adsorbed hydrogen via the partial hydrogenation to form enolic (HCOH) groups. Their results showed that the added alcohol or aldehydes was able to initiate chain growth.

Figure 4 The oxygenate (enol) mechanism [29]

2.2.3 CO insertion mechanism

This mechanism is the insertion phenomena of CO into a metal-hydrogen, metal-methyl or metal-methylene to the formation of alcohol products. Fig. 2.3 shown the mechanism of CO insertion; after insertion step, the alcohol precursor can eliminate oxygen atom to produce an alkene.
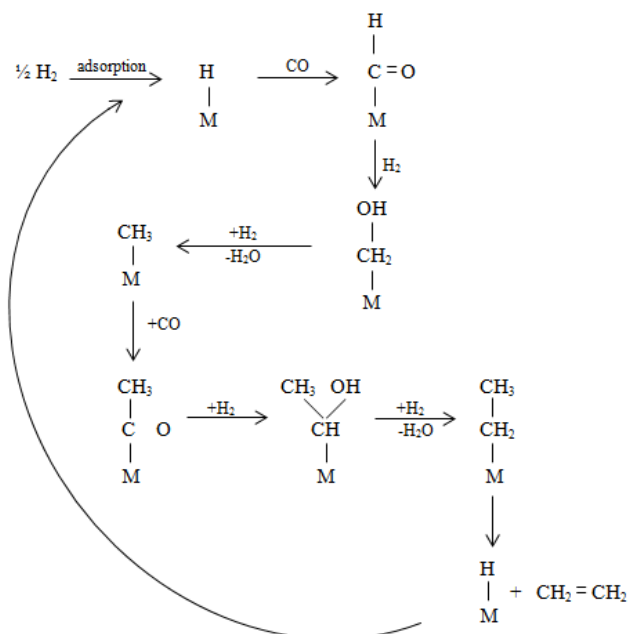
Figure 5 CO insertion mechanism [29]

2.3 Fischer-Tropsch Synthesis catalyst

Hinchiranan and her co-worker [13] investigated effect of TiO_2 promote Co/SiO_2 catalyst. Their SiO_2 supports were prepared by incipient wetness impregnation method and Co was impregnated onto the obtained supports.

Table 1 Properties of Co/SiO_2 catalysts with different TiO_2 loading [13]

Catalyst	TiO_2 loading (wt. %)	Co particle size(nm)	Reduction degree (%)	Co dispersion (%)	CO conversion (%)
Q-10	0	14.3	59.7	7.0	50.4
2-TiO$_2$	2	7.1	40.4	13.8	68.7
5-TiO$_2$	5	6.8	29.2	14.6	64.9
10-TiO$_2$	10	6.2	26.8	15.5	64.5

The activity of cobalt catalyst were depends on the number of active sites on the surface of cobalt metal. They found the unpromoted catalyst (Q-10) can form largest Co particle caused to lower Co surface area and dispersion result to less

catalytic activity. In case of titania promoted catalysts, the small amount of titania induced to the highest CO conversion, because of titania can promoted the adsorption of CO. On the other hand, the reduction performance of catalysts was obstructed with increased titania loading due to the strong interaction between supported cobalt and added titania leading to lower CO conversion when increase titania more than 2 wt. %.

In 2012, Maria Venezia and her co-worker [8] were studied about effect of SiO_2 support modification by TiO_2. The supports include SiO_2 and SiO_2 modified by TiO_2 were prepared by sol-gel procedure. Then the Co catalysts were synthesis by impregnation method. They found that all most the results; specific surface area, reducibility and Co particle sizes, has similar to Hinchiranan.

But they reported space time yields of hydrocarbon for the two differently cobalt catalysts supported on SiO_2 and $Ti-SiO_2$. At high space velocity the results showed the modified support by TiO_2 enhanced CO conversion rate and C5+ selectivity. At low space velocity and constant conversion, higher catalyst time yield and C5+ selectivity was obtained for titania doped catalysts.

Table 2 Catalytic performances in period A and B [8]

Sample	Period A				Period B	
	Conversion	CTY (mol CO/ g cat*h)	S_{c5+} (%)	GHSV	CTY (mol CO/ g cat*h)	S_{c5+} (%)
6Co/SiO$_2$	3.4	0.005	73.4	3100	0.006	77.9
6Co/TiSiO$_2$	8.5	0.013	76.3	4100	0.016	80.8
12Co/SiO$_2$	8.5	0.013	73.1	4200	0.017	80.4
12Co/TiSiO$_2$	18.7	0.030	79.7	7200	0.031	81.5

Park et al. [30] studied about the effect of titanium over Co supported on alumina. The modified support was prepared by sol-gel method and Co loading was prepared by impregnation method. The weight percentage of Ti on $Ti-Al_2O_3$ was vary

as 0, 0.1, 0.2, 0.5 and 1.0 wt. %. The results showed the catalyst which modified by titanium had high reducibility more than without titanium. The added titanium can suppress aggregation of cobalt particle that caused to enhance the FTS activity.

In 2013, TiO_2 supported Co catalysts were investigated by Shimura and his co-worker [2]. They reasoned for use TiO_2 as support that due to the low cost and strength of Co-support interaction on Co/TiO_2 was in the middle of those on Co/SiO_2 and Co/Al_2O_3. The Co/TiO_2 catalysts were prepared by the incipient wetness impregnation method. They found phase of TiO_2 had effect to reducibility and activity on Co catalysts in Fischer Tropsch reaction.
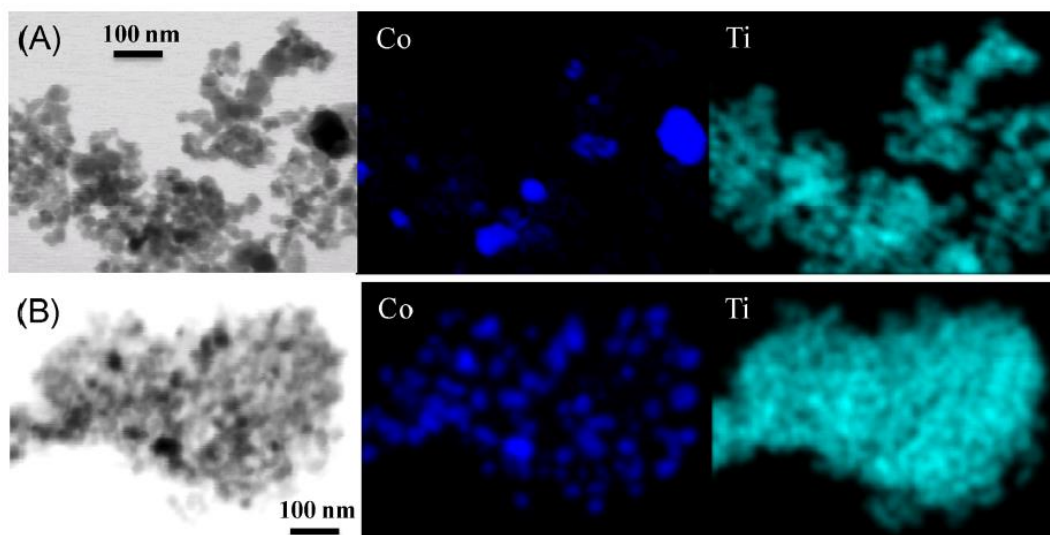
Figure 6 TEM images and EDS maps of (A) pure anatase phase and (B) 85% anatase phase [2]

Anatase phase had weak Co-support interaction leading to easily Co oxide reduction and poor Co dispersion that cause to low CO conversion rate. The catalyst which prepared from TiO_2 with 15% of rutile phase exhibited higher CO conversion rate because rutile phase in titania had effect to decrease reducibility of catalyst at low temperature that leading to low the catalyst activity. But the large Co particle size catalysts which supported on anatase phase can propagate long chain hydrocarbon product more than rutile phase.

Table 3 Catalytic performance of various Co/TiO$_2$ samples in FT synthesis [2]

Support	Conversion rate (mmol/g cat h)	Product selectivity (%)			
		C$_1$	C$_2$-C$_4$	C$_5$	CO$_2$
2% anatase	5.8	19	11	68	2
85% anatase	6.1	20	13	66	1
100% anatase	1.5	15	7	72	6

Moradi et al. (2003) [5] were studied about the Co/SiO$_2$ promoted by zirconium catalysts performance. From TPR results, they found the addition of zirconium can decrease the reduction temperature of cobalt silicate and suppress the formation of cobalt silicate at high zirconium content. The catalytic test showed, the addition of zirconium had effect to increase CO conversion and heavy hydrocarbon product selectivity.
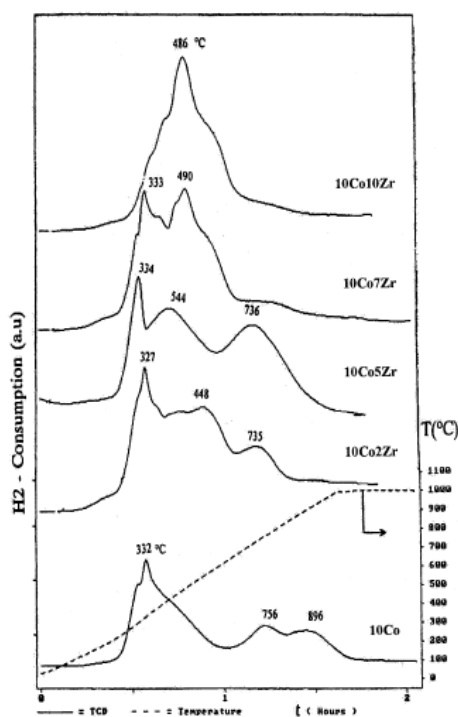
Figure 7 TPR profiles for the unpromoted and promoted catalysts [5]

Xiong et al. (2005) [6] investigated the catalyst performance of zirconium modified Co supported on alumina. They studied about the amount of zirconium (0.5, 1, 5, 9 and 15 wt. %) that addition to Co/Al_2O_3. They found the H_2 consumption from H_2-TPR results showed peak area at 573-723 K increased with increasing zirconium loading. Moreover, CO conversion and C_{5+} hydrocarbons selectivity were slightly increase with increasing zirconium loading. They concluded that the added zirconium can suppress the formation of cobalt aluminate that caused to increase the cobalt metal site and cobalt oxide reducibility.

Zirconium promoted Co/SiO_2 was investigated by Johnson et al. (2016) [31]. They studied about role of ZrO_2 on activity and selectivity of cobalt catalyst. The catalyst which modified by zirconium can improve the CO adsorption ability that caused to high CO on the surface and shift to the formation of heavy hydrocarbons. They found the suitable atomic ratio of Zr:Co was 1.

Koizumi et al. (2011) [32] studied about the interaction between Co and ZrO_x on the $Co/ZrO_x/SiO_2$ catalyst. From TPR and H_2-chemisorption results, the modified catalyst enhanced Co dispersion and maintained high reducibility of Co. They found the addition of zirconium did not have effect to the selectivity of C_{10+}. For the FT activity, they found the suitable of ZrO_2 loading was about 4 wt %.

In 2004, Enache et al. [25] studied about catalytic properties of cobalt supported on zirconia and alumina. From H_2-TPD results, they found the hydrogen atom to metallic Co atom was equal to 2 on catalyst with zirconium support. They concluded that the hydrogen was adsorbed by metal center, and then it migrated to the support via a spillover mechanism. When operated at low temperature, they found the Co/ZrO_2 showed high CO conversion and heavy hydrocarbons selectivity than Co/Al_2O_3. When compared between ZrO_2 and amorphous ZrO_2, they found the cobalt supported on amorphous ZrO_2 had low Co metallic reducibility that caused to low active site.

Wu et al. (2015) [14] investigated about mixed TiO_2-ZrO_2 with varied molar ratio were incorporated into Co catalysts supported on SiO_2. Mixed oxides that added

to silica support with weight ratio 1:4 were prepared by impregnation method. They found only anatase phase appeared on XRD patterns for all support. In case of TiO_2-SiO_2 support, the results showed the highest Co dispersion and catalyst activity due to strong interaction between Co and support.
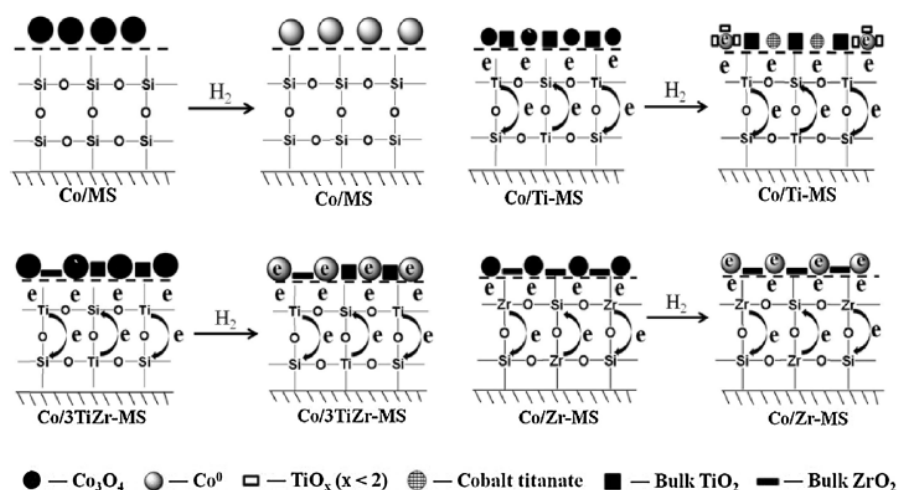
Figure 8 Model of the surface structure of Co/nTiZr–MS catalysts [14]

However, the lowest Co oxide reduction degree was observed on this catalyst due to high cobalt-support interaction and blockaged of cobalt metallic by TiO_x (x < 2) from partial reduction of TiO_2. The addition of ZrO_2 into Co/SiO_2 enhanced H_2 adsorption but suppressed CO adsorption, which increased hydrogen to carbon ratio cause to increased CO conversion and methane selectivity. On Co/Ti-Zr-SiO_2 catalysts, the results showed ZrO_2 suppressed the blockaged of Co by TiO_x and formation of non-reducible cobalt titanate caused to higher reducibility than Co/Ti-SiO_2.

CHAPTER III

FLAME SPRAY PYROLYSIS

3.2 Literature reviews about FSP

Li et al. (2013) [33] investigated metallic iron nanoparticles with a core-shell structure that prepared by FSP method. The TEM image had showed the diameters ranging from 30 to 80 nm. From XRD pattern, they found the product from this method had many phases such as $CF_{15.1}$, Fe/C and Fe_3O_4. The formation mechanism of solid particles was competition between reduction and oxidation reactions. They assumed that the formation of product phases depended on the model of droplet to particle.
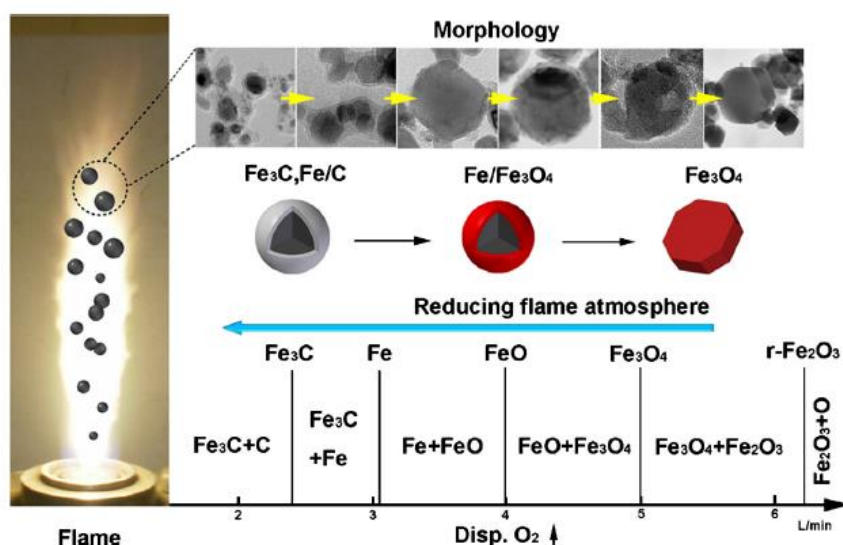
Figure 9 Illustration of the evolution of morphology and composition of FSP catalyst [33]

Bettini et al. (2015) [34] studied TiO_2 nanostructured powder were prepared by the flame spray pyrolysis. The catalysts were studied under the conditions of type of solvent, precursor concentration, precursor flow rate and the flow rate of oxygen. The XRD results showed many titania phases appeared such as anatest, rutile and brookite. They found the physical and chemical properties of the catalysts depend on the FSP synthesis conditions.
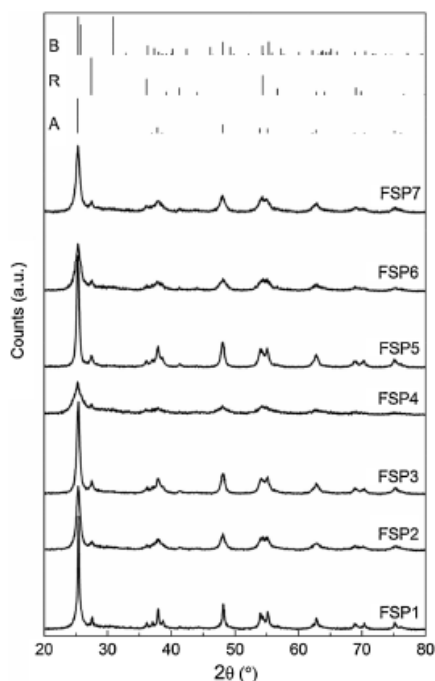
Figure 10 XRD diffractograms of synthesized FSP-made TiO$_2$ powder [34]

Boningari et el. (2012) [35] was studied about structure of V/ZrO$_2$ which prepared by FSP. They varied V/Zr atomic ratio (0.05, 0.11, 0.17, 0.25, 0.33 and 0.42) and they found, the atomic ratio affected the product phase. The increasing of vanadia content led to the formation of ZrV$_2$O$_7$, because of the migration of ZrO$_2$ into V$_2$O$_5$. They gave the reason of this phenomena that atom of oxygen around V were decrease and form to the new structure. This results proved that the catalyst which prepared by FSP can caused the formation of new compound.
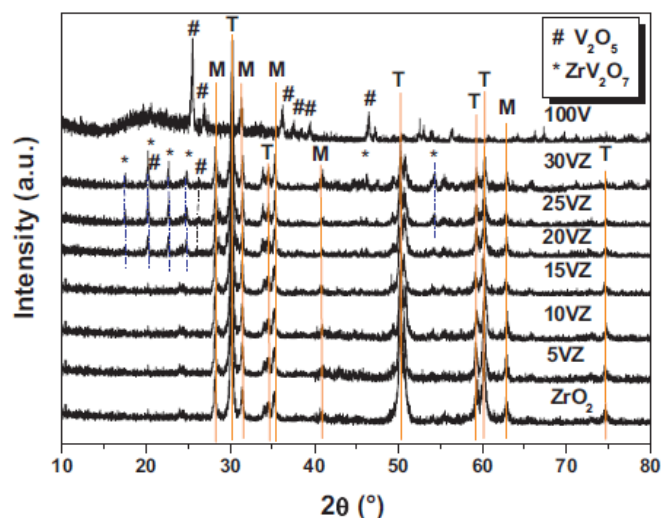
Figure 11 Powder X-ray patterns of the FSP-made vanadia-based catalysts based on atomic ratio [35]

In 2013, Boningari and co woker [36] studied about V over metal oxide support (CeO_2, TiO_2, Al_2O_3, ZrO_2, CeO_2-ZrO_2, TiO_2-Al_2O_3 and CeO_2-Al_2O_3) that prepared by FSP. The XRD pattern showed alumina, titania and zirconia support from FSP had many phases; α, γ, anatase, rutile, monoclinic and tetragonal, similar to his previously research. From their results, the catalyst supported on binary support showed the physicochemical properties that difference from the primary support.

Chaisuk et al. (2011) [37] investigated Co/ZrO_2 catalyst which prepared by one-step FSP under different flame conditions. They found for similar Co loading, the crystallite size of ZrO_2 increased (10 to 19 nm.) with increasing precursor feed rate (3 to 8 ml/min). For varied Co loading (5-10 wt. %), they found XRD results showed same peak pattern of tetragonal phase. From H_2-TPR, they found that the formation of solid solution; Co_xO_y-ZrO_2, appeared due to the interaction between cobalt and support. They found the increasing of precursor flow rate affect increase the CO hydrogenation reaction rate.
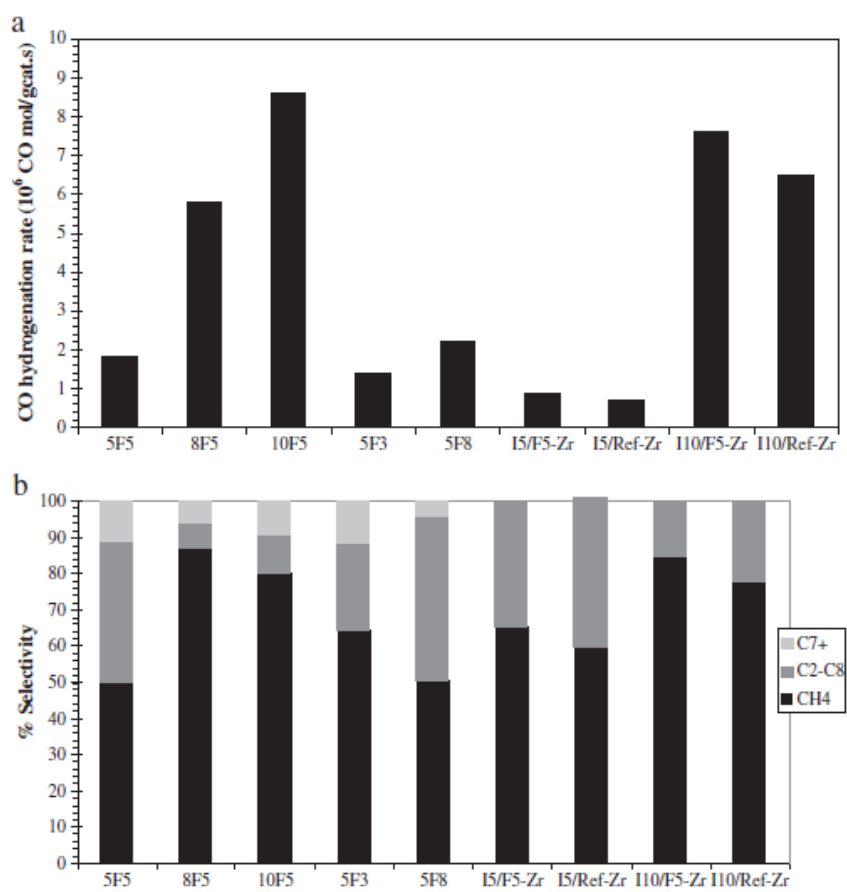
Figure 12 The catalytic performance in CO hydrogenation [37]

3.1 Flame spray pyrolysis

Flame spray pyrolysis (FSP) process is a rapidly technique for catalyst synthesis method which gas phase combustion to the formation of nanostructure materials in metal oxide form; high specific surface area and high catalytic performance, such as silica, alumina and titania.

Flame spray pyrolysis technique is a single-step preparation method which based on the exothermic combustion of the precursor. First step, the liquid precursor was injected by syringe pump into the flame supplied gas (O_2 and CH_4). Then, the precursor was dispersion and evaporation to generating a small cluster. Finally, the clusters will growth and coagulation to the nanoparticle powder [38].
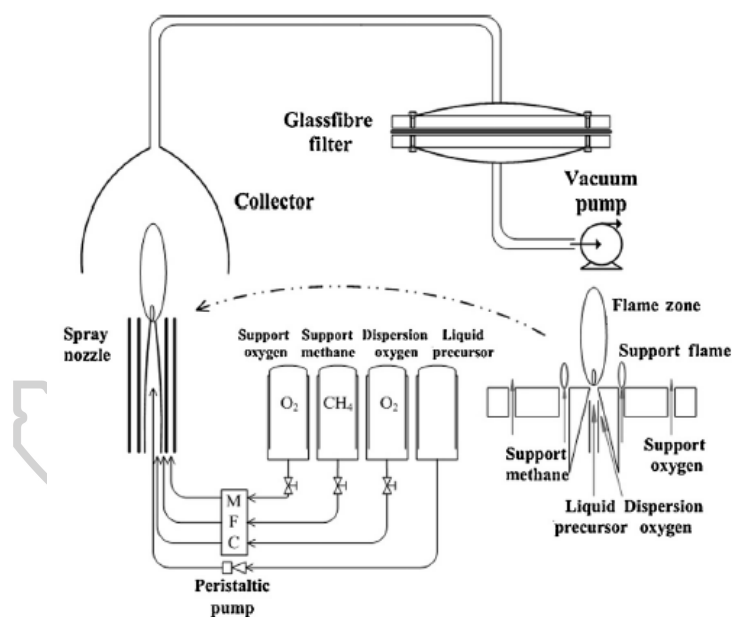
Figure 13 Illustration of flame spray pyrolysis [39]

CHAPTER IV

RESEARCH METHODOLOGY

4.1 Catalyst preparation

The chemicals used in the catalyst preparation are shown in the table 5

Table 4 The details of chemical used in the catalyst preparation

Chemicals	Formula	Grade	Manufacture
Cobalt (II) nitrate hexahydrate	$Co(NO_3)_2 \cdot 6H_2O$	98%	Ajax Finechem
Cobalt naphthenate	$CoC_{22}H_{14}O_4$	6 wt. % in mineral spirits	Sigma-Aldrich
Titanium (IV) butoxide	$Ti(OCH_2CH_2CH_2CH_3)_4$	97%	Sigma-Aldrich
Zirconium (IV) butoxide	$Zr(OCH_2CH_2CH_2CH_3)_4$	80 wt. % in 1-butanol	TCI
Xylene	C_8H_{10}	99.8%	Modern Chemical

4.1.1 Support preparation

All of supports in this research were prepared by FSP technique. Titanium (IV) butoxide, zirconium (IV) butoxide and cobalt naphthenate was used as Ti, Zr and Co precursors. The precursors were diluted with xylene to a 0.5 M solution as a liquid precursor for FSP. The precursor was fed into the center of O_2 (3 l/min) and CH_4 (1.5 l/min) by syringe pump with 5 ml/min. The dispersed oxygen was fed with 5 l/min and the pressure drop at nozzle was held constant at 150 kPa. The support powder was collected on a glass microfiber filter (Whatman) with the aid of a vacuum pump.

Table 5 The nomenclature of all catalysts

Sample	Amount of inserted-Co (wt %)	Ti-to-Zr ratio
Co/TiO$_2$	0	1:0
Co/5Co-TiO$_2$	5	1:0
Co/10Co-TiO$_2$	10	1:0
Co/20Co-TiO$_2$	20	1:0
Co/30Co-TiO$_2$	30	1:0
Co/ZrO$_2$	0	0:1
Co/5Co-ZrO$_2$	5	0:1
Co/10Co-ZrO$_2$	10	0:1
Co/20Co-ZrO$_2$	20	0:1
Co/30Co-ZrO$_2$	30	0:1
Co/4Ti:1Zr	0	4:1
Co/5Co-4Ti:1Zr	5	4:1
Co/10Co-4Ti:1Zr	10	4:1
Co/20Co-4Ti:1Zr	20	4:1
Co/30Co-4Ti:1Zr	30	4:1
Co/3Ti:2Zr	0	3:2
Co/5Co-3Ti:2Zr	5	3:2
Co/10Co-3Ti:2Zr	10	3:2
Co/20Co-3Ti:2Zr	20	3:2
Co/30Co-3Ti:2Zr	30	3:2
Co/2Ti:3Zr	0	2:3
Co/5Co-2Ti:3Zr	5	2:3
Co/10Co-2Ti:3Zr	10	2:3
Co/20Co-2Ti:3Zr	20	2:3
Co/30Co-2Ti:3Zr	30	2:3
Co/1Ti:4Zr	0	1:4
Co/5Co-1Ti:4Zr	5	1:4
Co/10Co-1Ti:4Zr	10	1:4
Co/20Co-1Ti:4Zr	20	1:4
Co/30Co-1Ti:4Zr	30	1:4

4.1.2 Catalyst preparation

Catalysts with 20 wt. % Co content were prepared with impregnation method. The above synthesized supports were impregnated with cobalt (II) nitrate hexahydrate solution. Then, the samples were dried at 120℃ for overnight and calcined at 500℃ for 4 h.
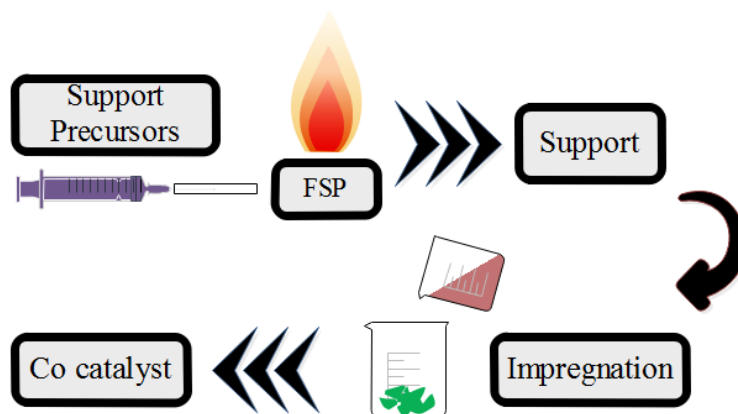
Figure 14 The support and catalysts preparation

4.2 Catalyst characterization

4.2.1 X-ray Diffraction (XRD)

X-ray diffraction (XRD) is a primary technique to study the crystal structures of catalysts sample. XRD measurements are performed using a D8-Discover X-ray diffractometer with Cu Kα connected with a computer with Diffract ZT version 3.3 for fully control of the XRD analyzer. The scans rate is a 2°/min and record in the range 2θ from 20° to 80°. Scherrer equation is use for estimate the crystallite size.

4.2.2 Nitrogen physisorption

The specific surface areas, average pore size diameter and pore size distribution of catalysts sample are determine by N_2 adsorption-desorption technique using a BELSORP-miniII, Japan. The samples are pretreatment in inert gas with volumetric flow rate of 50 ml/min at 180°C for 3 h.

4.2.3 Temperature Programmed Reduction (TPR)

H_2 temperature programmed reduction experiment use to determine the reducibility of the surface of catalyst samples using a Micromeritics AutoChem 2910 instrument. The sample (0.1 g) are put in a quartz reactor and pretreatment in a N_2 flow (30 ml/min) up to 150°C and keep for 30 min to remove the adsorbed water follow by cooling to ambient temperature. The reducing gas with 10% H_2 in N_3 content (30 ml/min) was passed over the sample with the heating rate of 10°C/min from ambient to 800°C for 1 h.

4.2.4 Hydrogen chemisorption

The active surface metal of the catalysts are measure by H_2 chemisorption using a Micromeritics AutoChem 2910 instrument. Prior to the adsorption, the catalysts (0.2 g) are reduced in H_2 (30 ml/min) at 350°C for 2 h and then cool down to 100°C by N_2 (30 ml/min). Then the pure H_2 (80 μl) are inject until the peak area of H_2 pluses are constant. The hydrogen uptake data are estimate by the method of Reuel and Bartholomew.

4.3 Catalyst evaluation

The catalytic performance was tested by Fischer-Tropsch synthesis. The reacting gases used in this test are shown in table 6.

Table 6 The details of gases used in the catalytic performance testing

Gas	Formula	Grade
Carbon monoxide	CO	30% in H_2
Helium	He	Ultra-high purity
Hydrogen	H_2	High purity

A flow diagram of the FTS system was shown in Figure 12. An apparatus consisted of a fixed-bed reactor, electrical furnace, temperature controller, gas controlling system and gas chromatography.
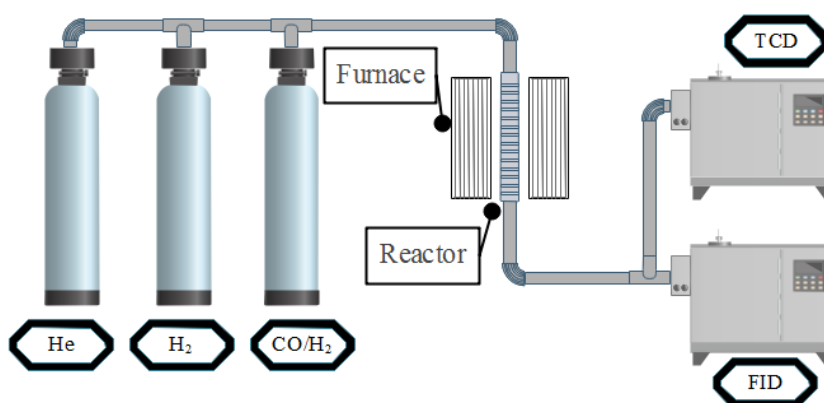
Figure 15 Illustration of Fischer-Tropsch synthesis system

Catalytic activity measurements were carried out in a down flow stainless steel fixed-bed reactor (I.D. 0.71 cm) with a catalyst loading of 0.3 ml. (GHSV = 5400 h^{-1}). The catalyst sample was placed between two quartz wool layers. The gas flows (30% CO in H_2, He and H_2) were adjusted by metering valves. The catalysts were heat up and cool down in He (30 ml/min) and the temperature was control by automation temperature controller (maximum voltage output of 220 V.).

Prior to reaction, the catalyst was reduced in situ in pure H_2 (30 ml/min) at 350°C for at atmospheric pressure 2 h (heating rate: 10°C/min). After reduction the catalyst was cooled at 230°C and switched to 30% CO in H_2 (30 ml/min).

Reactant and product streams were analyzed on-line using a gas chromatograph (GC) equipped with sample loop, Thermal Conductivity Detectors (TCD) used for the analysis of carbon monoxide and Flame Ionization Detector (FID) used for the analysis of hydrocarbon products. The operation conditions for GC instrument are shown in the Table 7 and 8.

Table 7 The operating conditions of TCD gas chromatographs for the catalytic activity test

Gas chromatograph	Shimadzu GC-14B
Detector	TCD
Column	Porapack Q
Carrier gas	He
Carrier gas flow	30 ml/min
Injector temperature	150°C
Detector temperature	150°C
Column temperature	40°C
Analysis gas	CO

Table 8 The operating conditions of FID gas chromatographs for the catalytic activity test

Gas chromatograph	Shimadzu GC-14B
Detector	FID
Column	DB-1
Carrier gas	N_2
Split/Splitless	40 ml/min
Purge flow rate	10 ml/min
Carrier pressure	40 kPa
Make up pressure	50 kPa
Injector temperature	200°C
Detector temperature	200°C
Column temperature	40°C (held 10 min) and then raised to 250 °C (5°C/min)
Analysis gas	Hydrocarbons
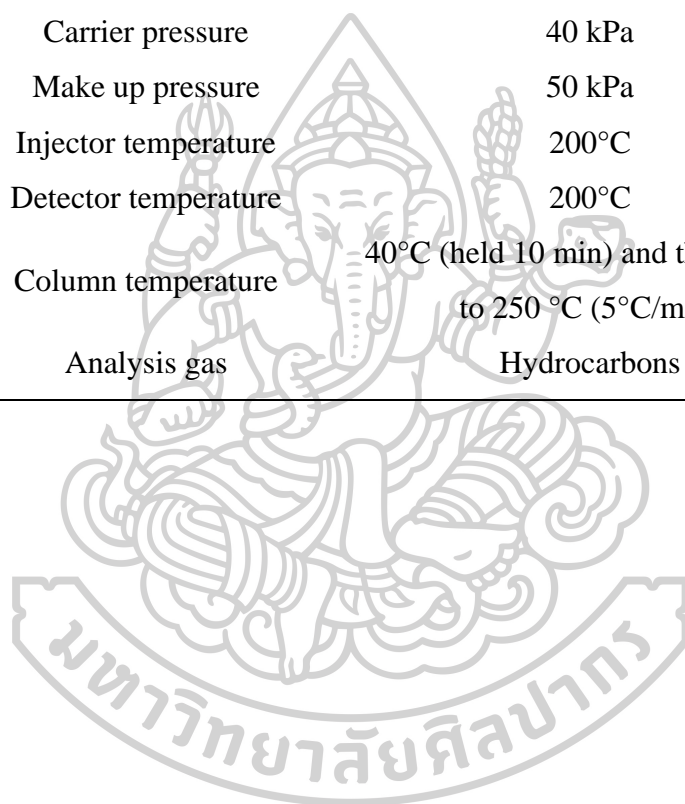
CHAPTER V

RESULTS AND DISCUSSION

In the fifth chapter, the main topic of this research about modification of the Co-based catalyst by inserting some part of cobalt in TiO_2-ZrO_2 support using the FSP method was presented. This catalyst was evaluated by the Fischer-Tropsch synthesis. In this chapter, the results and discussion were divided into two parts. In the first part, the cobalt catalyst supported on the Co-inserted in both TiO_2 and ZrO_2 were studied. In the second part, the effect of Co-inserted in mixed metal oxide support (TiO_2-ZrO_2) was investigated. For both parts, the physical and chemical properties of cobalt catalysts consisted of the phase analysis analyzed by X-ray diffraction (XRD), the specific surface area and pore characteristic determined by N_2-physisorption, the reducibility evaluated by temperature programmed reduction (TPR) and the amount of cobalt metal active sites determined by H_2-chemisorption. The catalytic activity and selectivity were tested by Fischer-Tropsch reaction.

5.1 Effect of FSP-inserted Co in single metal oxide

5.1.1 Co/TiO_2 and Co/Co-TiO_2 catalysts

5.1.1.1 Physicochemical properties of catalysts

The phase analysis by X-ray diffraction

The XRD patterns of the Co/TiO_2 and Co/Co-TiO_2 catalysts are shown in Figure 15. The measurements were carried out at the diffraction angles (2Θ) between 20º and 80°. The characteristic peaks of Co_3O_4 at 2Θ=36° (major), 31°, 44°, 59°, and 65° [40] were found in all of catalysts. The catalyst without the inserted-cobalt showed the characteristic peaks of the crystalline phases of TiO_2 consisting of anatase phase at 2Θ=25° (major), 37°, 38°, 48°, 53°, 55° and 62° [41] and small peaks of rutile phase at 2Θ = 27° (major), 36°, 41°, and 54° [42]. The insertion of cobalt in TiO_2 support promoted the formation of rutile phase. These results were consistent with Teoh and co-workers [43]. They found that the addition of second element in TiO_2 by flame spray pyrolysis increased the rutile phase. They proposed that the

addition of second element established higher number of defects, most likely oxygen vacancies, inside the TiO_2 crystals and affected the phase transformation of anatase to rutile. The support preparation using mixture liquid precursors by flame spray pyrolysis can produce the mixture of metallic phases or alloy [26, 27]. The alloys that possibly occur in this research were divided into two types. One was the alloy consisting of two metallic mixture such as cobalt titanate, titanium zirconate and zirconium titanate. The other one was the alloy of three metallic components; Co-Ti-Zr. At high amount of cobalt insertion; 20 and 30%, the XRD pattern of cobalt titanate appeared at $2\Theta=32°$ (major), $35°$, $40°$, $49°$, $53°$, and $61°$ [44].

The average crystallite sizes of cobalt oxide were calculated by the Scherrer's equation from the full width at half maximum of the XRD peak at $2\Theta=36°$. The results are summarized in Table 8. The crystallite sizes of Co_3O_4 were nearly about 24-31 nm.

Table 9 Physical properties of Co/TiO_2 and $Co/Co-TiO_2$ catalysts

Catalyst	N₂-physisorption			XRD
	$S_{BET}{}^a$ (m²/g)	$V_p{}^b$ (cm³/g)	$dp_{av}{}^c$ (nm)	$d_{Co3O4}{}^d$ (nm)
Co/TiO$_2$	27.2	0.10	15.0	24.8
Co/5Co-TiO$_2$	30.5	0.13	17.8	27.3
Co/10Co-TiO$_2$	34.0	0.13	16.1	25.6
Co/20Co-TiO$_2$	29.9	0.08	11.0	27.3
Co/30Co-TiO$_2$	28.9	0.08	12.2	31.4

[a] Specific surface area
[b] Total pore volume
[c] Average pore diameter
[d] Crystallite size of Co_3O_4

Specific surface area and pore characteristic

The results by N₂-physisorption are shown in Table 8 and Figure 16. The catalysts showed the BET surface area, total pore volume and average pore diameter in range of 27-34 nm, 0.08-0.13 cm³/g and 11-18 nm, respectively. The amount of inserted Co hardly affected the specific surface area and pore characteristics of the Co catalysts.
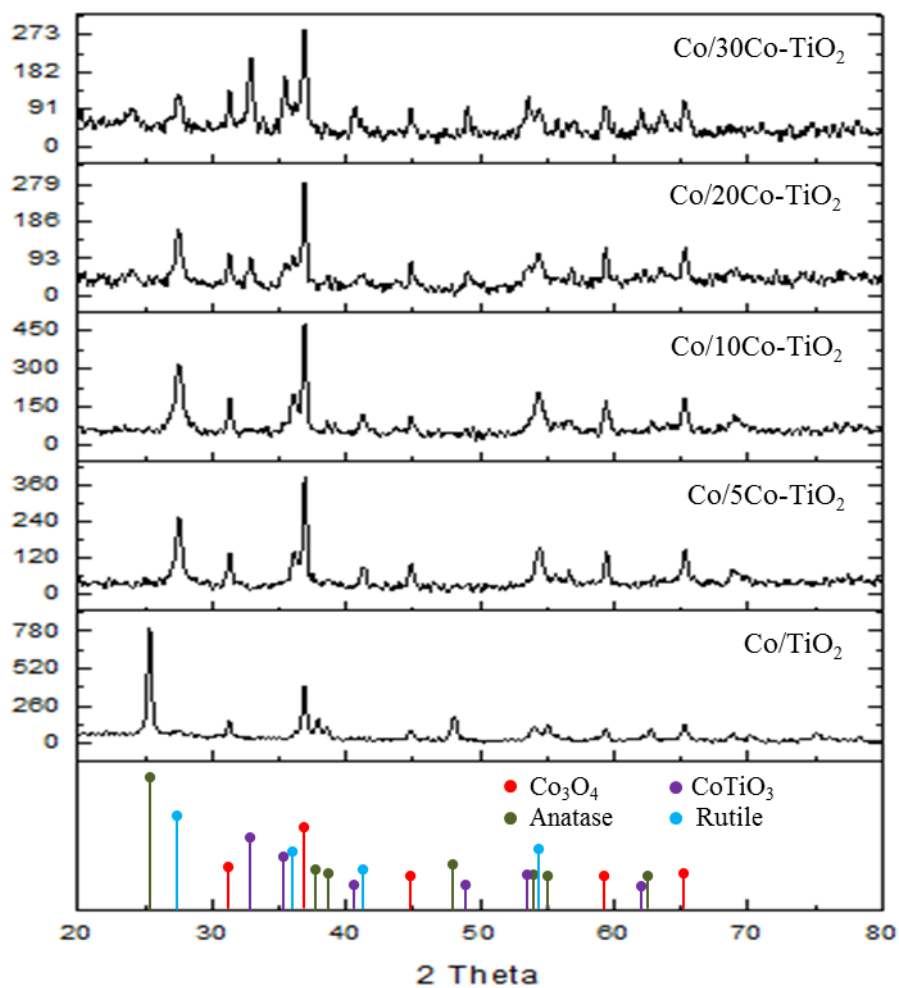
Figure 16 XRD patterns of Co/TiO$_2$ and Co/Co-TiO$_2$ catalysts

The adsorption-desorption isotherm of Co/TiO$_2$ and Co/Co-TiO$_2$ catalysts showed hysteresis loop that indicated the porous structure. The types of isotherm and hysteresis loop were type IV and H3, respectively. This was characteristic of the mesoporous structure within the catalyst consistent with the results of the mean pore diameter. The pores were associated with slit-shaped pores [45].
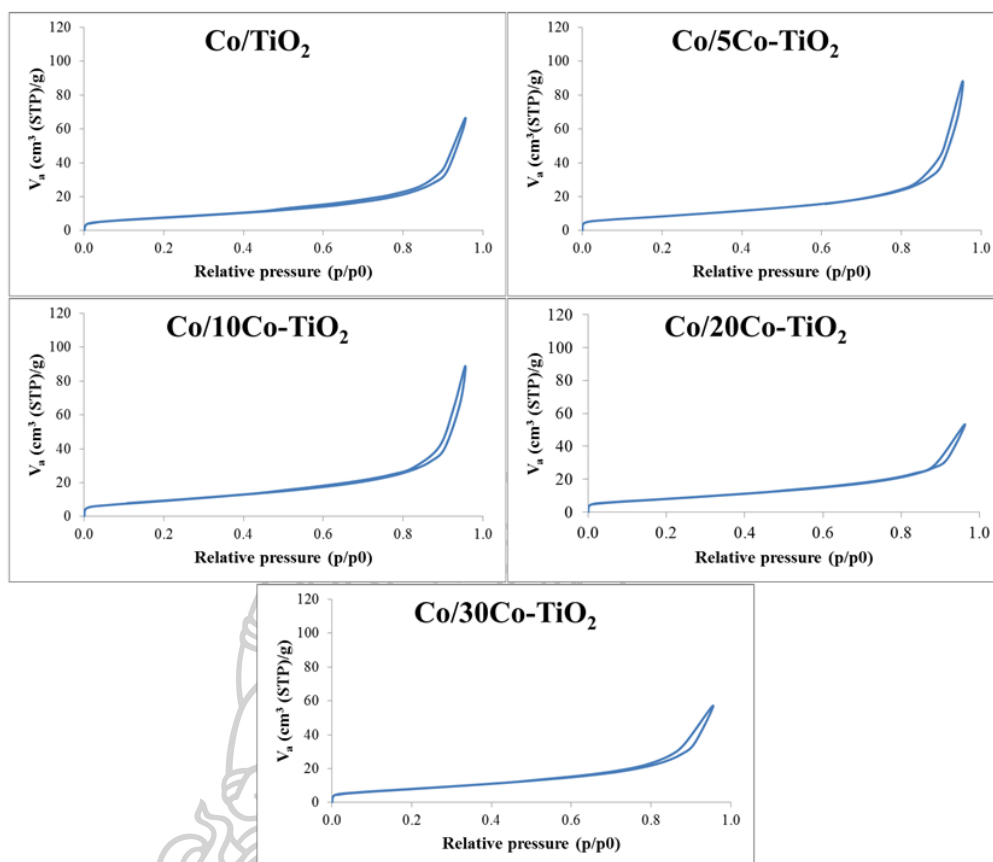
Figure 17 Adsorption-desorption isotherm of Co/TiO$_2$ and Co/Co-TiO$_2$ catalysts
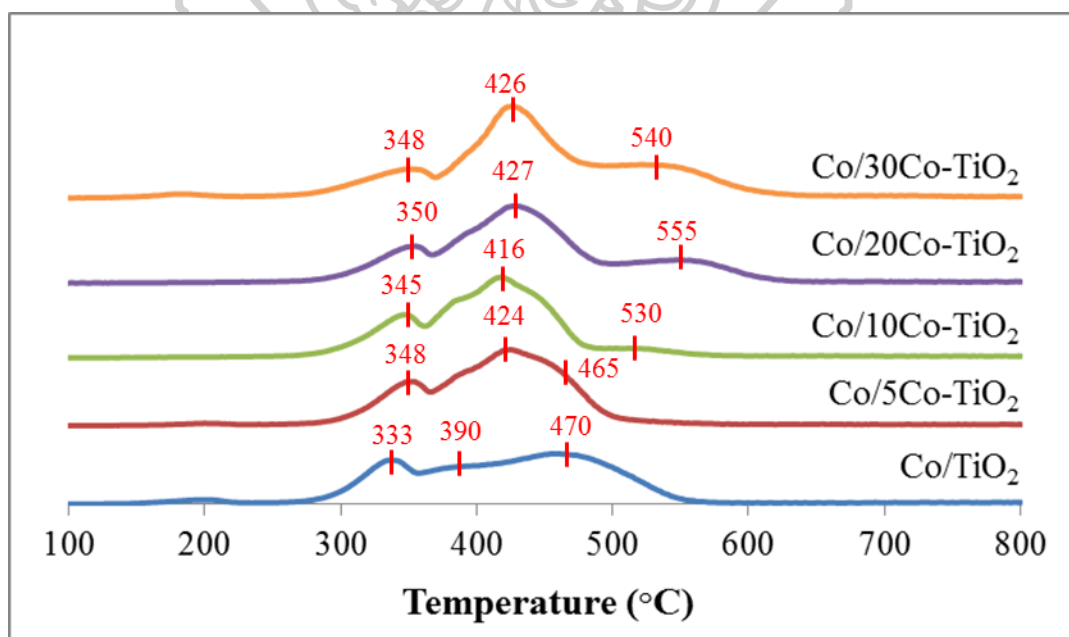
Figure 18 H$_2$-TPR profiles of Co/TiO$_2$ and Co/Co-TiO$_2$ catalysts

The reduction characteristic by TPR

The reduction behaviors of Co catalysts are shown in Figure 17. The Co/TiO_2 catalyst showed the reduction peaks at 333-470°C. It was well known that these peaks typically assigned to the reduction of weak interaction Co_3O_4 to Co metal [46]. For $Co/5Co-TiO_2$ catalyst, the reduction peaks was narrowed than Co/TiO_2 catalyst. The other catalysts showed the reduction peak at high temperature. It was attributed to the reduction of other cobalt species or strongly interaction cobalt oxide with support [47]. The further increase inserted-cobalt led to increase amount of H_2 consumption. According to this results, the reduction peak at high temperature represents to the reduction of FSP-inserted Co [27].

Table 9 shows the reducibility of Co/TiO_2 and $Co/Co-TiO_2$ catalysts. There were two reduction regions at temperature below and above 500°C assigned as the reduction of impregnated- and inserted-cobalt, respectively. All catalysts showed reducibility of impregnated-cobalt in range of 79-90%. The $Co/5Co-TiO_2$ catalyst did not show the reduction peak of inserted-cobalt probably due to the strong interaction of inserted-cobalt and TiO_2. For high amount of inserted-cobalt in support (more than 10%), the reducibility of inserted-cobalt showed around 20%. This result was related to an increase of non-reducible cobalt species confirmed by XRD results. The total reducibility was calculated by summarizing both reduction regions. The total reducibility decreased with increasing the amount of inserted-cobalt.

Table 10 Reducibility of Co/TiO_2 and $Co/Co-TiO_2$ catalysts

Catalyst	Reducibility (%)		
	Impregnated Co	Inserted Co	Total
Co/TiO_2	87.5	-	87.5
$Co/5Co-TiO_2$	87.1	0	73.5
$Co/10Co-TiO_2$	79.7	22.5	63.3
$Co/20Co-TiO_2$	82.6	22.0	55.6
$Co/30Co-TiO_2$	89.8	20.5	52.0

Cobalt metallic sites by H_2 chemisorption

The relative amount of active Co metal surface on the catalyst samples was calculated from H_2 chemisorption based on the assumption that one hydrogen atom adsorbed on one Co site. It was well known that only surface Co metal atom was active for the Fischer-Tropsch synthesis. The results of H_2 chemisorption as shown in Figure 18 indicated the information of the number of cobalt active sites. Among all the catalysts, it was found that the Co/TiO_2 catalyst exhibited the highest cobalt active sites. The inserted-cobalt accelerated the agglomeration of the impregnated-cobalt. Then, the number of active sites decreased.
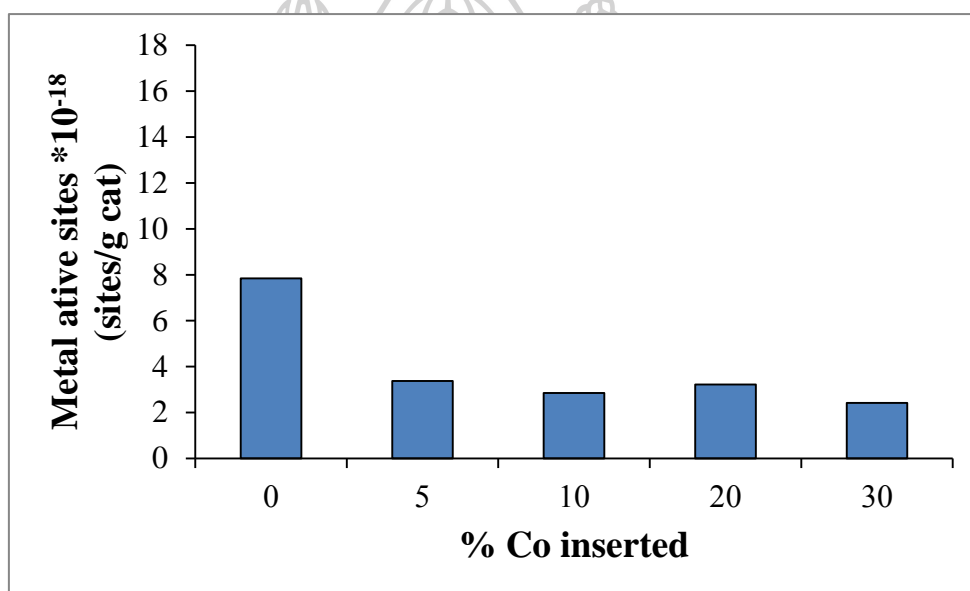
Figure 19 Metal active sites of Co/TiO₂ and Co/Co-TiO₂ catalysts

5.1.1.2 The catalytic activity and product selectivity by FTS

The reaction rate, turnover frequency (TOF) and product distribution of the Co/TiO_2 and Co/Co-TiO₂ catalysts are shown in Figures 19 and 20. It was found that insertion of cobalt affected both reaction rate and TOF. The Co/TiO_2 catalyst showed the highest reaction rate and methane formation. The increase of inserted Co by FSP showed low reaction rate but long-chain hydrocarbon selectivity increased. Except 10% inserted Co, the catalyst showed low reaction rate and kerosene selectivity.
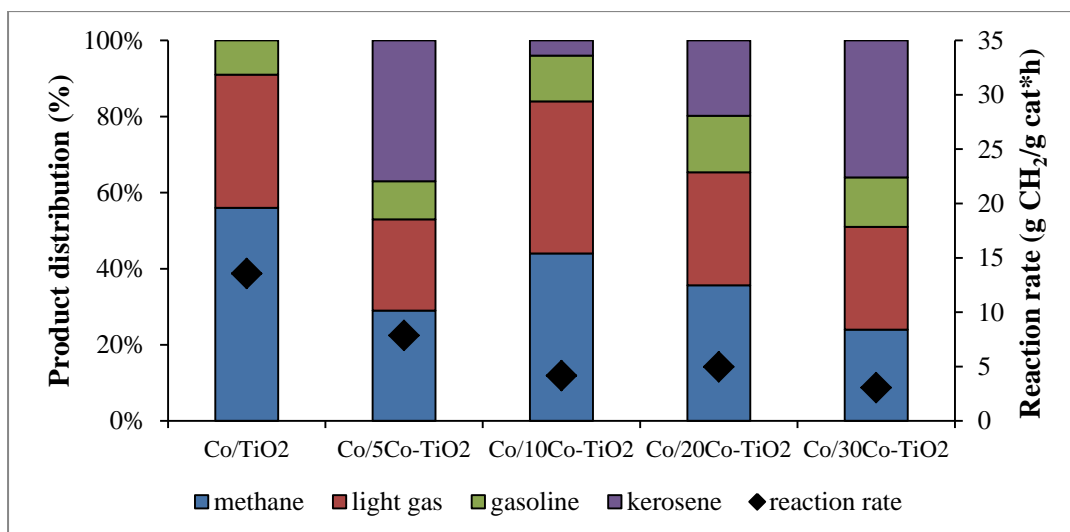
Figure 20 Catalytic properties of Co/TiO$_2$ and Co/Co-TiO$_2$ catalysts
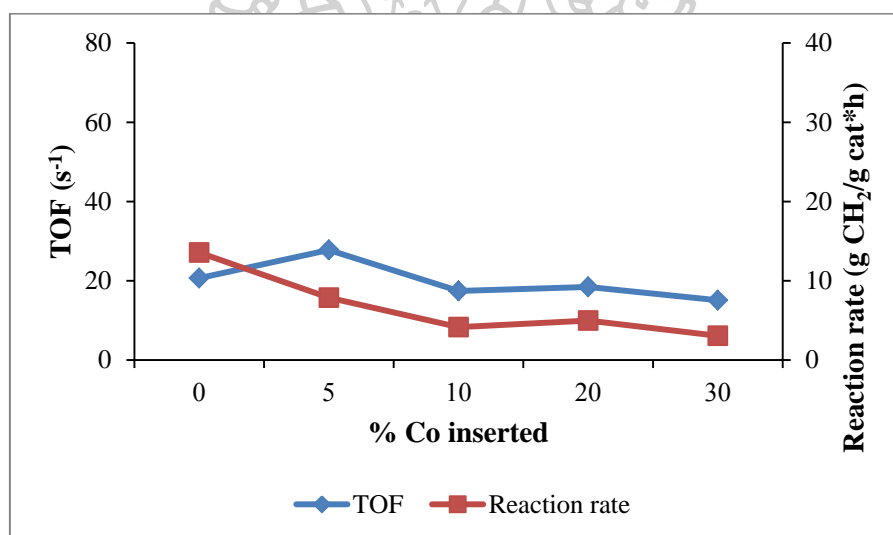
Figure 21 The reaction rate and TOF of Co/TiO$_2$ and Co/Co-TiO$_2$ catalysts

Figure 21 shows the speculation of Co/TiO$_2$ and Co/Co-TiO$_2$ catalysts structure. For the Co/TiO$_2$ catalyst, the cobalt oxide dispersed on titania support that was in agreement with XRD result. For the Co/5Co-TiO$_2$ catalyst, the inserted-cobalt was divided into two cobalt species consisting of cobalt embedded in the support and cobalt titanate. It was possible that the cobalt titanate suppressed the dispersion of the impregnated-cobalt that was confirmed by the H$_2$ chemisorption result. The decrease of metal active sites retarded the rate of reaction but promoted the selectivity to heavy hydrocarbon. The composition on the catalyst surface was changed when more than

10% inserted Co was added. Besides two cobalt species, the cobalt oxides formed by the FSP insertion were pronounced. They were strongly interacted with the TiO_2 support confirmed by the TPR results. The high amount of these cobalt oxides possibly aggomerated and then became larger particle. This was reason to increase the kerosene selectivity.
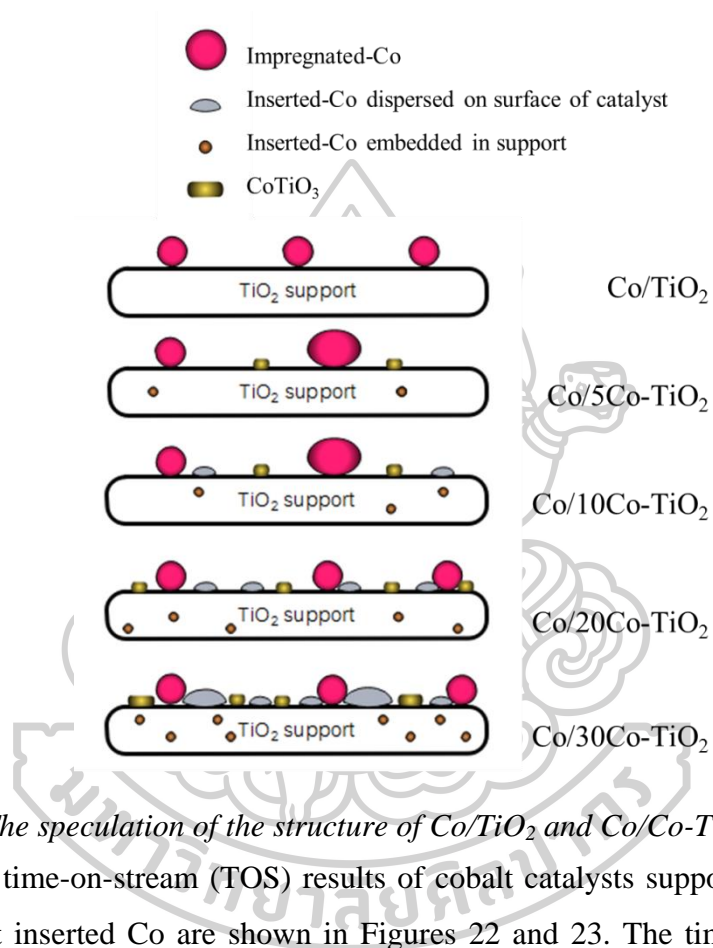
Figure 22 The speculation of the structure of Co/TiO$_2$ and Co/Co-TiO$_2$ catalysts

The time-on-stream (TOS) results of cobalt catalysts supported on TiO_2 with and without inserted Co are shown in Figures 22 and 23. The time for steady-state was independent on the amount of inserted-cobalt. The reaction rate and product distribution of all catalysts hardly changed with time-on-stream.
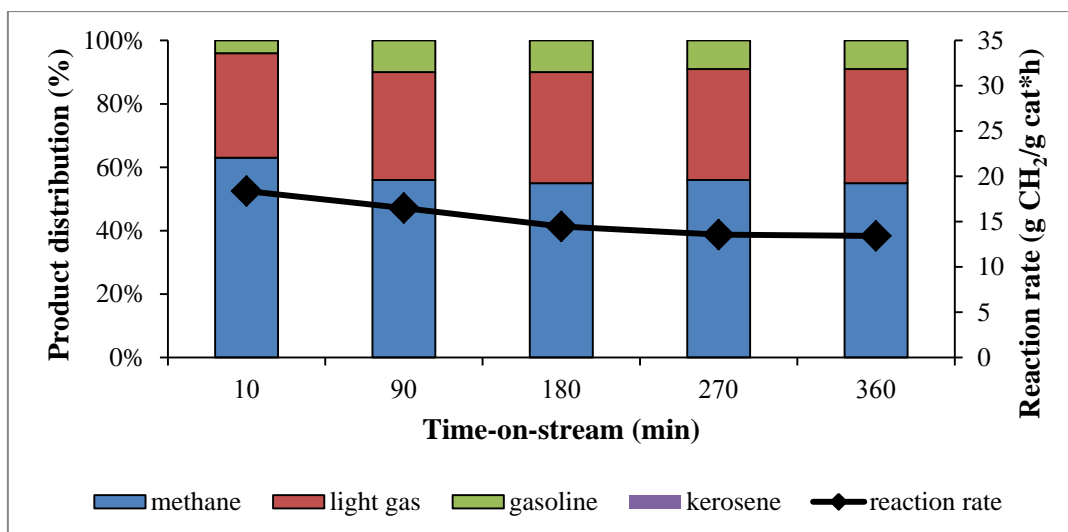
Figure 23 Time-on-stream profile of reaction rate and product distribution over Co/TiO₂ catalyst
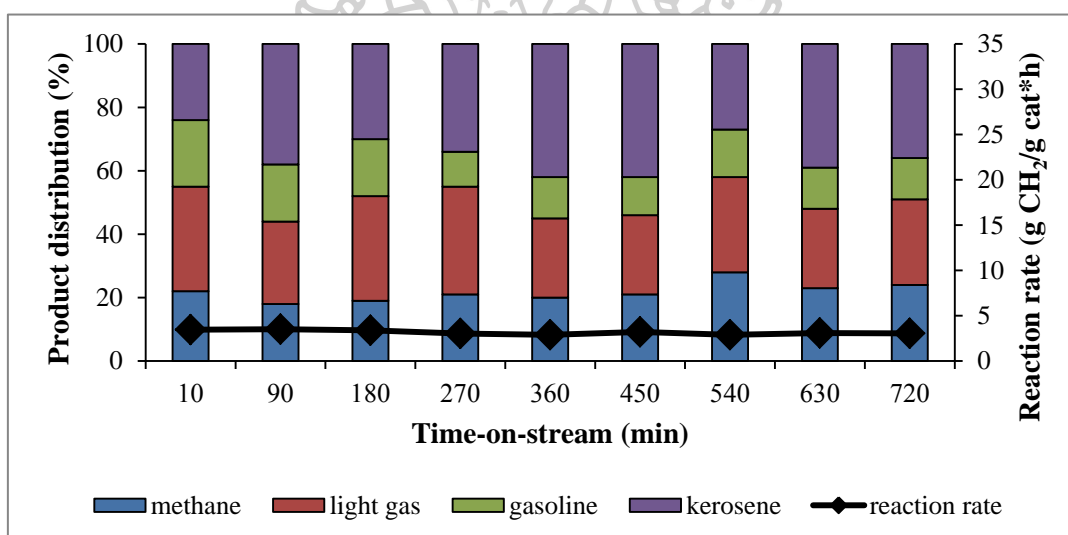
Figure 24 Time-on-stream profile of reaction rate and product distribution over Co/30Co-TiO₂ catalyst

5.1.2 Co/ZrO$_2$ and Co/Co-ZrO$_2$ catalysts

5.1.2.1 Physicochemical properties of catalysts

The phase analysis by X-ray diffraction

Figure 24 shows the XRD results of the Co/ZrO$_2$ and Co/Co-ZrO$_2$. All of catalysts showed the pattern of Co$_3$O$_4$ at 2Θ=36° (major), 31°, 44°, 59°, and 65°. The Co/ZrO$_2$ catalyst showed the characteristic peaks of the ZrO$_2$ consisting of monoclinic phase at 2Θ=27° (major), 24°, 31°, 34°, 35°, 38°, 40°, 49° and 54° [48] and tetragonal phase at 2Θ=30° (major), 50° and 60° [49]. The insertion of cobalt by FSP in ZrO$_2$ support affected the phase formation of tetragonal. The addition of Co as a second element by FSP created a defect in ZrO$_2$ crystal thus accelerating the monoclinic to tetragonal transition. For high amount of inserted-cobalt, the characteristic peaks of monoclinic were disappeared.

The average crystallite sizes of cobalt oxide are shown in Table 10. The Co/ZrO$_2$ catalyst showed the largest Co$_3$O$_4$ crystallite size. In case of FSP-inserted Co, the crystallite size was decreased to 17-20 nm.

Table 11 Physical properties of Co/ZrO$_2$ and Co/Co-ZrO$_2$ catalysts

Catalyst	N$_2$-physisorption			XRD
	S$_{BET}$ (m^2/g)	V$_p$ (cm^3/g)	dp$_{av}$ (nm)	d$_{Co3O4}$ (nm)
Co/ZrO$_2$	20.2	0.07	15.1	31.4
Co/5Co-ZrO$_2$	32.3	0.11	14.8	18.3
Co/10Co-ZrO$_2$	34.8	0.15	17.2	19.6
Co/20Co-ZrO$_2$	27.3	0.08	12.1	19.2
Co/30Co-ZrO$_2$	29.8	0.13	18.3	17.5
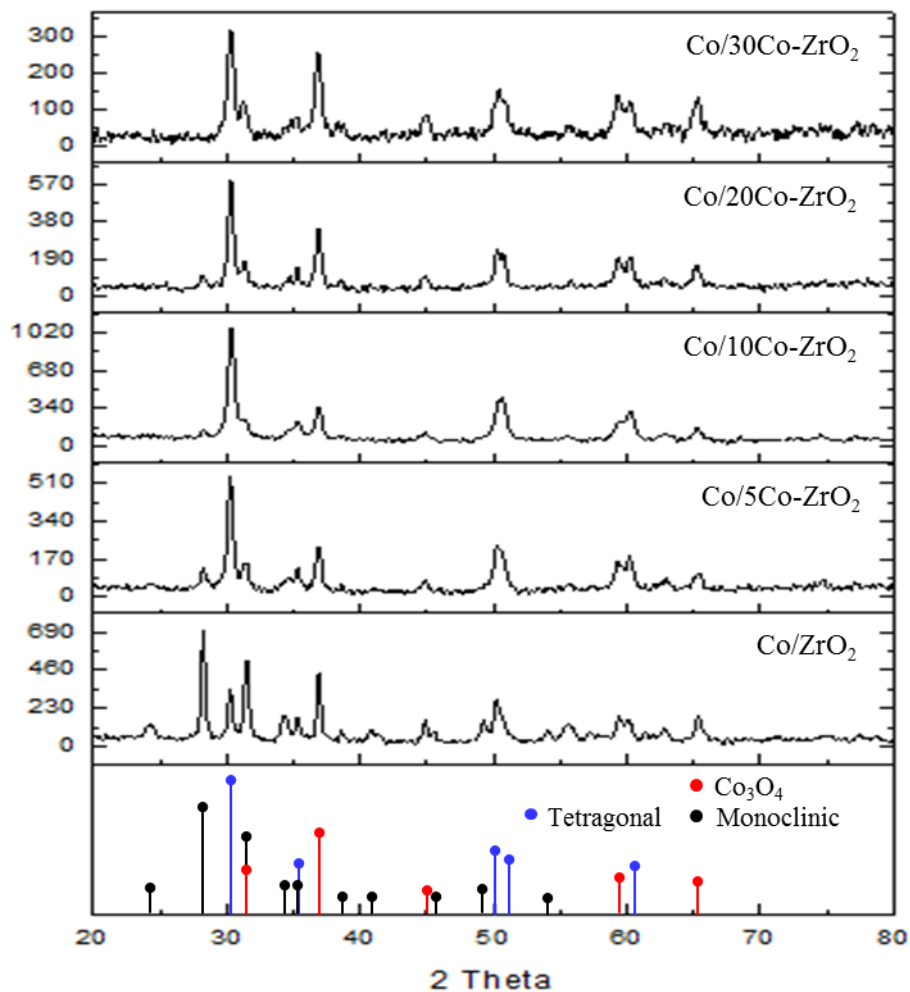
Figure 25 XRD patterns of Co/ZrO$_2$ and Co/Co-ZrO$_2$ catalysts

Specific surface area and pore characteristic

The BET surface area, total pore volume and average pore diameter are shown in Table 10. The Co-based catalysts with inserted cobalt showed higher specific surface area than the Co/ZrO$_2$ catalyst but it did not affect pore characteristics.

The adsorption-desorption isotherm of Co catalysts are shown in Figure 25 with a type IV isotherm, which was characteristic of the mesoporous structure in the catalyst. The hysteresis loop of Co/ZrO$_2$ showed type H3 similar to Co/TiO$_2$.
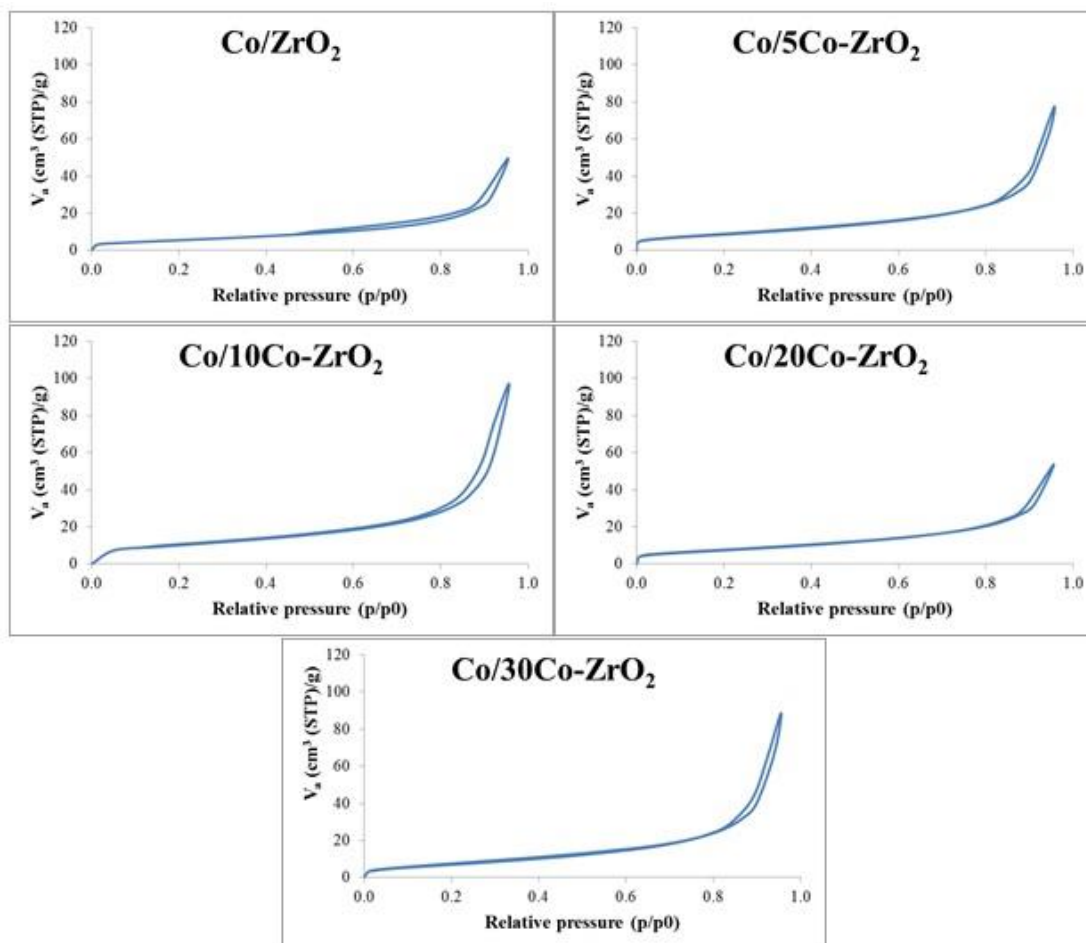
Figure 26 Adsorption-desorption isotherm of Co/ZrO$_2$ and Co/Co-ZrO$_2$ catalysts

The reduction characteristic by TPR

Figure 26 shows the reduction profiles of Co/ZrO$_2$ and Co/Co-ZrO$_2$ catalysts. The Co/ZrO$_2$ catalyst showed the reduction peaks of cobalt oxide at temperature below 400°C (LT). The TPR profiles of catalysts with inserted-cobalt in the support showed the additional reduction peaks at higher temperature (HT). The H$_2$ consumption of the HT peak increased with increasing the amount of inserted-cobalt. It was possible that the reduction peak at high temperature represented the reduction of inserted-cobalt. This result attributed to a strong metal-support interaction of inserted-cobalt and the ZrO$_2$ support. The HT peak was the reduction of small particle of Co$_3$O$_4$ that interacted with support [50].
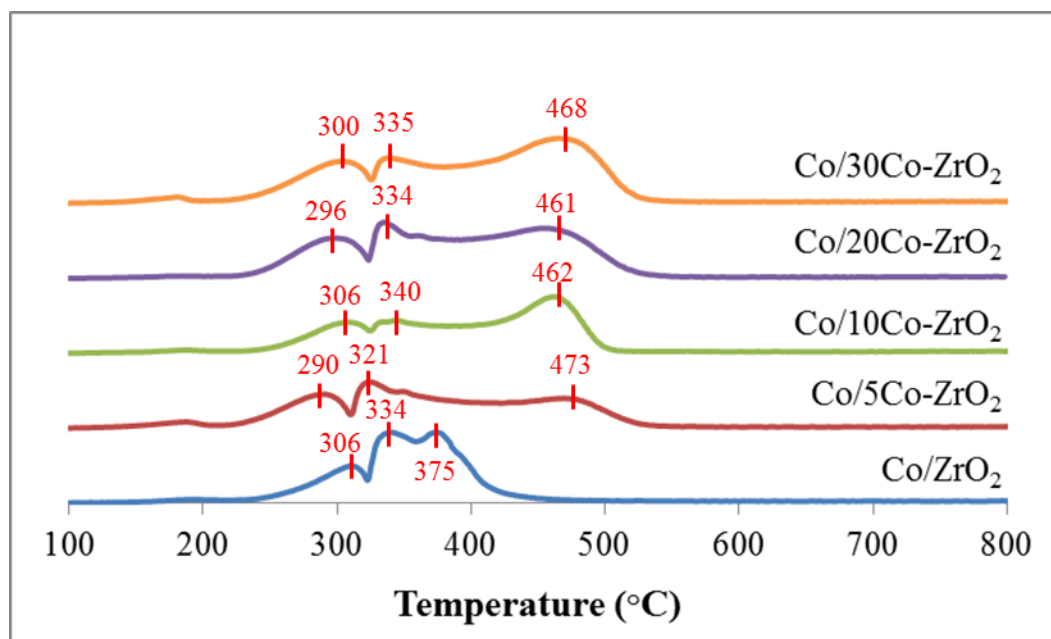
Figure 27 H₂-TPR profiles of Co/ZrO₂ and Co/Co-ZrO₂ catalysts

Table 11 shows reducibility of cobalt supported on zirconia and modified zirconia. The reduction regions at temperature below and above 400°C were assigned to the reduction of impregnated- and inserted-cobalt, respectively. The reducibility of Co/ZrO₂ catalyst was around 79%. The reducibility of impregnated-cobalt slightly decreased when adding inserted-cobalt until 10 wt%. On the other hand, the high amount of inserted-cobalt enhanced reducibility of impregnated-cobalt. The reducibility of inserted-cobalt decreased with increasing inserted-cobalt in the support.

Table 12 Reducibility of Co/ZrO₂ and Co/Co-ZrO₂ catalysts

Catalyst	Reducibility (%)		
	Impregnated Co	Inserted Co	Total
Co/ZrO₂	79.3	-	79.3
Co/5Co-ZrO₂	72.6	87.6	75.1
Co/10Co-ZrO₂	65.5	54.9	62.5
Co/20Co-ZrO₂	84.9	35.6	63.0
Co/30Co-ZrO₂	91.8	29.6	57.9

Cobalt metallic site by H_2 chemisorption

The cobalt metallic active sites of Co/ZrO_2 and $Co/Co-ZrO_2$ are shown in Figure 27. The Co/ZrO_2 catalyst showed the lowest cobalt active sites; 7.54×10^{18} sites/g cat. A 5 wt. % of inserted-cobalt gave the highest active sites; 1.65×10^{19} sites/g cat. The insertion of cobalt by FSP can promote the ability of H_2 chemisorption. It was possible that the inserted-cobalt dispersed on the catalyst surface due to weak interaction between metal and support.
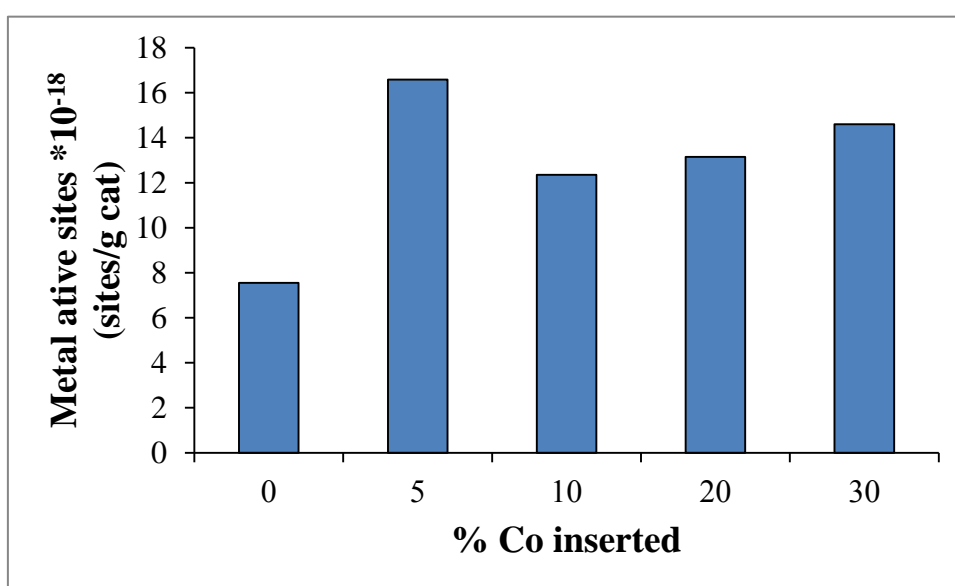
Figure 28 Metal active sites of Co/ZrO_2 and $Co/Co-ZrO_2$ catalysts

5.1.2.2 The catalytic activity and product selectivity by FTS

The catalytic properties of catalysts are shown in Figures 28 and 29. The reaction rate of all catalysts related to the results by H_2 chemisorption. Insertion of cobalt via FSP in ZrO_2 support hardly affected product distribution in the FTS. The methane formation of all catalysts exhibited in range of 29 to 41%. The $Co/5Co-ZrO_2$ catalysts showed the highest rate of reaction. TOF decreased when adding inserted Co. However, at more than 10 wt. % loadings, TOF was rather kept constant.
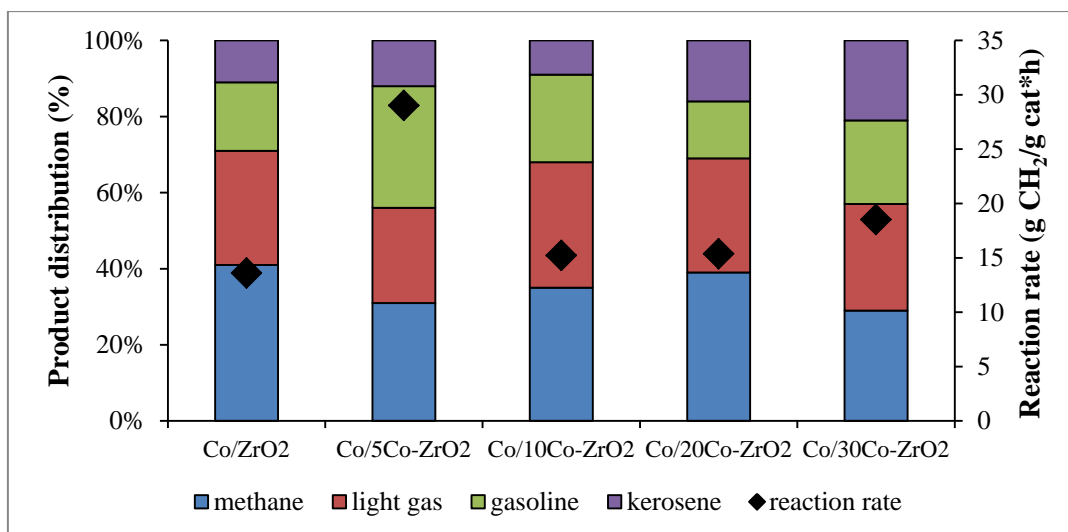
Figure 29 Catalytic properties of Co/ZrO$_2$ and Co/Co-ZrO$_2$ catalysts
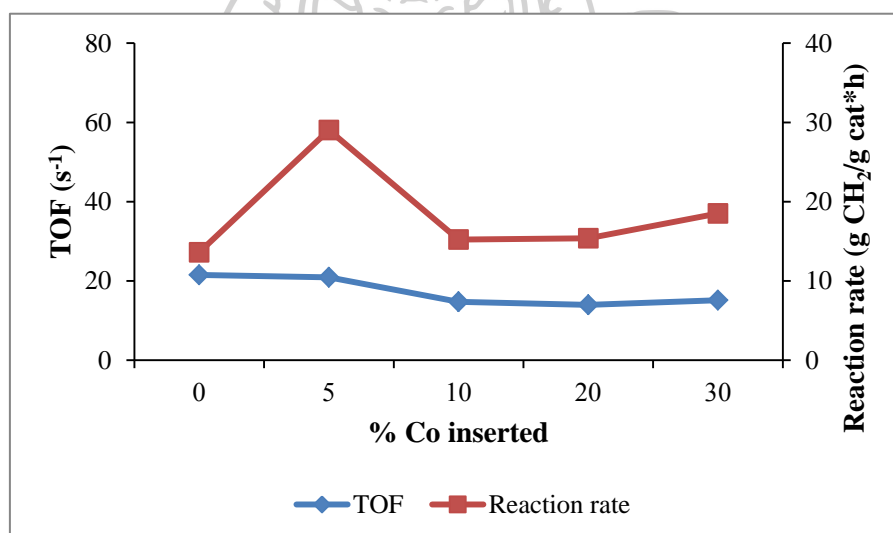
Figure 30 The reaction rate and TOF of Co/ZrO$_2$ and Co/Co-ZrO$_2$ catalysts

The structure of the Co/ZrO$_2$ and Co/Co-ZrO$_2$ catalysts is speculated as shown in Figure 30. For the Co/ZrO$_2$, the cobalt oxide was dispersed on zirconia support. The addition of the inserted-cobalt possibly represented cobalt oxides dispersed on surface of catalyst and embedded in the support. For the Co/5Co-ZrO$_2$, the inserted-cobalt might be well dispersed on surface of catalyst. It showed good agreement with H$_2$ chemisorption leading to the highest rate of reaction. For a high amount of inserted cobalt in the support (more than 10%), Co$_3$O$_4$ size was increased that related to a decrease of reaction rate and simultaneously an increase of kerosene formation.
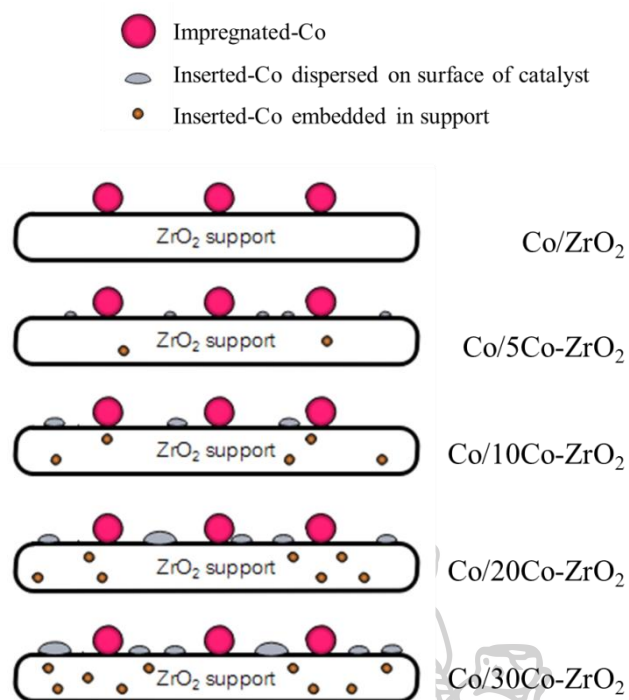
Figure 31 The speculation of the structure of Co/ZrO$_2$ and Co/Co-ZrO$_2$ catalysts

The time-on-stream results of cobalt catalysts are shown in Figures 31 and 32. Unlike Co/TiO$_2$, the reaction rate and product distribution of all Co/ZrO$_2$ catalysts were clearly changed on time. All of catalysts exhibited high reaction rate and methane selectivity at initial time but the activity and methane production decreased with time until steady-state. It was noted that both FTS activity and methanation were sharply decreased for some of inserted Co catalysts. It might be deactivation of catalysts.
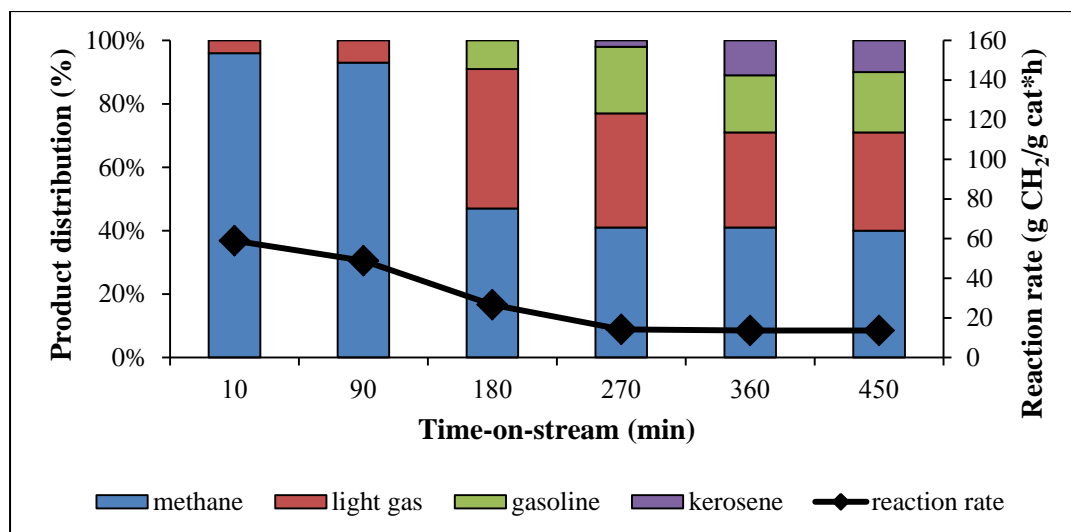
Figure 32 Time-on-stream profile of reaction rate and product distribution over Co/ZrO₂ catalyst
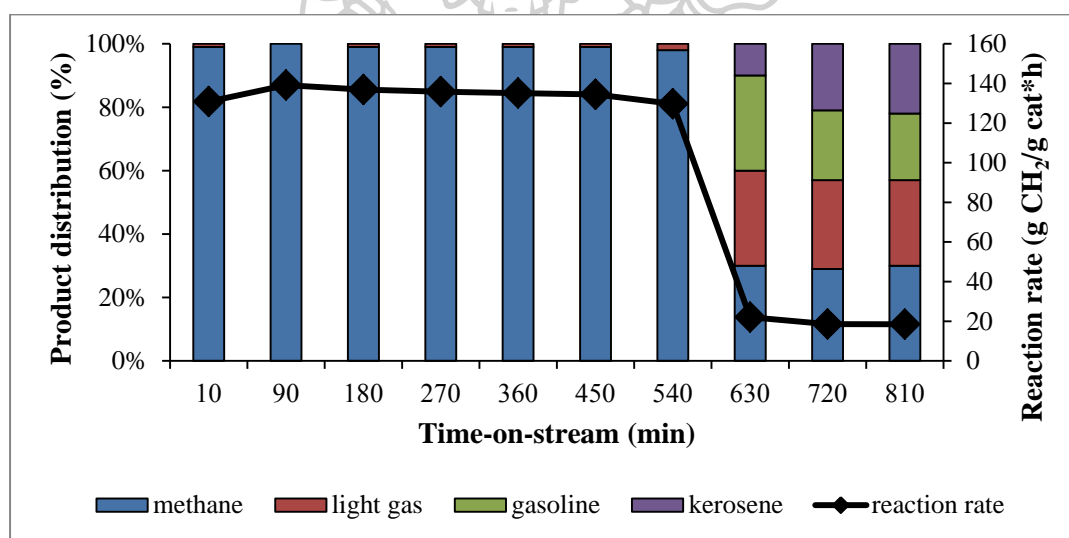
Figure 33 Time-on-stream profile of reaction rate and product distribution over Co/30Co-ZrO₂ catalyst

5.2 Effect of FSP-inserted Co in mixed metal oxide

5.2.1 Mixed TiO_2-ZrO_2 support with weight ratio 4:1

5.2.1.1 Physicochemical properties of catalysts

The phase analysis by X-ray diffraction

The XRD results of the Co/Co-4Ti:1Zr catalysts are shown in Figure 33. The Co/Co-4Ti:1Zr catalyst showed phase composition similar to Co/Co-TiO_2 catalyst. The Co/4Ti:1Zr catalyst showed the peak of Co_3O_4 and TiO_2. In case of insertion Co, the characteristic peaks of anatase were disappeared but rutile was obviously appeared. The insertion of Co by FSP in TiO_2 and 4Ti:1Zr support can suppress the formation of anatase and promoted rutile phase. The further addition of inserted-Co more than 20% promoted the formation of $CoTiO_3$. The crystallite size of Co_3O_4 is shown in Table 12.

Table 13 Physical properties of Co/4Ti:1Zr and Co/Co-4Ti:1Zr catalysts

Catalyst	N_2-physisorption			XRD
	S_{BET} (m^2/g)	V_p (cm^3/g)	dp_{av} (nm)	d_{Co3O4} (nm)
Co/4Ti:1Zr	37.9	0.16	17.6	22.8
Co/5Co-4Ti:1Zr	37.8	0.14	15.5	21.6
Co/10Co-4Ti:1Zr	35.0	0.11	12.9	24.8
Co/20Co-4Ti:1Zr	30.4	0.09	12.0	27.3
Co/30Co-4Ti:1Zr	33.0	0.11	13.5	18.3
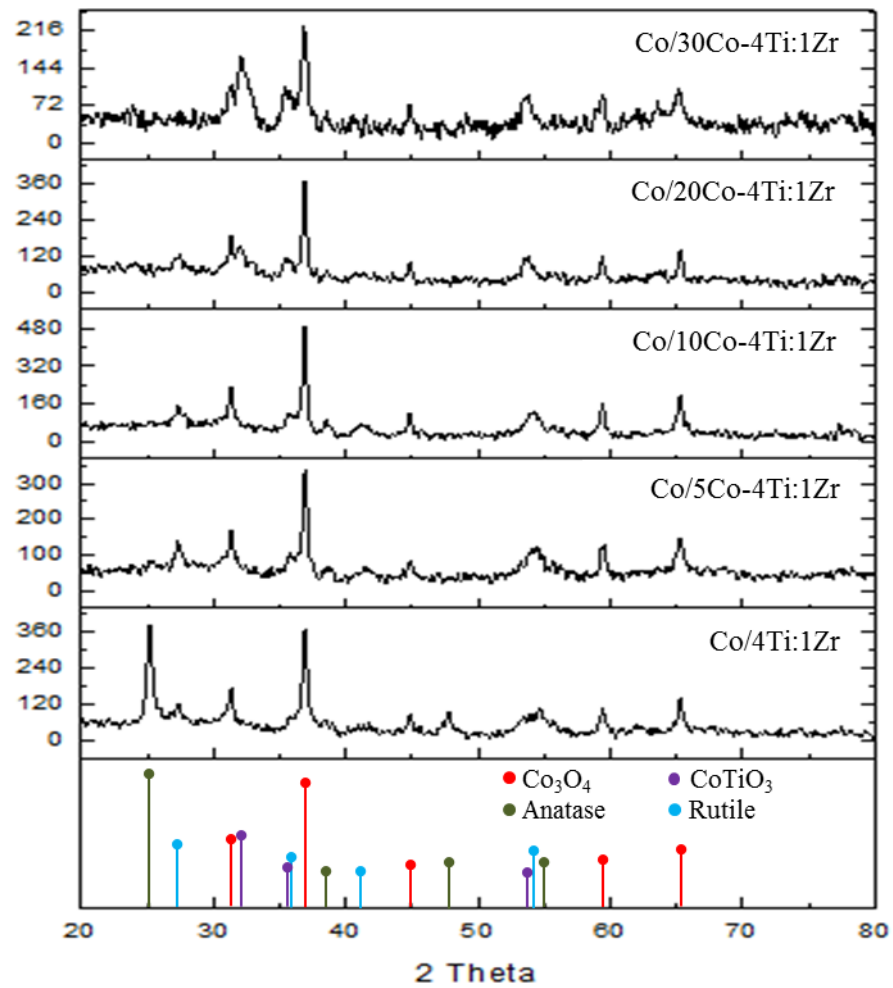
Figure 34 XRD patterns of Co/4Ti:1Zr and Co/Co-4Ti:1Zr catalysts

Specific surface area and pore characteristic

Table 12 shows N_2-physisorption results. BET surface area, total pore volume and average pore diameter were slightly decreased with increasing FSP-inserted Co to 20 wt. %. The adsorption-desorption isotherm of catalysts are shown in Figure 34. All catalysts showed isotherm and hysteresis loop in type VI and H3 respectively. The cobalt-insertion did not affect the catalyst's pore structure.
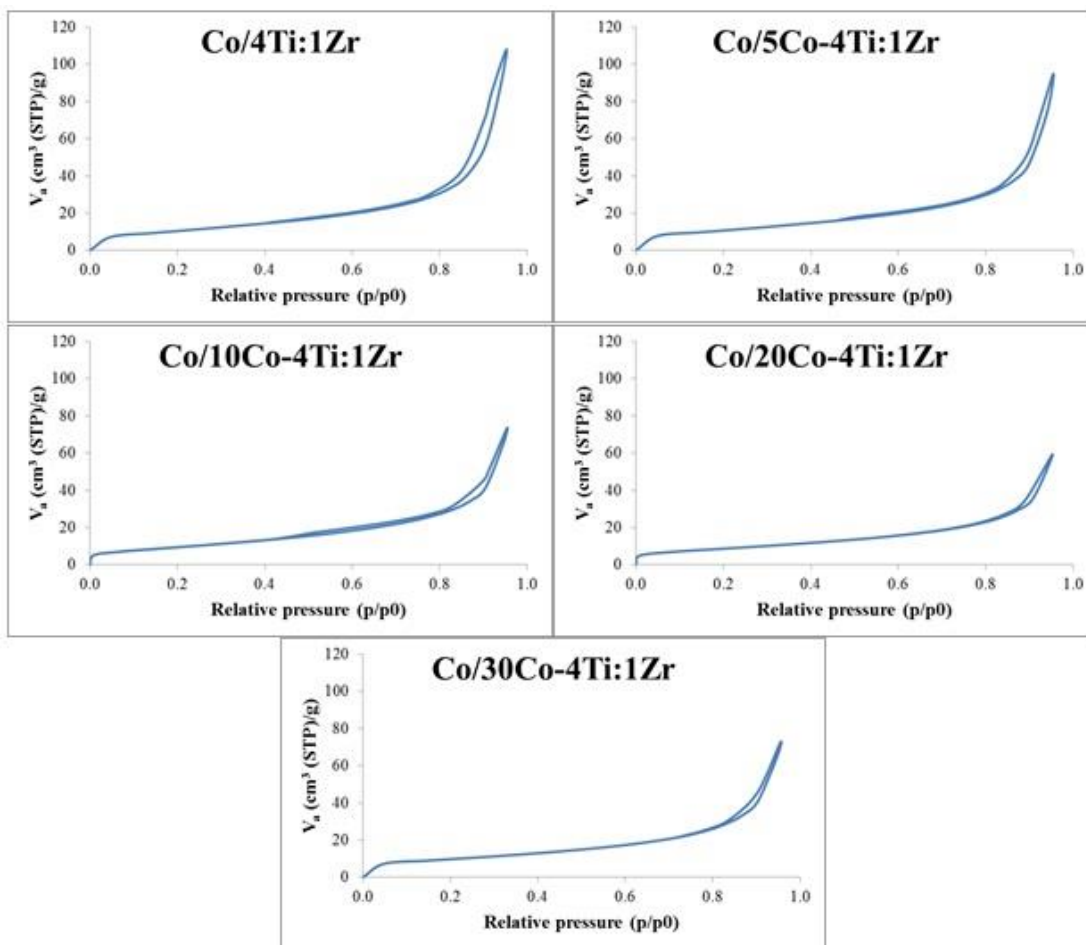
Figure 35 Adsorption-desorption isotherm of Co/4Ti:1Zr and Co/Co-4Ti:1Zr catalysts

The reduction characteristic by TPR

TPR profiles and catalysts reducibility are shown in Figure 35 and Table 13. All catalysts showed three reduction regions of cobalt oxide at below 400°C, 400-500°C and above 500°C. The catalyst without Co inserted and low Co inserted showed the similar pattern. It can be described that at without and low cobalt content, the cobalt particle size was closely corresponding to the XRD result. At 20 and 30 wt. % of cobalt in mixed support showed the same pattern, the second peak had high H_2 consumption that difference from other catalysts.
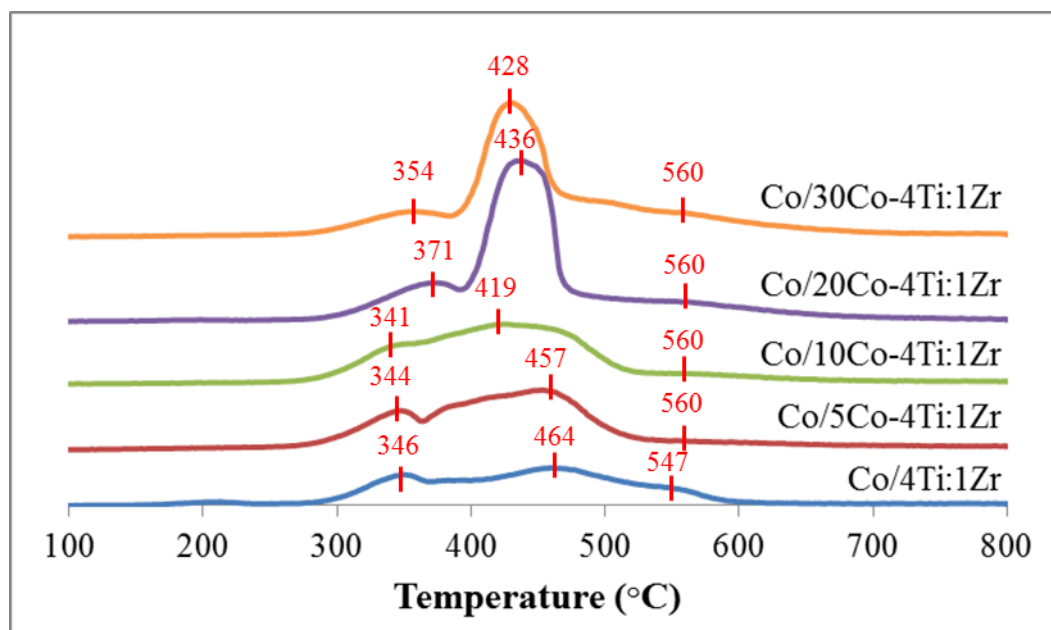
Figure 36 H$_2$-TPR profiles of Co/4Ti:1Zr and Co/Co-4Ti:1Zr catalysts

Table 14 Reducibility of Co/4Ti:1Zr and Co/Co-4Ti:1Zr catalysts

Catalyst	Reducibility (%)
Co/4Ti:1Zr	67.9
Co/5Co-4Ti:1Zr	82.5
Co/10Co-4Ti:1Zr	70.2
Co/20Co-4Ti:1Zr	74.7
Co/30Co-4Ti:1Zr	55.8

Cobalt metallic site by H$_2$ chemisorption

The results of H$_2$ chemisorption are shown in Figure 36 indicating the amount of cobalt metallic on surface. The Co/4Ti:1Zr catalyst exhibited the highest cobalt actives sites; 4.5×10^{18} sites/g cat. At low inserted-Co, the active sites of catalyst slightly deceased. The further increase inserted-cobalt to 20 and 30 wt. % led to clearly decreased of active sites to 2.23×10^{18} and 0.88×10^{18} sites/g cat respectively. The Co insertion affected the increasing of strong metal-support interaction.
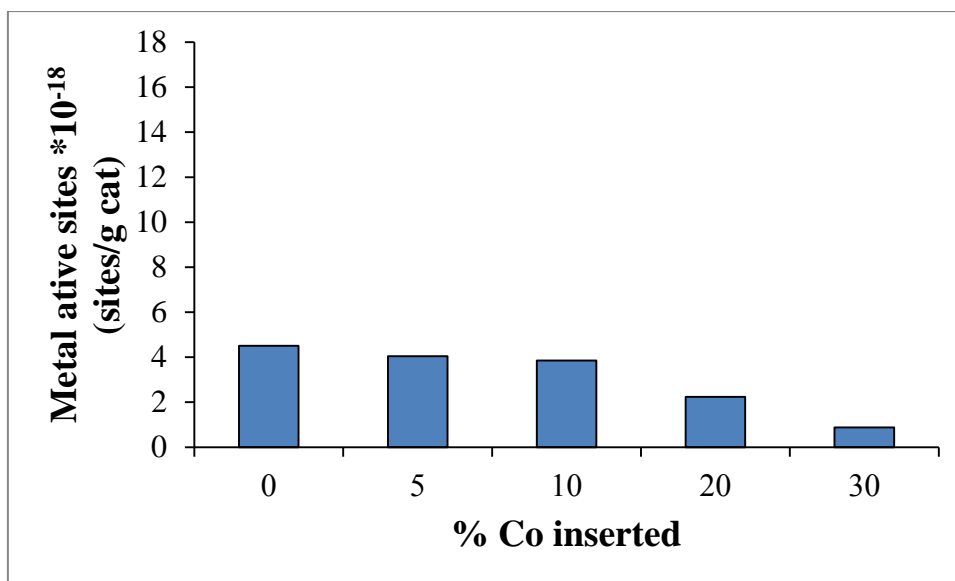
Figure 37 Metal active sites of Co/4Ti:1Zr and Co/Co-4Ti:1Zr catalysts
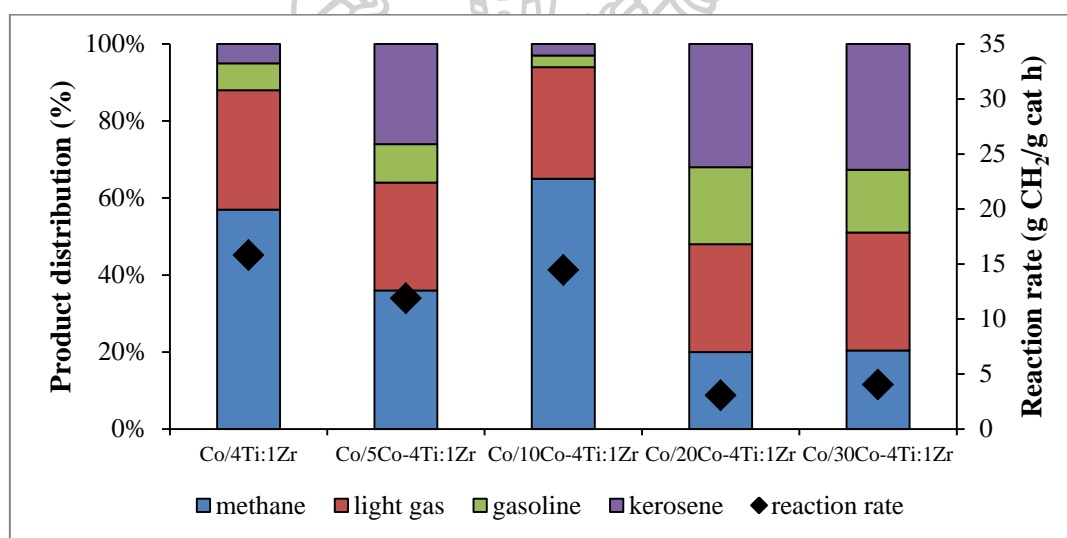
Figure 38 Catalytic properties of Co/4Ti:1Zr and Co/Co-4Ti:1Zr catalysts

5.2.1.2 The catalytic activity and product selectivity by FTS

The catalytic properties are shown in Figures 37 and 38. The catalyst without and with low inserted-Co showed nearly reaction rate at steady-state; 11-15 g CH_2/g cat·h. The catalysts with high Co insertion by FSP showed low reaction rate but they exhibited high kerosene selectivity. At 20 and 30 wt. % Co inserted showed the similar reaction rate and product distribution. The TOF and reaction rate of all

catalysts were similar trend. Except 30% Co inserted, showed the highest TOF with low cobalt metallic site.
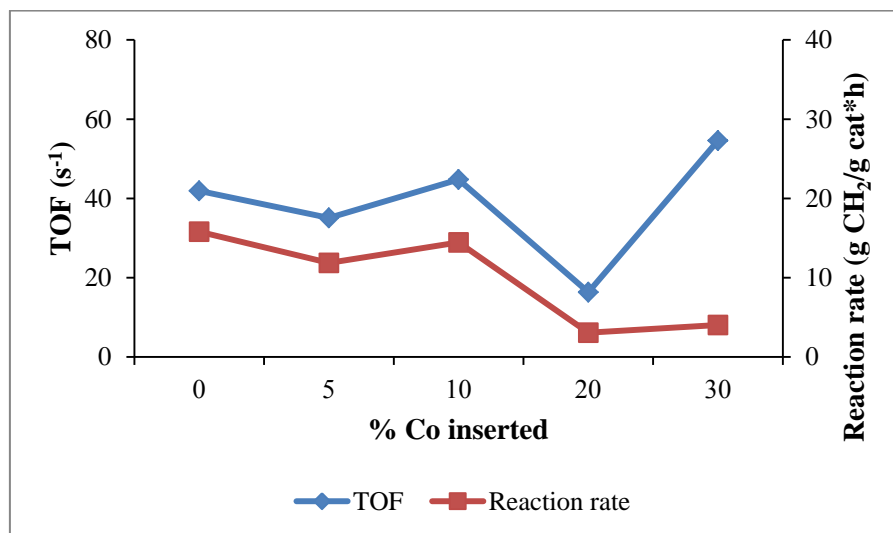
Figure 39 The reaction rate and TOF of Co/4Ti:1Zr and Co/Co-4Ti:1Zr catalysts
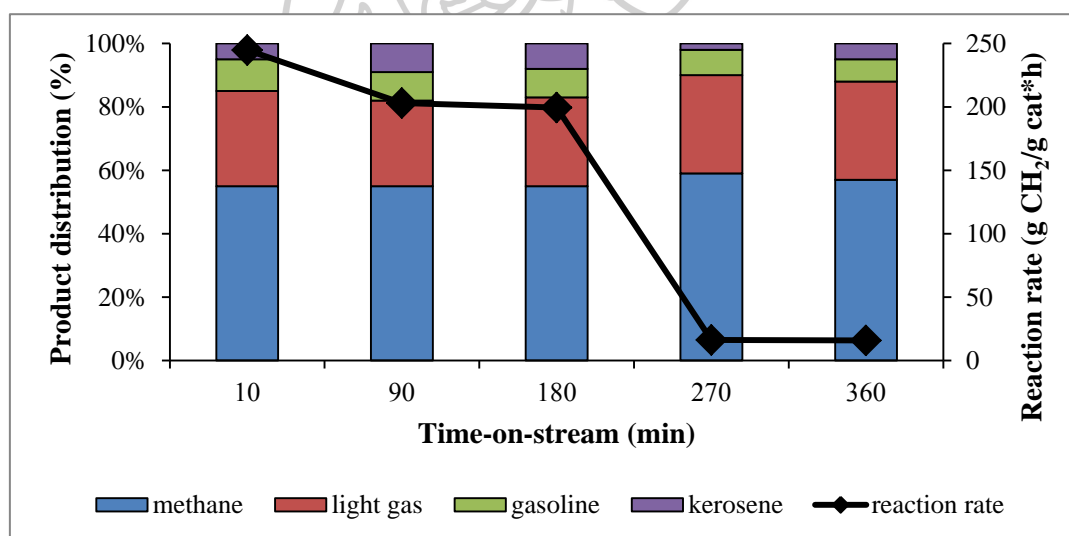
Figure 40 Time-on-stream profile of reaction rate and product distribution over Co/4Ti:1Zr catalyst
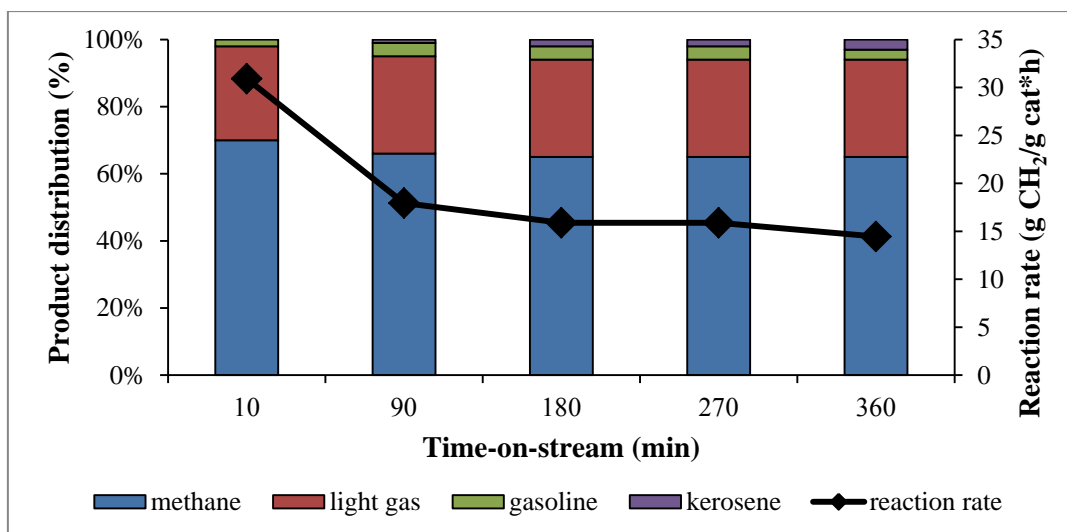
Figure 41 Time-on-stream profile of reaction rate and product distribution over Co/10Co-4Ti:1Zr catalyst
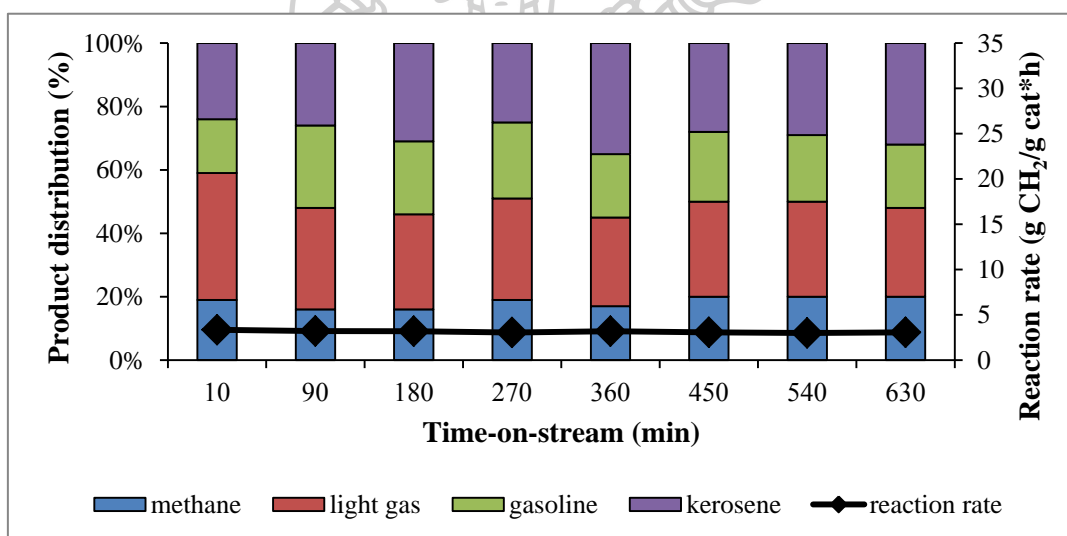
Figure 42 Time-on-stream profile of reaction rate and product distribution over Co/20Co-4Ti:1Zr catalyst

The time-on-stream (TOS) of catalysts supported on 4Ti:1Zr with and without Co-inserted are shown in Figures 39, 40 and 41. Product distribution of all catalysts was constant with time-on-stream result. In term of reaction rate, Co/4Ti:1Zr showed drastically decreased with increasing the reaction time, while 5 and 10% Co inserted showed slightly decreased. For high Co inserted, the reaction time did not affect rate of reaction.

5.2.2 Mixed TiO$_2$-ZrO$_2$ support with weight ratio 3:2

5.2.2.1 Physicochemical properties of catalysts

The phase analysis by X-ray diffraction

The XRD results of Co/3Ti:2Zr and Co/Co-3Ti:2Zr with various amount of cobalt inserted are shown in Figure 42. The pattern of Co$_3$O$_4$ appeared in all catalysts. The peaks of Ti$_2$ZrO$_6$ at 2Ө=30° (major), 24°, 35°, 53° and 54° [51] were showed in Co/3Ti:2Zr and low amount of cobalt inserted. For high cobalt inserted, these peaks were disappeared, while the peaks of CoTiO$_3$ were appeared. The average crystallite sizes of cobalt oxide are shown in Table 14. The increasing of FSP-inserted Co, the crystallite size decreased to 31-21 nm.

Table 15 Physical properties of Co/3Ti:2Zr and Co/Co-3Ti:2Zr catalysts

| Catalyst | N$_2$-physisorption | | | XRD |
	S$_{BET}$ (m^2/g)	V$_p$ (cm^3/g)	dp$_{av}$ (nm)	d$_{Co3O4}$ (nm)
Co/3Ti:2Zr	28.1	0.11	16.6	27.3
Co/5Co-3Ti:2Zr	22.2	0.06	11.3	31.4
Co/10Co-3Ti:2Zr	31.6	0.09	11.6	24.8
Co/20Co-3Ti:2Zr	26.7	0.07	11.8	22.8
Co/30Co-3Ti:2Zr	30.3	0.08	11.6	21.6

Specific surface area and pore characteristic

The results by N$_2$-physisorption are shown in Table 14 and Figure 43. The Co/Co-3Ti:2Zr catalysts showed the adsorption-desorption isotherm and hysteresis loop similar to the Co/Co-4Ti:1Zr catalysts. But it was smaller BET surface area than Co/Co-4Ti:1Zr catalysts due to the low amount of titania. The catalysts showed the BET surface area in range of 22-31 nm. The increasing of inserted-cobalt in support from 5 to 30% did not affect pore characteristic of catalysts.
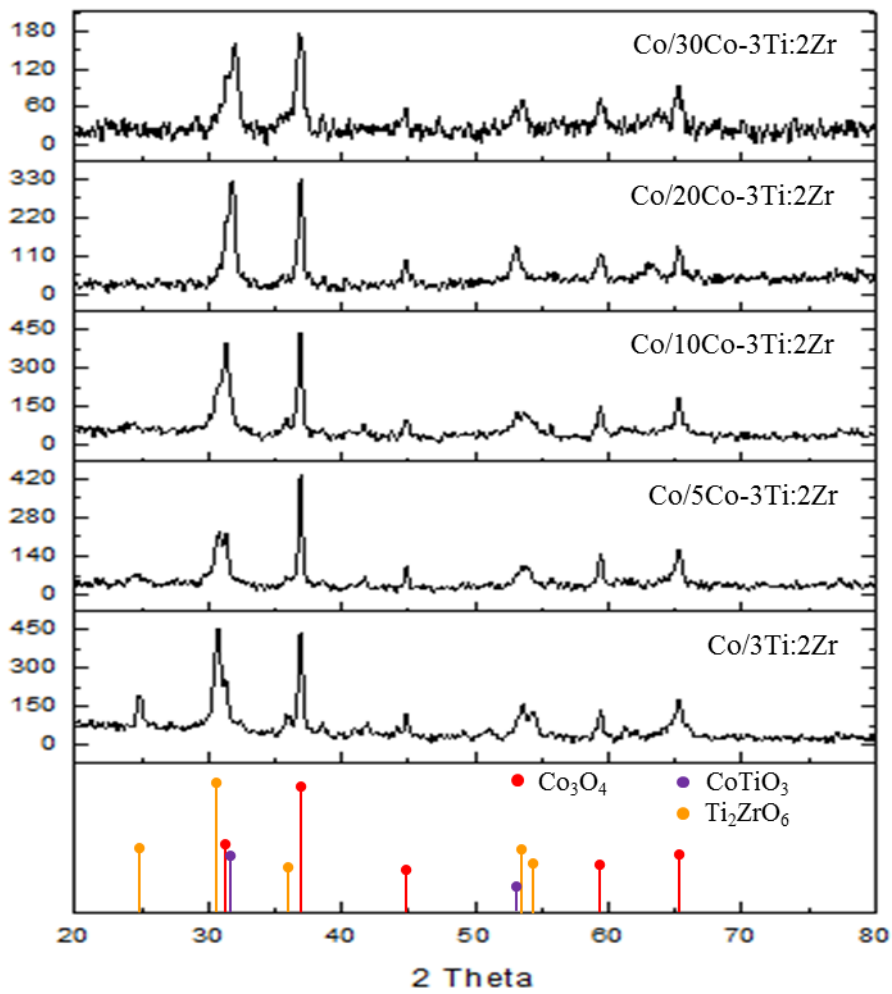
Figure 43 XRD patterns of Co/3Ti:2Zr and Co/Co-3Ti:2Zr catalysts
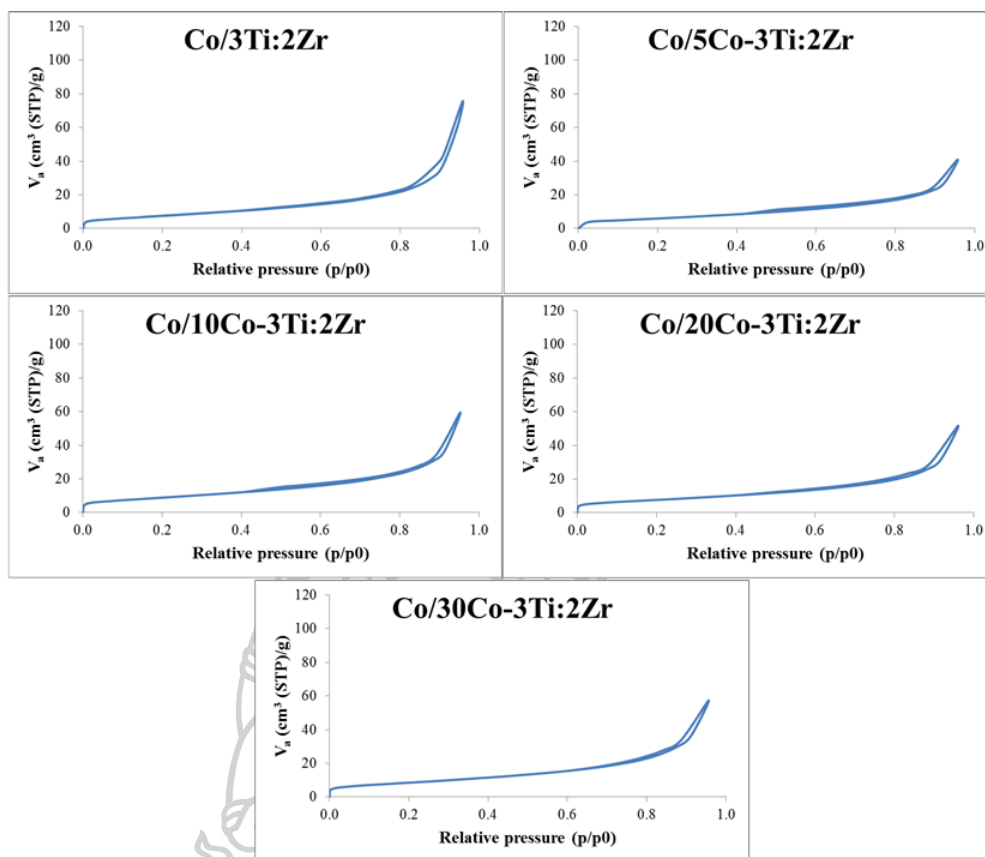
Figure 44 Adsorption-desorption isotherm of Co/3Ti:2Zr and Co/Co-3Ti:2Zr catalysts

The reduction characteristic by TPR

The reduction behaviors are shown in Figure 44. The TPR profile of all catalysts divided two main peaks. Co/3Ti:2Zr showed the wide board peak resulting in the reduction of heterogeneous distribution of cobalt oxide particle [30]. The increasing amount of inserted-cobalt led to H_2 consumption and reduction temperature increased. This result indicated the metal-support interaction increased with increasing the inserted-Co. The reduction degrees of catalysts are shown in Table 15. The reducibility slightly decreased with increasing insertion of cobalt in mixed support.
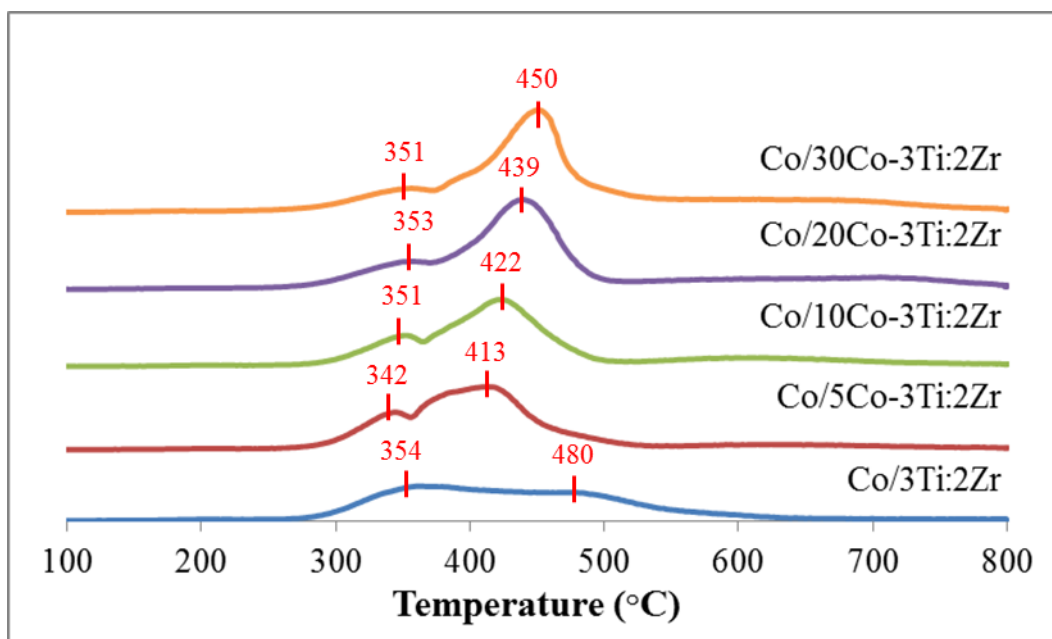
Figure 45 H₂-TPR profiles of Co/3Ti:2Zr and Co/Co-3Ti:2Zr catalysts

Table 16 Reducibility of Co/3Ti:2Zr and Co/Co-3Ti:2Zr catalysts

Catalyst	Reducibility (%)
Co/3Ti:2Zr	80.2
Co/5Co-3Ti:2Zr	74.9
Co/10Co-3Ti:2Zr	64.9
Co/20Co-3Ti:2Zr	64.7
Co/30Co-3Ti:2Zr	60.1

Cobalt metallic site by H₂ chemisorption

The cobalt metallic active site of catalyst is shown in Figure 45. Amount of active site decreased from 7.81×10^{18} to 1.41×10^{18} site/g cat with increasing FSP-inserted cobalt from 0 to 30%. The decreasing of active sites was in agreement with the metal-support interaction of TPR profile.
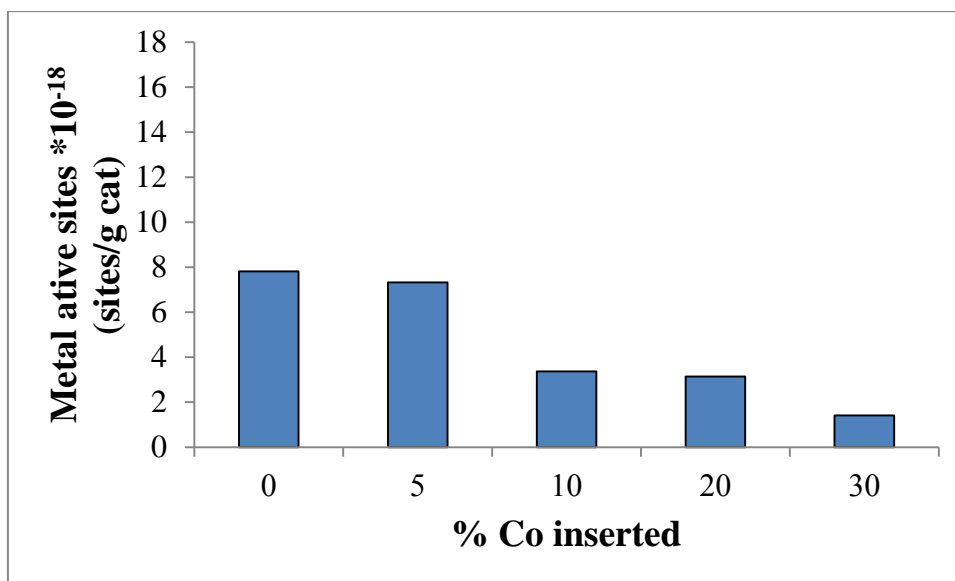
Figure 46 Metal active sites of Co/3Ti:2Zr and Co/Co-3Ti:2Zr catalysts

5.2.2.2 The catalytic activity and product selectivity by FTS

The Fischer–Tropsch activities are shown in Figure 46. Reaction rate and methane selectivity decreased from 12 to 2 g CH_2/g cat·h and 67 to 23%, respectively with increasing cobalt contain in catalysts that related to H_2 chemisorption results. But the amount of cobalt metallic site did not affect light gas selectivity. TOF of Co catalysts are shown in Figure 47.
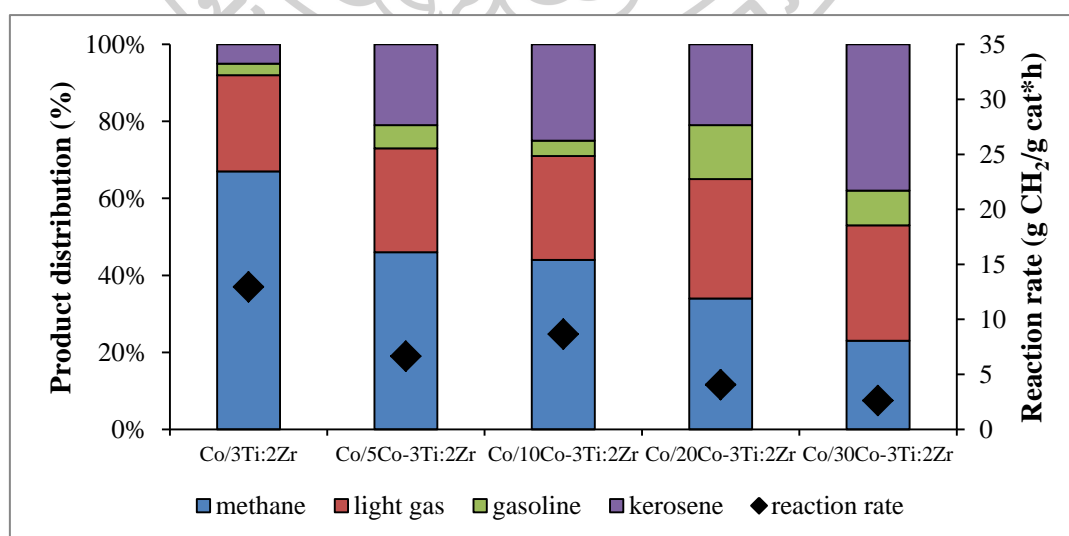
Figure 47 Catalytic properties of Co/3Ti:2Zr and Co/Co-3Ti:2Zr catalysts
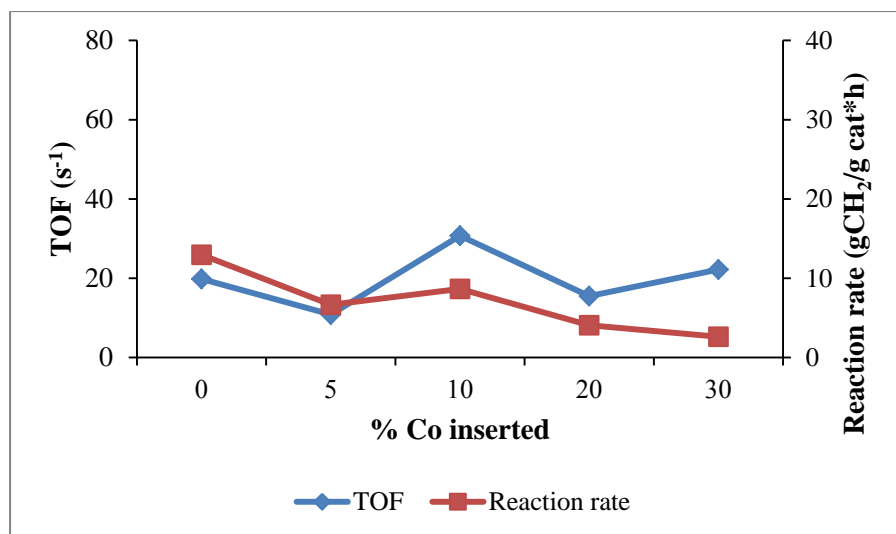
Figure 48 The reaction rate and TOF of Co/3Ti:2Zr and Co/Co-3Ti:2Zr catalysts

Figures 48 and 49 are show time-on-stream results. The Co/3Ti:2Zr showed drastically decreased of reaction rate and methane selectivity with increasing reaction time to 270 min; from 67 to 13 g CH_2/g cat·h and 98 to 67% respectively. For catalysts with inserted-cobalt, the differentiations of reaction rate and methane selectivity decreased with increasing amount of cobalt.
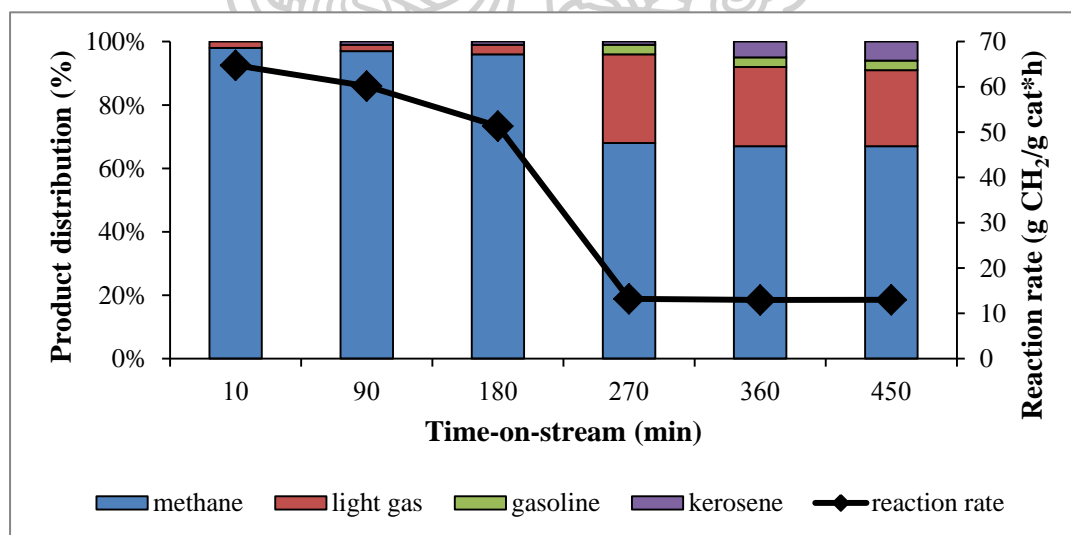
Figure 49 Time-on-stream profile of reaction rate and product distribution over Co/3Ti:2Zr catalyst
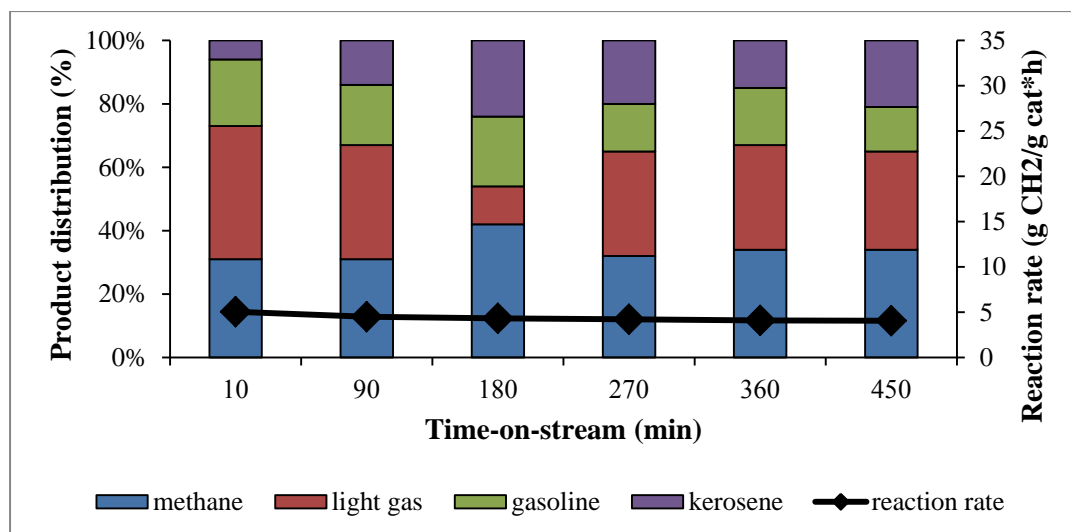
Figure 50 Time-on-stream profile of reaction rate and product distribution over Co/20Co-3Ti:2Zr catalyst

5.2.3 Mixed TiO_2-ZrO_2 support with weight ratio 2:3

5.2.3.1 Physicochemical properties of catalysts

The phase analysis by X-ray diffraction

The XRD results of Co supported on mixed TiO_2-ZrO_2 support in weight ratio 2:3 with and without Co inserted by FSP are shown in Figure 50. Cobalt oxide was showed in XRD result of all catalysts. The peaks of $ZrTiO_4$ at 2Θ=30° (major), 24°, 32°, 48°, and 53° [52] were observed on Co/2Ti:3Zr. Because of the ZrO_2 was increased to 60 wt. %, the peaks of tetragonal were appeared on Co/Co-2Ti:3Zr catalyst. The insertion of cobalt in mixed support suppressed the formation of zirconia-titania composite led to the disappearance of $ZrTiO_4$. For high cobalt loading, peaks of tetragonal were disappeared. At inserted-cobalt more than 10%, the peaks of $CoTiO_3$ were appeared. The crystallite sizes of Co_3O_4 are shown in Table 16. The small amount of cobalt content in support did not affected Co_3O_4 crystallite sizes, while further increase inserted-cobalt more than 20% resulted in Co_3O_4 size slightly decreased.
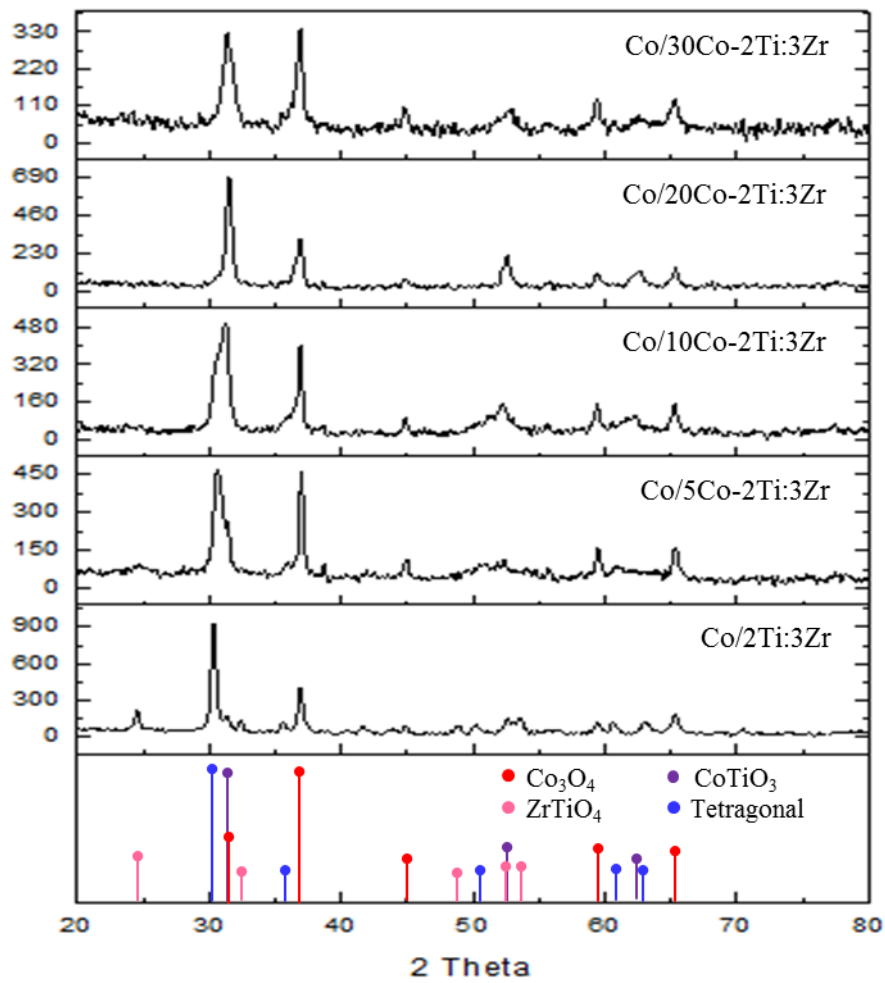
Figure 51 XRD patterns of Co/2Ti:3Zr and Co/Co-2Ti:3Zr catalysts

Table 17 Physical properties of Co/2Ti:3Zr and Co/Co-2Ti:3Zr catalysts

| Catalyst | N$_2$-physisorption | | | XRD |
	S_{BET} (m^2/g)	V_p (cm^3/g)	dp_{av} (nm)	d_{Co3O4} (nm)
Co/2Ti:3Zr	30.2	0.11	14.6	26.4
Co/5Co-2Ti:3Zr	31.9	0.09	11.3	26.4
Co/10Co-2Ti:3Zr	29.4	0.08	11.2	26.4
Co/20Co-2Ti:3Zr	29.3	0.08	11.6	22.2
Co/30Co-2Ti:3Zr	31.9	0.11	14.0	23.4
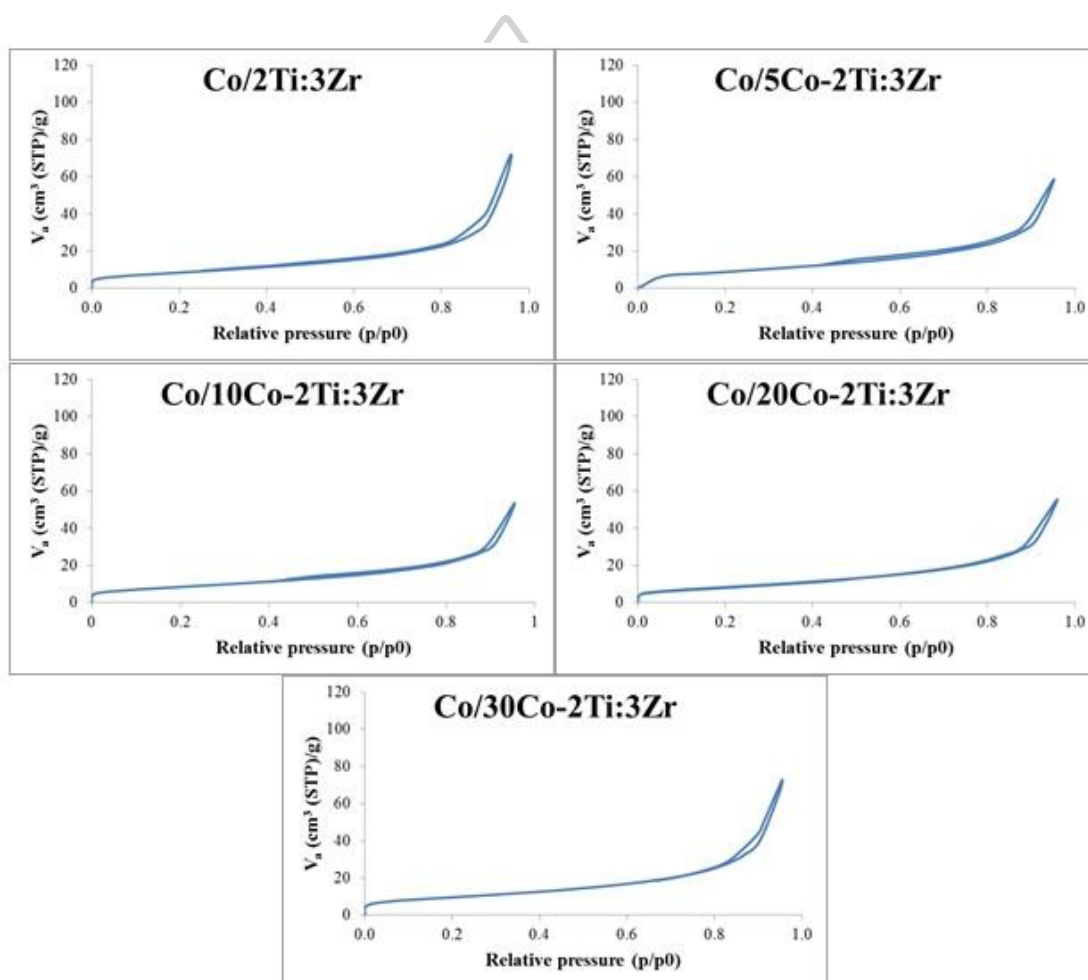
Figure 52 Adsorption-desorption isotherm of Co/2Ti:3Zr and Co/Co-2Ti:3Zr catalysts

Specific surface area and pore characteristic

BET surface area, total pore volume, average pore diameter and adsorption isotherm are shown in Table 16 and Figure 51. The insertion of cobalt did not affect surface area and porous structure. The isotherm exhibited type IV with hysteresis loop, corresponding to the characteristic of mesoporous materials with pore diameters between 2 and 50 nm. The shape characteristics of hysteresis loop for all catalysts were type H3, which describes a slit-shaped pore.

The reduction characteristic by TPR

The reduction behaviors of the catalysts supported on 2Ti:3Zr mixed support were studied by H_2-TPR technique. The results are shown in Figure 52 and Table 17. All catalysts showed the reduction peaks of Co_3O_4 to Co metal. Co/2Ti:3Zr and Co/5Co-2Ti:3Zr showed the board peak at 389-486°C that indicated cobalt oxide particles with a wide range of sizes in these catalyst [50]. For increasing amount of Co inserted from 10 to 30%, the board peak was merged to 425°C and shifted to 461°C. That indicated the increase of metal-support interaction with increasing inserted-Co.
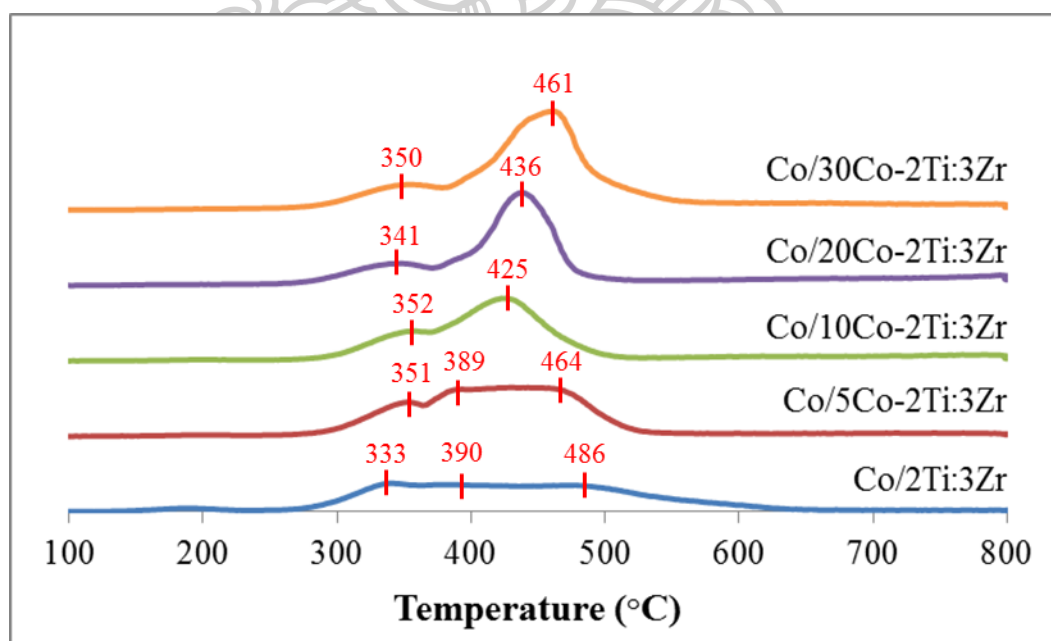
Figure 53 H_2-TPR profiles of Co/2Ti:3Zr and Co/Co-2Ti:3Zr catalysts

Table 18 Reducibility of Co/2Ti:3Zr and Co/Co-2Ti:3Zr catalysts

Catalyst	Reducibility (%)
Co/2Ti:3Zr	77.5
Co/5Co-2Ti:3Zr	77.7
Co/10Co-2Ti:3Zr	62.6
Co/20Co-2Ti:3Zr	75.1
Co/30Co-2Ti:3Zr	59.0
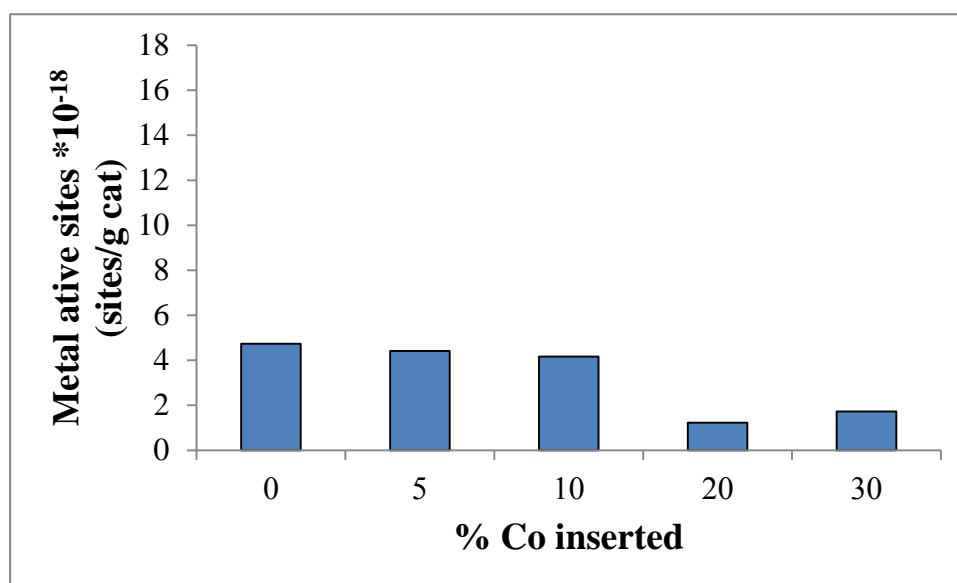
Figure 54 Metal active sites of Co/2Ti:3Zr and Co/Co-2Ti:3Zr catalysts

Cobalt metallic site by H_2 chemisorption

The results of H_2 chemisorption are shown in Figure 53. It provided the information of active cobalt metals on the catalyst samples. Catalysts with low inserted-Co showed the amount of active site nearly to Co/2Ti:3Zr catalyst. The addition of inserted-cobalt more than 20% decreased the ability of H_2 chemisorption.

5.2.3.2 The catalytic activity and product selectivity by FTS

Figures 54 and 55 show the product distribution, reaction rate and TOF number for FTS. The insertion of cobalt in mixed metal oxide support suppressed methanation and promoted the formation of long-chain hydrocarbon product. The amount of cobalt content in support did not affect rate of reaction. Except 5% Co

inserted, showed the highest FT reaction rate with low methane selectivity. The trend of reaction rate of Co/Co-2Ti:3Zr catalysts were similar to Co/Co-ZrO$_2$.
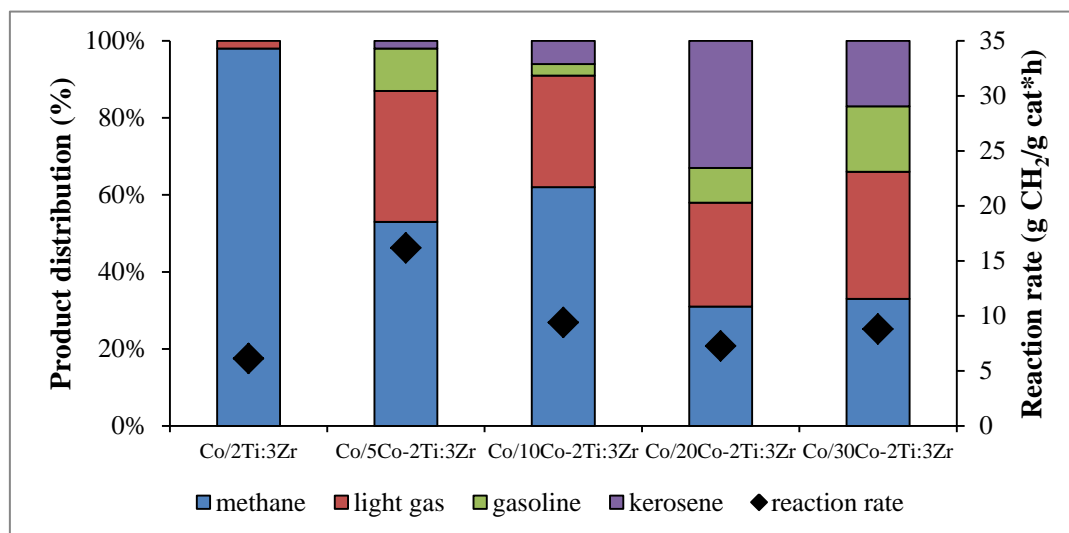
Figure 55 Catalytic properties of Co/2Ti:3Zr and Co/Co-2Ti:3Zr catalysts
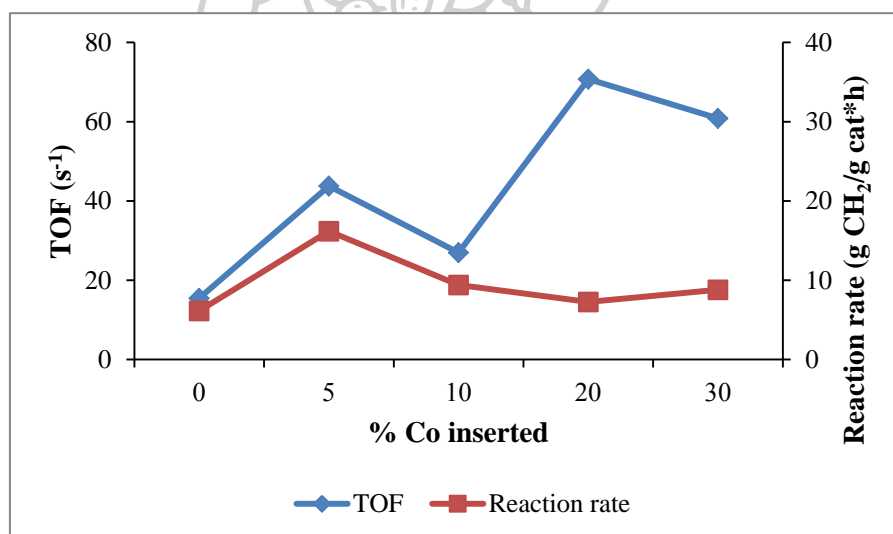
Figure 56 The reaction rate and TOF of Co/2Ti:3Zr and Co/Co-2Ti:3Zr catalysts

The time-on-stream (TOS) of catalysts are shown in Figures 56 and 57. Product distribution of Co/Co-2Ti:3Zr catalysts did not depend on the reaction time. The reaction rate of Co/2Ti:3Zr rapidly decreased with increasing reaction time to 3 h. On the other hand, the reaction rate of modified catalysts with inserted-Co slightly decreased from initial time to steady-state.
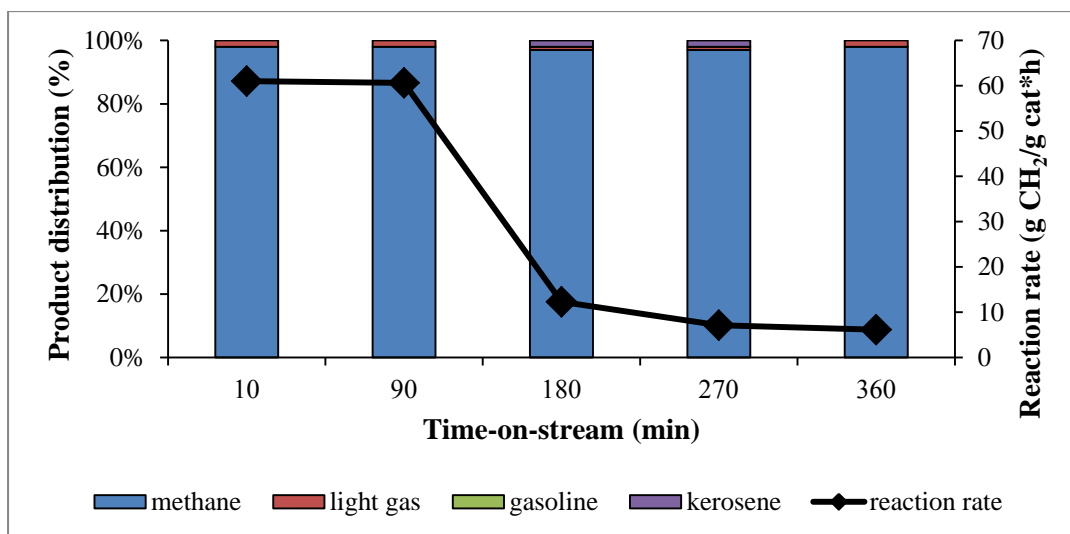
Figure 57 Time-on-stream profile of reaction rate and product distribution over Co/2Ti:3Zr catalyst
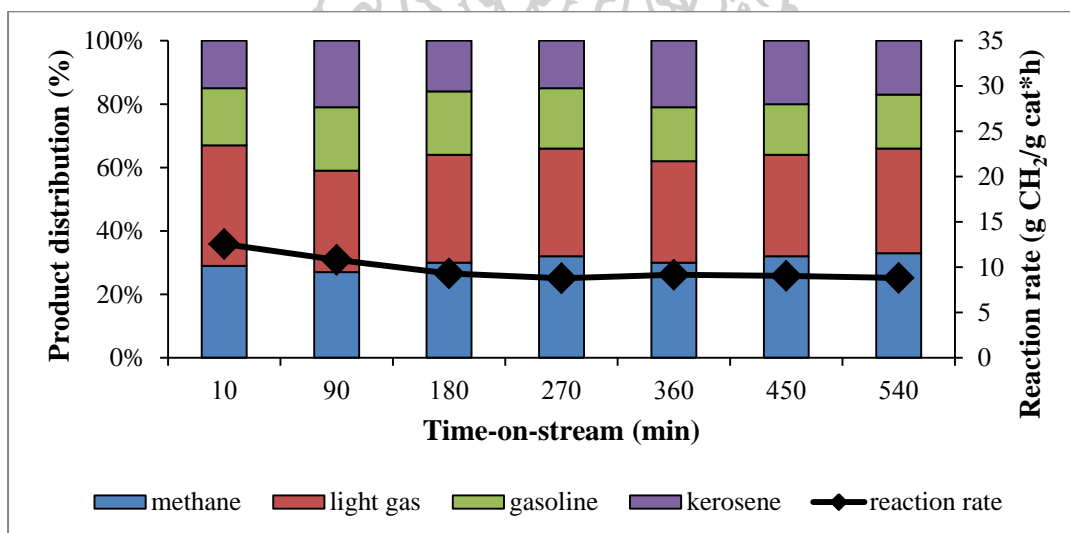
Figure 58 Time-on-stream profile of reaction rate and product distribution over Co/30Co-2Ti:3Zr catalyst

5.2.4 Mixed TiO$_2$-ZrO$_2$ support with weight ratio 1:4

5.2.4.1 Physicochemical properties of catalysts

The phase analysis by X-ray diffraction

Figure 58 and Table 18 shows the results of XRD analyze of the Co catalysts supported on mixed 1Ti:4Zr support with various FSP-cobalt inserted. The patterns of Co$_3$O$_4$ appeared in all catalysts.. The catalysts without and with low amount of cobalt inserted showed the present of monoclinic and tetragonal zirconia phase. The further addition inserted-cobalt to 20 and 30% suppressed the formation of monoclinic phase. Amount of 5% of cobalt inserted did not affected the Co$_3$O$_4$ size, however Co$_3$O$_4$ size decreased with increasing cobalt inserted more than 10%.
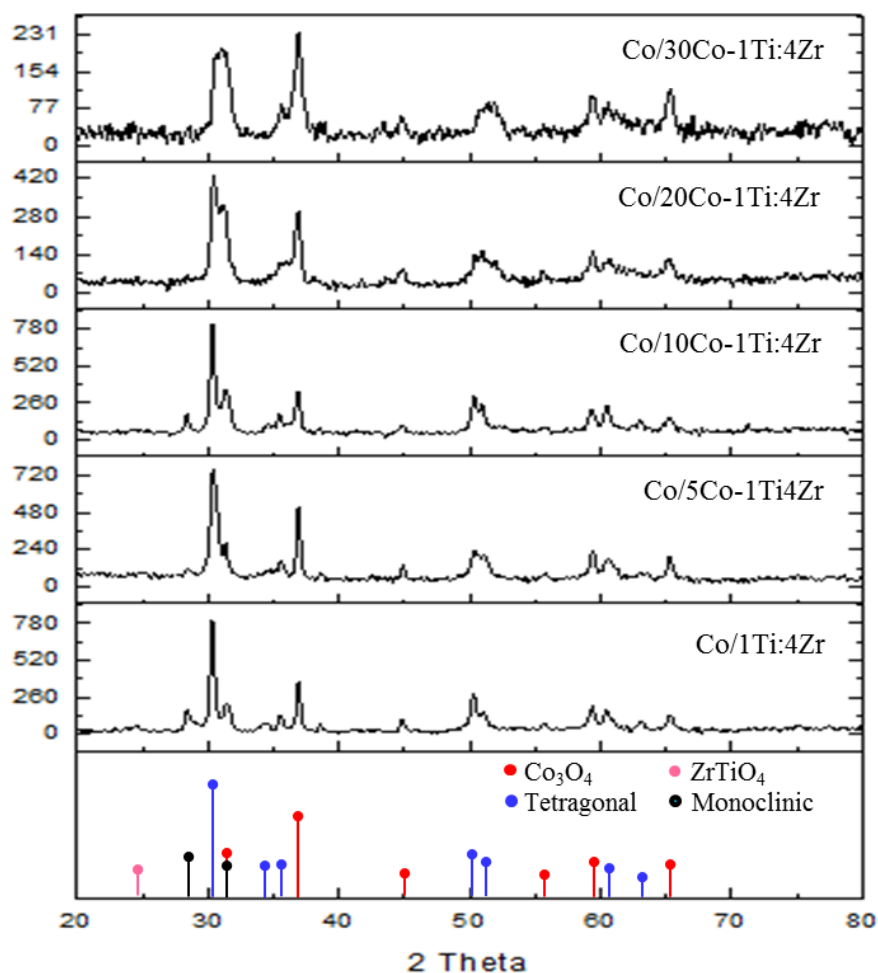
Figure 59 XRD patterns of Co/3Ti:2Zr and Co/Co-1Ti:4Zr catalysts

Specific surface area and pore characteristic

The specific surface area, total pore volume, average pore diameter and the N_2 adsorption-desorption isotherm of the cobalt catalysts are shown in Table 18 and Figure 59. Figure 59 shows a type-IV isotherm with hysteresis loop, which is characteristic of the mesoporous structure within the catalyst. This was consistent with the results of the average pore diameter.

Table 19 Physical properties of Co/1Ti:4Zr and Co/Co-1Ti:4Zr catalysts

Catalyst	N$_2$-physisorption			XRD
	S_{BET} (m^2/g)	V_p (cm^3/g)	dp$_{av}$ (nm)	d_{Co3O4} (nm)
Co/1Ti:4Zr	25.9	0.08	12.5	27.3
Co/5Co-1Ti:4Zr	31.2	0.11	15.2	29.2
Co/10Co-1Ti:4Zr	27.5	0.08	11.9	22.2
Co/20Co-1Ti:4Zr	31.7	0.09	11.9	19.2
Co/30Co-1Ti:4Zr	40.4	0.14	14.6	20.0
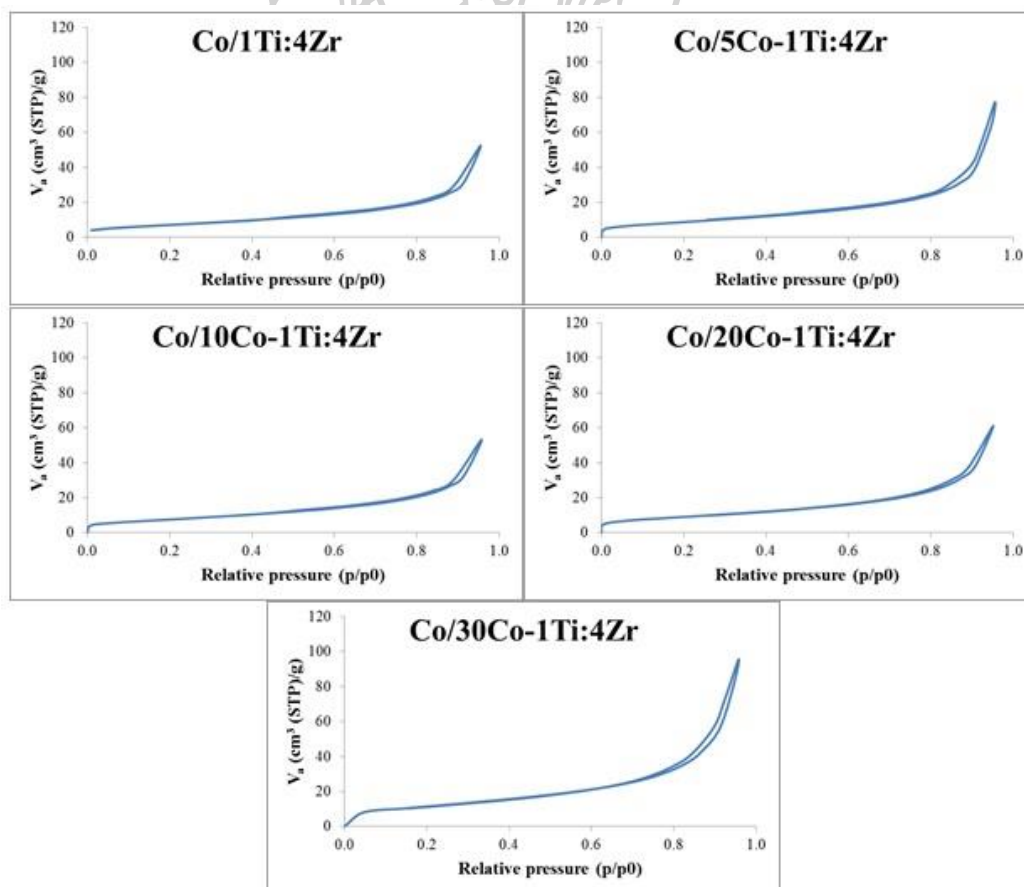
Figure 60 Adsorption-desorption isotherm of Co/1Ti:4Zr and Co/Co-1Ti:4Zr catalysts
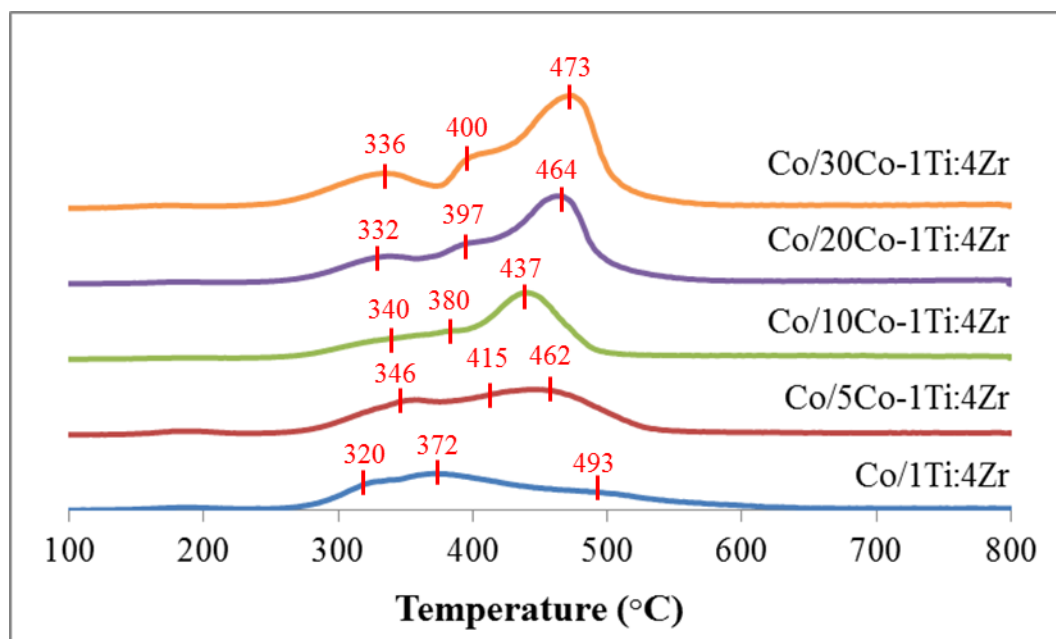
Figure 61 H₂-TPR profiles of Co/1Ti:4Zr and Co/Co-1Ti:4Zr catalysts

The reduction characteristic by TPR

The TPR profiles are shown in Figure 60 and Table 19. As can be seen, Co/1Ti:4Zr showed a wide broad reduction peak of Co_3O_4 and shifted to higher temperature than Co/ZrO_2 catalyst. It was indicated that the wide range of Co_3O_4 particle size on the surface catalyst due to the increasing of metal-support interaction. This was probably due to the presence of titanium in mixed oxide support. For FSP-Co inserted, the third reduction peak showed the amount of H_2 for reduction increased with increasing inserted-Co. This result indicated that the inserted-cobalt by FSP in mixed support was able to transform to cobalt oxide and used high temperature (437-473°C) for reduction to cobalt metallic. The reducibility of Co catalysts was slightly decreased from 78% to 63% with increasing Co content in catalyst. This was indicated that the addition of cobalt increased the interaction between cobalt and support.

Table 20 Reducibility of Co/1Ti:4Zr and Co/Co-1Ti:4Zr catalysts

Catalyst	Reducibility (%)
Co/1Ti:4Zr	78.5
Co/5Co-1Ti:4Zr	71.7
Co/10Co-1Ti:4Zr	60.5
Co/20Co-1Ti:4Zr	64.1
Co/30Co-1Ti:4Zr	63.6

Cobalt metallic site by H_2 chemisorption

The results from H_2 chemisorption are shown in Figure 61. Co/1Ti:4Zr exhibited the highest active site about 9.69×10^{18} site/g cat. The increasing of cobalt content by FSP affected decreasing of active site on surface catalyst; 5.50×10^{18} to 2.46×10^{18} site/g cat for 5 to 30% Co inserted. It showed relating to TPR results, the strong metal-support interaction in catalyst led to hydrogen adsorption was poorly.
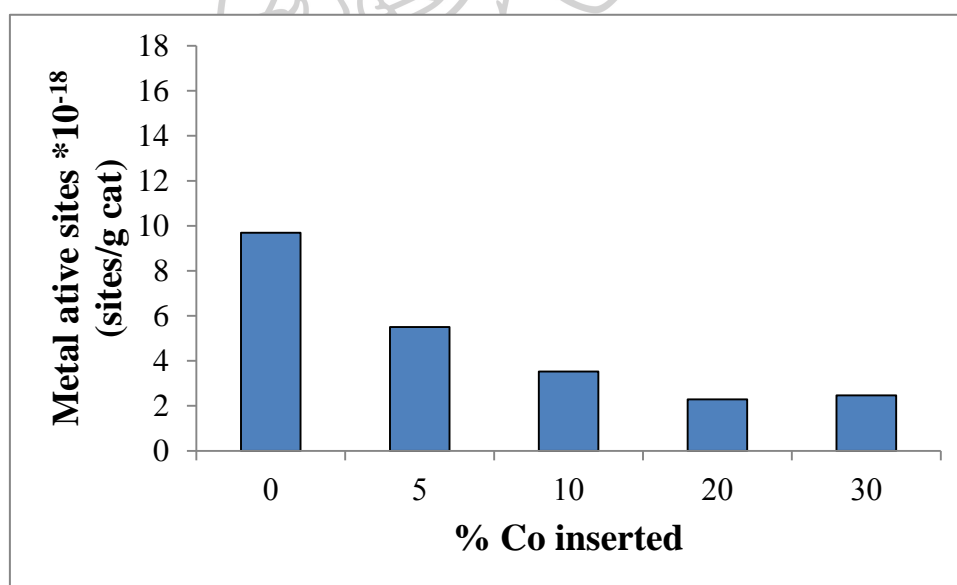
Figure 62 Metal active sites of Co/1Ti:4Zr and Co/Co-1Ti:4Zr catalysts

5.2.4.2. The catalytic activity and product selectivity by FTS

The FT activities of catalysts are shown in Figures 62 and 63. The catalyst without cobalt insertion showed the methane selectivity up to 98%, while the rate of reaction was approaching 6.5 g CH_2/g cat·h. The addition of cobalt in mixed support

affected products distribution of all catalysts. It suppressed methanation reaction and increased kerosene selectivity. On the other hand, the rate of reaction did not change for increasing amount of Co. The further increase inserted-cobalt up to 30% resulted in TOF increased to 31 s^{-1}.
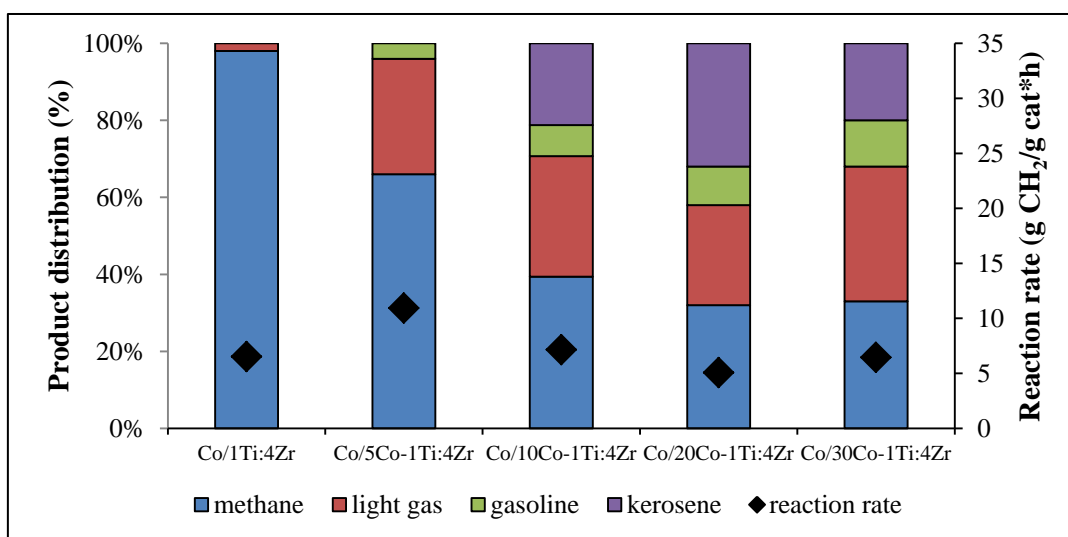
Figure 63 Catalytic properties of Co/1Ti:4Zr and Co/Co-1Ti:4Zr catalysts
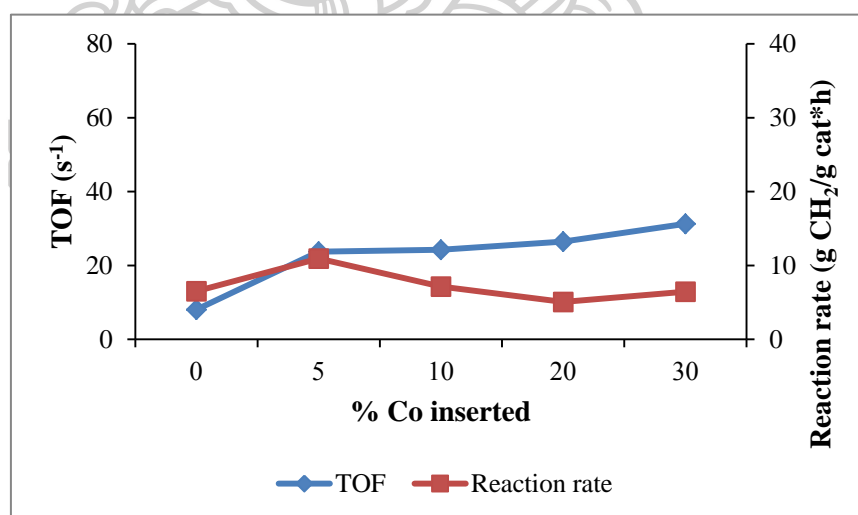
Figure 64 The reaction rate and TOF of Co/1Ti:4Zr and Co/Co-1Ti:4Zr catalysts

The time-on-stream profiles of products distribution and reaction rate for Co/Co-1Ti:4Zr catalysts are shown in Figures 64, 65 and 66. The Co/1Ti:4Zr and Co/5Co-1Ti:4Zr catalysts showed high reaction rate at initial time and rapidly decreased to ~ 10 g CH$_2$/g cat·h after 180 min on stream. However, Co/5Co-1Ti:4Zr

improve product distribution by decreasing methane formation. The products selectivity with TOS of the other catalysts was different to Co/1Ti:4Zr and Co/5Co-1Ti:4Zr catalyst. The initial rate of reaction over these catalysts showed in range of 8 to 11 g CH_2/g cat·h. and slightly decreased with TOS. The product distribution did not depend on time-on-stream.
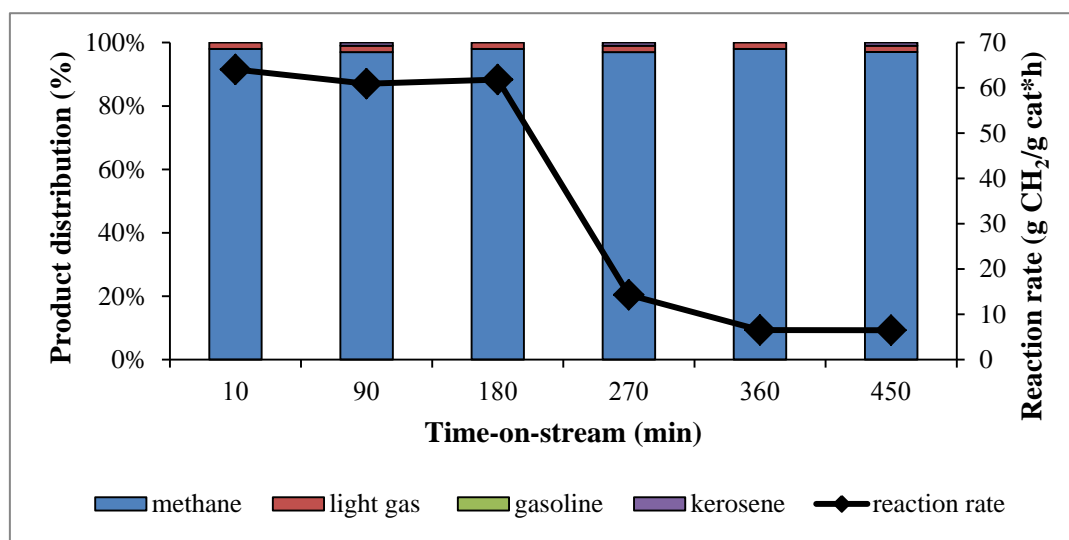
Figure 65 Time-on-stream profile of reaction rate and product distribution over Co/1Ti:4Zr catalyst
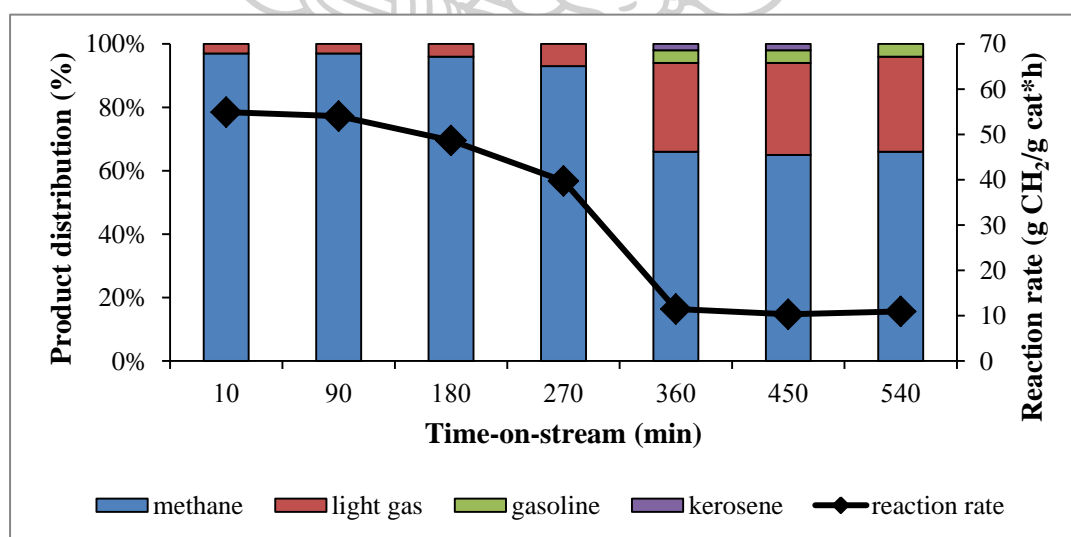
Figure 66 Time-on-stream profile of reaction rate and product distribution over Co/5Co-1Ti:4Zr catalyst
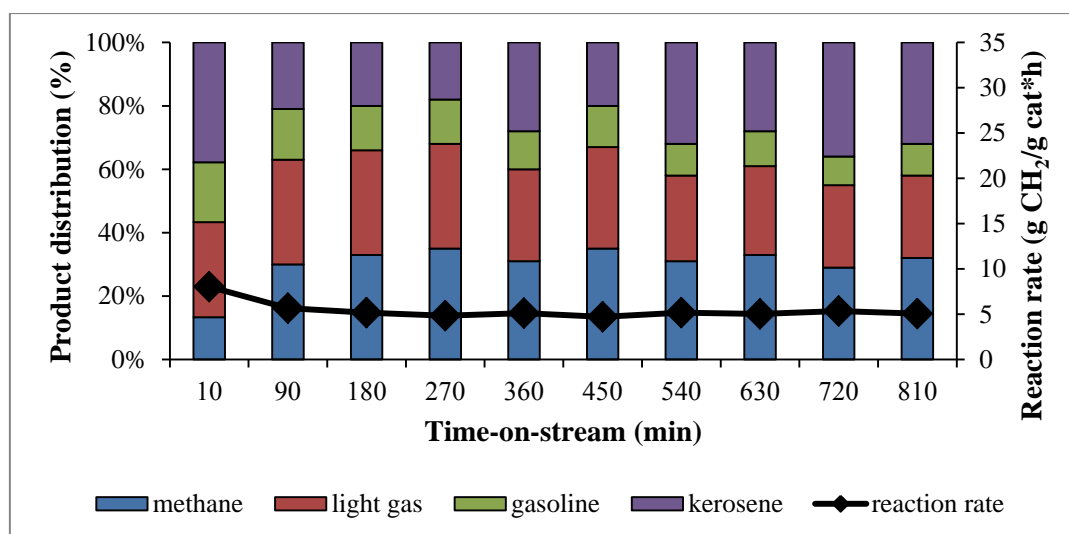
Figure 67 Time-on-stream profile of reaction rate and product distribution over Co/20Co-1Ti:4Zr catalyst
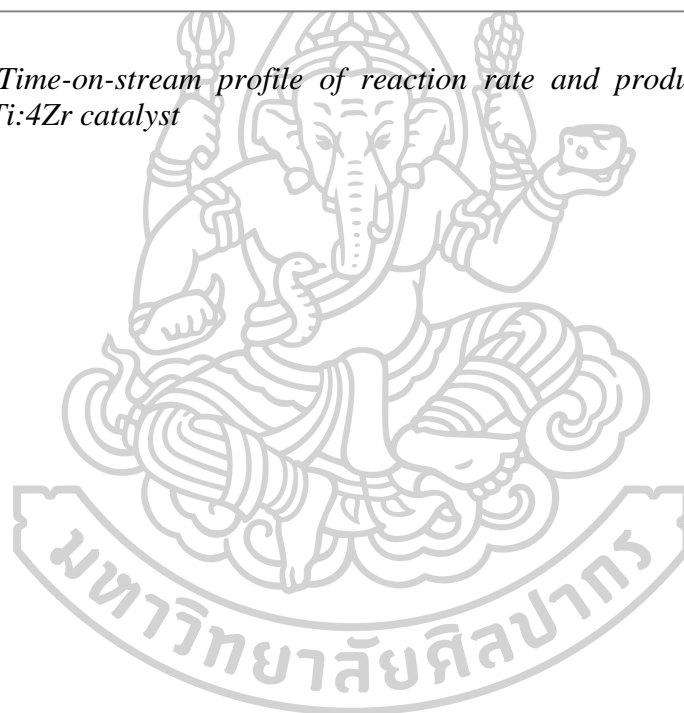
CHAPTER VI
CONCLUSIONS AND RECOMMENDATIONS

6.1 Conclusions

6.1.1 Effect of FSP-inserted Co in single metal oxide

The roles of inserted-cobalt in TiO_2 support were divided to three functions as following;

- Embedded in support

- Dispersed on surface of catalyst

- Transform to other cobalt species

While the addition of 5% Co insertion did not present the inserted-cobalt dispersed on surface of catalyst. The increasing of inserted-cobalt related to increased cobalt on surface of catalyst that induced to poorly dispersion of impregnated-Co. The large particle of coblat oxide decreased number of active sites, reflected to decrease of reaction rate and selective to kerosene production.

For the zirconia support, roles of inserted-cobalt was difference with titania support due to the weak interaction between zirconia and cobalt, therefore did not form to cobalt zirconate species. The increasing of inserted-cobalt in zirconia support led to Co_3O_4 particle growth, reflected to decrease of cobalt metallic sites and promotion of kerosene. Rate of reaction and methane formation decreased for long time because deactivation of catalyst which was significant due to weak interaction between metal-support.

6.1.2 Effect of FSP-inserted Co in mixed metal oxide

The effects of FSP-inserted Co were folloing;

- Suppress the formation of Ti-Zr alloy

- Promote the phase transformation of anatase and monoclinic phase

- Enhance the strong metal-support interaction

- Inhibit the methanation on mixed support with high Zr loading

The modified catalysts supported on mixed TiO_2-ZrO_2 support with 4:1 and 3:2 weight ratio showed the catalytic properties similar to Co/Co-TiO_2 catalysts. The high Co insertion affect decreased rate of reaction and methane selectivity.

On the other hand, the catalysts supported on mixed TiO_2-ZrO_2 support with 2:3 and 1:4 weight ratio showed the trend of reaction rate similar to Co/Co-ZrO_2 catalysts. The addition of 5% inserted-Co showed the highest reaction rate, while the other amount of inserted-Co exhibited closely reaction rate.

The Co/5Co-4Ti:1Zr catalyst exhibited the highest yield of kerosene than other mixed support catalysts.

6.2 Recommendations

Using X-ray photoelectron spectroscopy (XPS) and scanning electron microscope (SEM-EDX) were determined the dispersion of inserted-cobalt on surface catalyst.
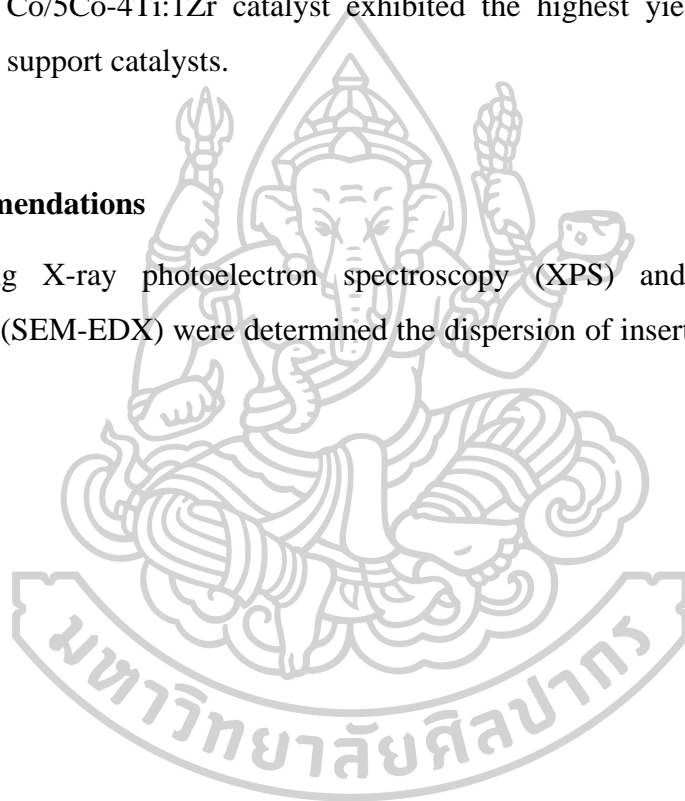
APPENDIX

APPENDIX A

CALCULATION FOR CATALYST PREPARATION

Chemical properties

Table 21 Chemical properties of catalyst precursors

Chemicals	MW	Chemical precursor	MW of precursor	Grade	Density (g/cm^3)
Co	58.9	$Co(NO_3)_2 \cdot 6H_2O$	291.03	98%	-
Co	58.9	$CoC_{22}H_{14}O_4$	407.25	6 wt. % in mineral spirits	0.92
TiO_2	79.86	$Ti(OCH_2CH_2CH_2CH_3)_4$	340.32	97%	1.00
ZrO_2	123.22	$Zr(OCH_2CH_2CH_2CH_3)_4$	383.68	80 wt. % in 1-butanol	1.05

Calculation of mixed metal oxide support prepared by flame spray pyrolysis

For example:

The calculation for the preparation of 20Co-4Ti:1Zr support, cobalt naphthenate,

Titanum (IV) butoxide and 80 wt% of zirconium (IV) butoxide in butanol were used as precursor and diluted with xylene to a 0.5 M solution.

The composition of the catalyst will be as follows:

Co $\quad = \quad$ 20 g

$TiO_2 \quad = \quad (100-20) \times \dfrac{4}{5} \quad = \quad$ 64 g

$ZrO_2 \quad = \quad (100-20) \times \dfrac{1}{5} \quad = \quad$ 16 g

Conversion to mole fraction

$$Co \quad = \quad 20 \text{ g Co} \times \frac{1 \text{ mol Co}}{58.9 \text{ g Co}} \quad = \quad 0.339 \text{ mol Co}$$

$$TiO_2 \quad = \quad 64 \text{ g TiO}_2 \times \frac{1 \text{ mol TiO}_2}{79.86 \text{ g TiO}_2} \quad = \quad 0.801 \text{ mol TiO}_2$$

$$ZrO_2 \quad = \quad 16 \text{ g ZrO}_2 \times \frac{1 \text{ mol ZrO}_2}{123.22 \text{ g ZrO}_2} \quad = \quad 0.129 \text{ mol ZrO}_2$$

∴ Total mole fraction = 0.339 + 0.801 + 0.129 = 1.269 mol

Basis on 500 ml of liquid precursor with 0.5 M

$$Co \quad = \quad 500 \text{ ml} \times \frac{0.5 \text{ mol}}{1000 \text{ ml}} \times \frac{0.339 \text{ mol Co}}{1.269 \text{ mol}} \quad = \quad 0.0668 \text{ mol Co}$$

$$TiO_2 \quad = \quad 500 \text{ ml} \times \frac{0.5 \text{ mol}}{1000 \text{ ml}} \times \frac{0.801 \text{ mol TiO}_2}{1.269 \text{ mol}} \quad = \quad 0.1576 \text{ mol TiO}_2$$

$$ZrO_2 \quad = \quad 500 \text{ ml} \times \frac{0.5 \text{ mol}}{1000 \text{ ml}} \times \frac{0.129 \text{ mol ZrO}_2}{1.269 \text{ mol}} \quad = \quad 0.0255 \text{ mol ZrO}_2$$

Calculation of usage chemical precursor

Co precursor $= 0.0668 \text{ mol Co} \times \dfrac{58.9 \text{ g Co precursor}}{1 \text{ mol Co}} \times \dfrac{1 \text{ ml}}{0.92 \text{ g}} \times \dfrac{1}{0.06}$ $=$

53.45 ml

TiO$_2$ precursor $= 0.1576 \text{ mol TiO}_2 \times \dfrac{340.32 \text{ TiO}_2 \text{ precursor}}{1 \text{ mol TiO}_2} \times \dfrac{1}{0.97}$ $=$

55.31 ml

ZrO$_2$ precursor $= 0.0255 \text{ mol ZrO}_2 \times \dfrac{383.7 \text{ ZrO}_2 \text{ precursor}}{1 \text{ mol ZrO}_2} \times \dfrac{1 \text{ ml}}{0.80 \text{ g}} \times \dfrac{1}{1.05} =$

11.67 ml

Calculation of cobalt catalyst prepared by impregnation method

For example:

Calculation for the preparation of 20Co/4Ti:1Zr catalyst with cobalt nitrate hexahydrate as Co precursor

Based on 100 g of catalyst used, the composition of the catalyst will be as follows:

Cobalt	= 20 g	
Mixed support	= 100-20	= 80 g

For 2 g of mixed support

Cobalt required	$= 2 \times (20/80)$	= 0.5 g

Thus, Cobalt 0.5 g was prepared from cobalt nitrate hexahydrate

$$\text{Cobalt nitrate required} = (0.5 \text{ g Co} \times \frac{291.03 \text{ g Co precursor}}{58.9 \text{ g Co}}) \times \frac{1}{0.98} = 2.5197 \text{ g}$$
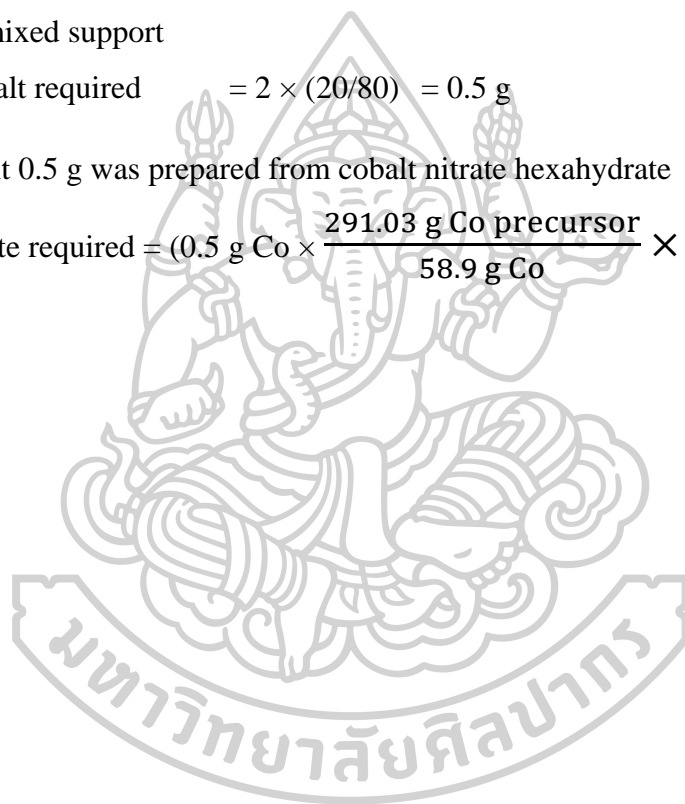
APPENDIX B

CALCULATION OF THE CRYSTALLITE SIZE BY XRD

Calculation of the crystallite size by Debye-Scherrer equation

The crystallite size was calculated from the half-height width of the diffraction peak of XRD pattern using the Debye-Scherrer equation.

Scherrer equation:

$$d = \frac{K\lambda}{\beta\cos\theta}$$

Where   d   =   Crystallite size, nm

K   =   Crystallite-shape factor = 0.9

λ   =   X-ray wavelength, 1.5418 Å for CuKα

β   =   X-ray diffraction broadening, radian

θ   =   Observed peak angle, degree

Warren's formula:

$$\beta = \sqrt{\beta_M{}^2 - \beta_S{}^2}$$

Where β_M =   The measured peak width in radians at half peak height

β_S =   The corresponding width of the standard material
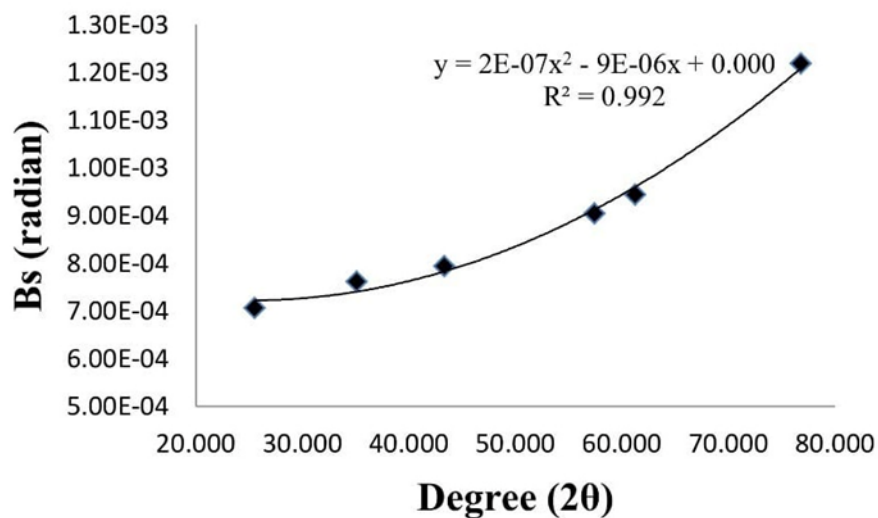
Figure 68 The plot indicating the value of line broadening due to the equipment. The data were obtained by using α-alumina as a standard

For example:

Calculation of the Co_3O_4 crystallite size of Co/4Ti:1Zr
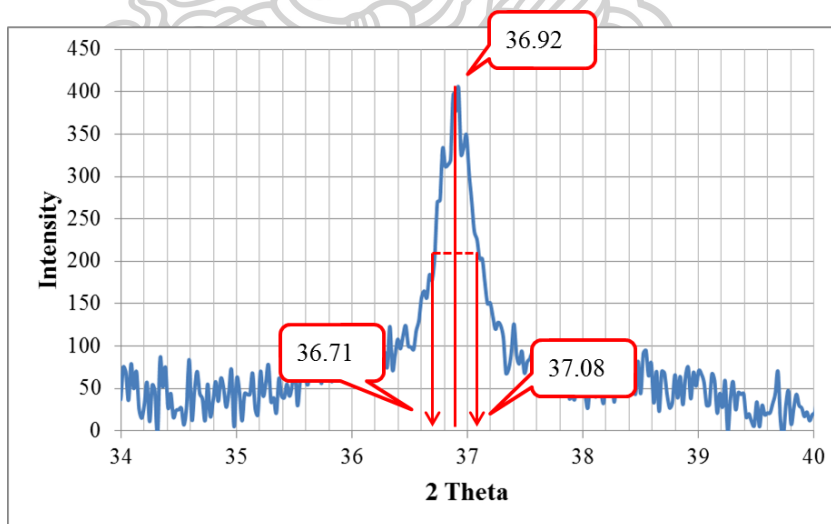
Figure 69 Calculation of the Co_3O_4 crystallite size

The half-height width of diffraction peak = 37.08°-36.71°

= 0.37°

$$= 0.37 \times \frac{\pi}{180}$$

= 0.00646 radian

The corresponding width of the standard material (Bs) at the 36.92° = 0.000745 radian

Warren's formula:

$$\beta = \sqrt{0.00646^2 - 0.000745^2}$$

= 0.006417 radian

2θ = 36.92°

θ = 18.46°

∴ The crystallite size = 22.79 nm
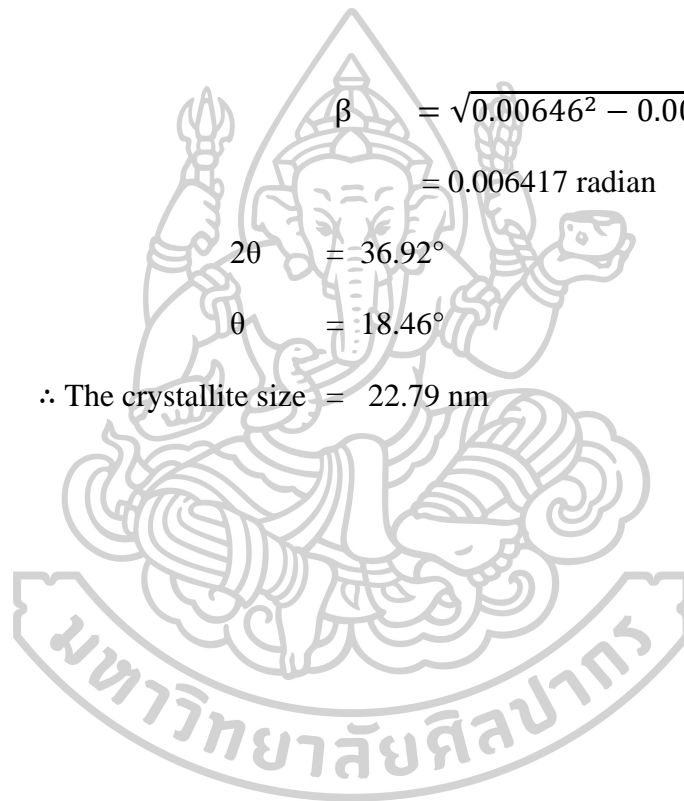
APPENDIX C

CALCULATION FOR REDUCIBILITY

Calculation of the catalyst reducibility

The reduction of Co_3O_4 to Co^0 was calculated as follows:

Molecular weight of Co = 58.93

Molecular weight of Co_3O_4 = 240.79

Integral area of hydrogen used to reduce Co_3O_4 standard 0.1 g   =   122.19   unit

Mole of Co3O4 $= \dfrac{0.1 \text{ g } Co_3O_4}{240.79/\text{mol } Co_3O_4}$ mole Co_3O_4

The reduction of cobalt oxide was follow by equation;

$$Co_3O_4 \ + 4H_2 \rightarrow 3Co + 4H_2O$$
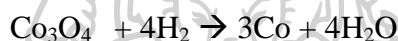
Mole of H_2 consumption $=$ $4 \times$ Mole of Co_3O_4 consumption

$=$ $4 \times 4.15 \times 10^{-4}$ mole H_2

$=$ 1.661×10^{-3} mole H_2

For example:

Calculation of the reducibility of Co/4Ti:1Zr catalyst

Integral area of the calcined catalyst   A   unit

Let the weight of calcined catalyst used   0.1   g

Concentration of Co   20   wt%

Mole of Co $= \dfrac{0.1 \text{ gcat} \times (20\text{wt\%}/100)}{58.93 \text{ g/mol Co}}$ mole

Mole of Co_3O_4 $= \dfrac{0.1 \text{ gcat} \times (20\text{wt\%}/100)}{3 \times 58.93 \text{ g/mol Co}}$ mole

Amount of H_2 from theoretical $= \dfrac{0.1 \text{ gcat} \times (20\text{wt\%}/100) \times 4}{3 \times 58.93 \text{ g/mol Co}}$ mole

$=$ 4.525×10^{-4} mole of H_2

Total reducibility (%) of Co catalyst

$$= \frac{\text{Amount of } H_2 \text{ uptake to reduce 0.1 g of catalyst}}{H_2 \text{ uptake to reduce Co3O4 to Co}^0 \text{ for 0.1 g catalyst}} \times 100$$

$$= \frac{1.661 \times 10^{-3} \times A}{4.525 \times 10^{-4} \text{ mole of } H_2} \times 100$$

APPENDIX D

CALCULATON OF REACTION RATE AND SELECTIVITY

Calculation of reaction rate

The catalyst performance for the CO hydrogenation was evaluated in terms of activity for CO conversion reaction rate and selectivity.

Activity of the catalyst performed in term of carbon monoxide conversion and reaction rate. Carbon monoxide conversion is defined as moles of CO converted with respect to CO in feed:

$$\text{CO coversion (\%)} = \frac{area\ of\ CO\ in\ feed - area\ of\ CO\ in\ product}{area\ of\ CO\ in\ feed} \times 100$$

Which area of CO peak obtained from computer program based plot on TCD (GC-14B).

Reaction rate was calculated from CO conversion that is as follows:

Let the weight of catalyst used	=	W	g
Flow rate of feed	=	30	ml/min
Volume of 1 mole of gas at 1 atm	=	25270	ml
Concentration of Co in catalyst	=	C	%wt
Reaction rate (g CH$_2$/g of catalyst $\times$ h)	=	$\dfrac{\%Conversion \times 30 \times 60 \times 14}{W \times 25270}$	

$$= A \quad \text{g CH}_2\text{/g of catalyst} \times \text{h}$$

Turnover frequencies (TOF)

Turnover frequencies (TOF) were calculated based on the number of Co active site from H2-Chemisorption.

$$\text{TOF} = \text{rate/site. Time}$$

Product Selectivity

Selectivity of product is defined as weight of product (B) form with respect to total area of product:

Selectivity of B (wt%) = 100 x [area of B form / total area of product]

Which area of product obtained from computer program based plot FID (GC-8A)

APPEBDIX E

SUPPLEMENTARY DATA

Figure 70 Time-on-stream profile of reaction rate and product distribution over Co/5Co-TiO₂ catalyst

Figure 71 Time-on-stream profile of reaction rate and product distribution over Co/10Co-TiO₂ catalyst

Figure 72 Time-on-stream profile of reaction rate and product distribution over Co/20Co-TiO₂ catalyst

Figure 73 Time-on-stream profile of reaction rate and product distribution over Co/5Co-ZrO₂ catalyst

Figure 74 Time-on-stream profile of reaction rate and product distribution over Co/10Co-ZrO₂ catalyst
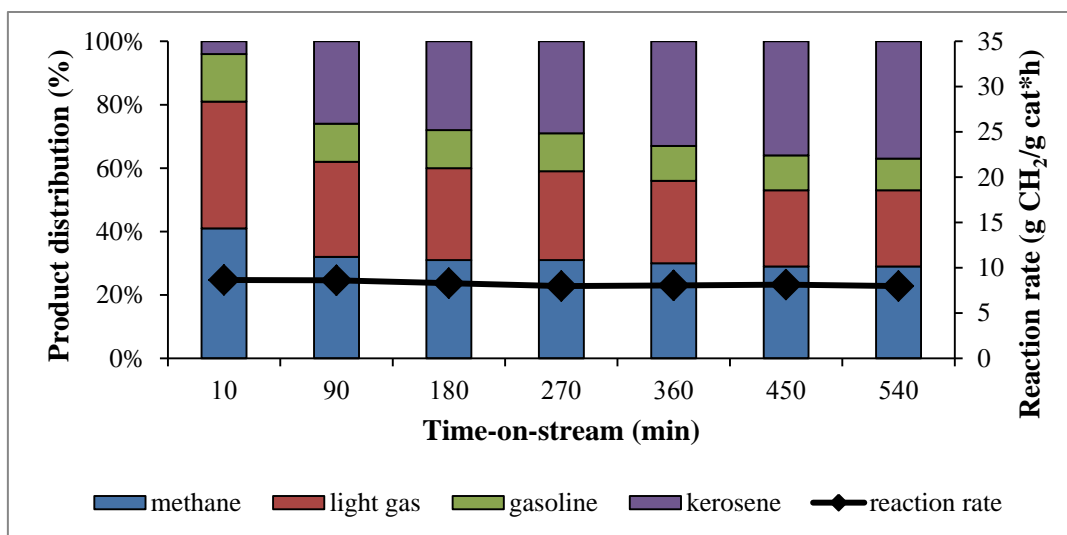

Figure 75 Time-on-stream profile of reaction rate and product distribution over Co/20Co-ZrO₂ catalyst

Figure 76 Time-on-stream profile of reaction rate and product distribution over Co/5Co-4Ti:1Zr catalyst

Figure 77 Time-on-stream profile of reaction rate and product distribution over Co/30Co-4Ti:1Zr catalyst
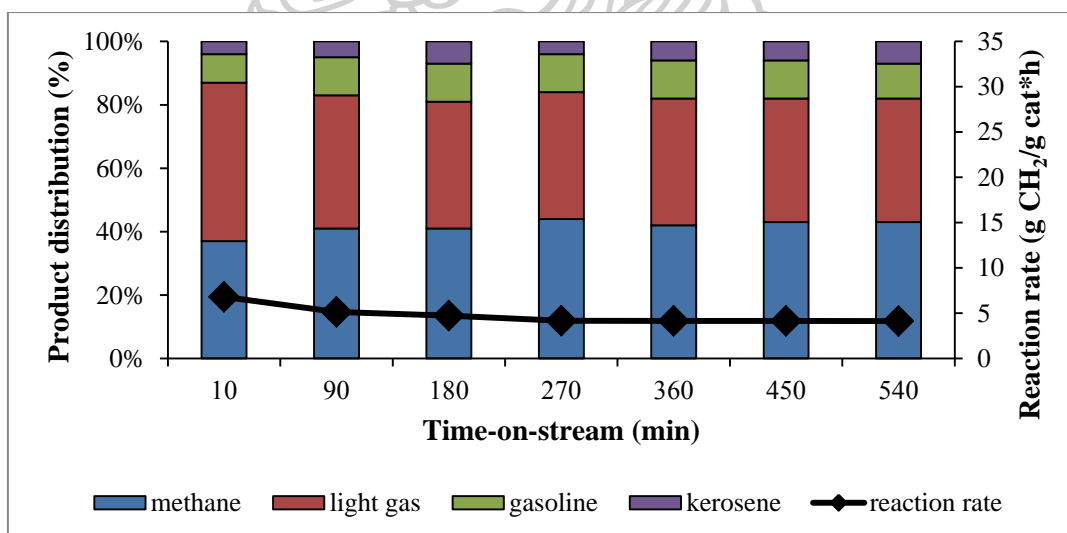
Figure 78 Time-on-stream profile of reaction rate and product distribution over Co/5Co-3Ti:2Zr catalyst
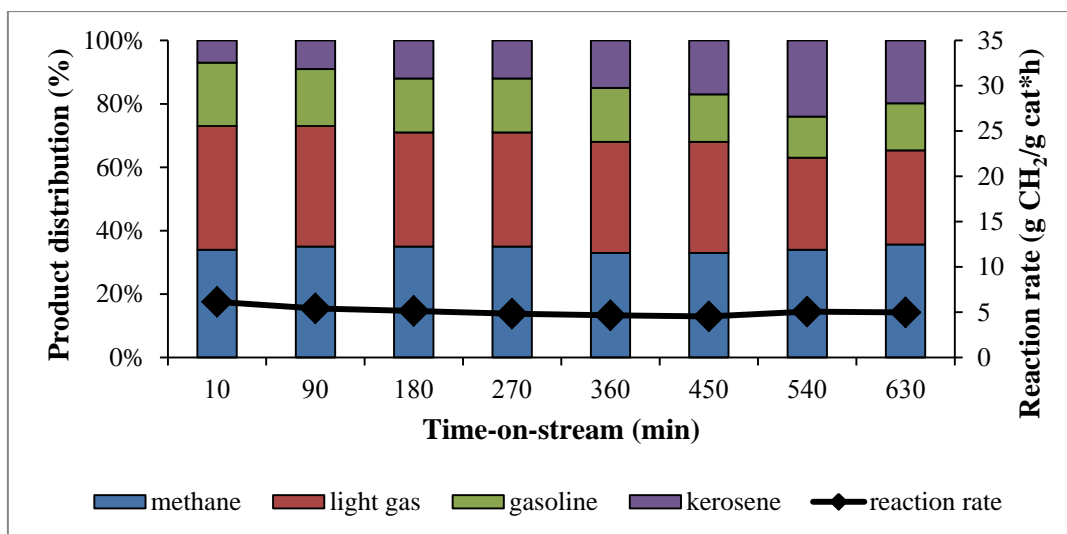

Figure 79 Time-on-stream profile of reaction rate and product distribution over Co/10Co-3Ti:2Zr catalyst

Figure 80 Time-on-stream profile of reaction rate and product distribution over Co/30Co-3Ti:2Zr catalyst

Figure 81 Time-on-stream profile of reaction rate and product distribution over Co/5Co-2Ti:3Zr catalyst

Figure 82 Time-on-stream profile of reaction rate and product distribution over Co/10Co-2Ti:3Zr catalyst
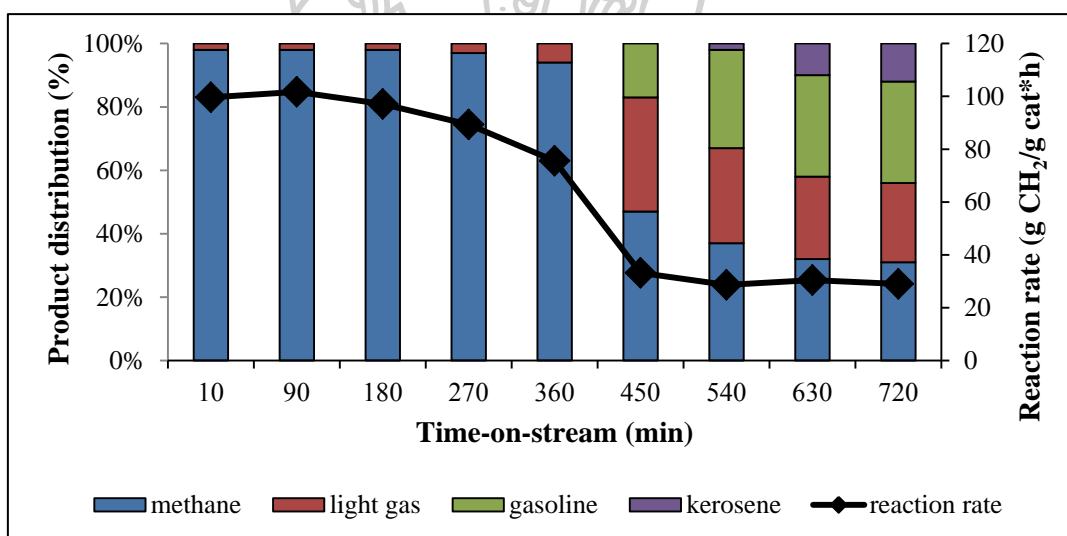

Figure 83 Time-on-stream profile of reaction rate and product distribution over Co/20Co-2Ti:3Zr catalyst
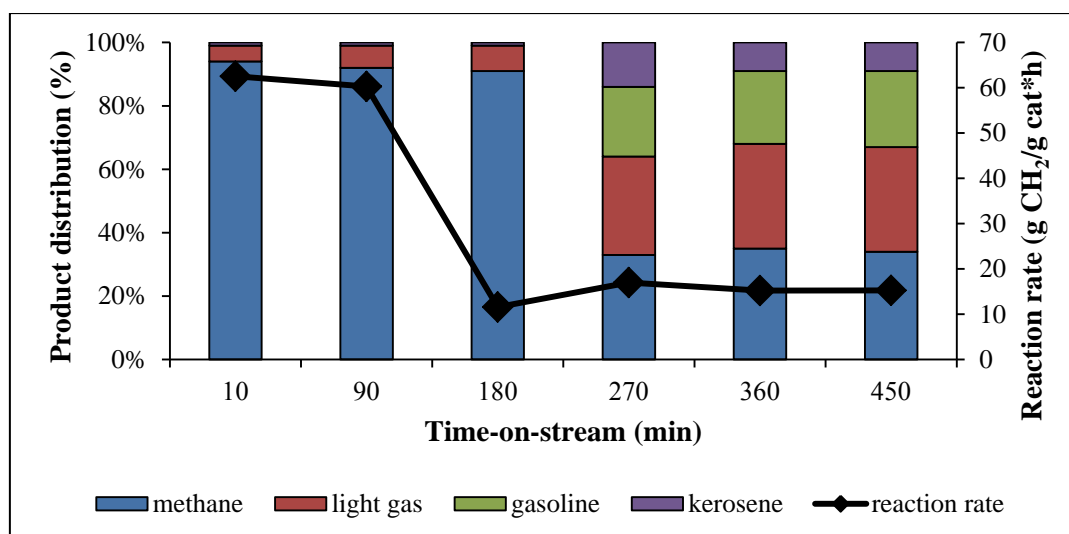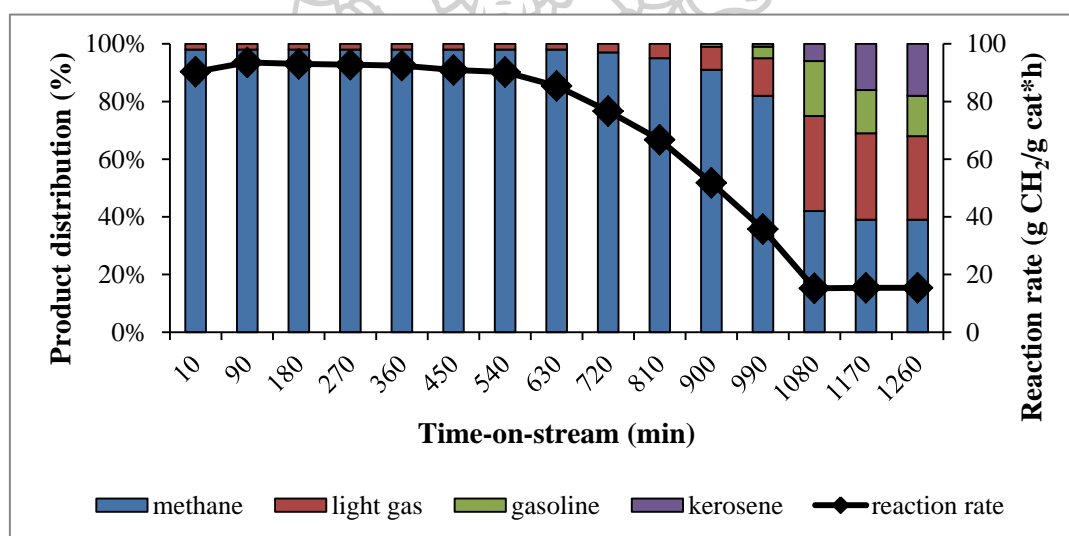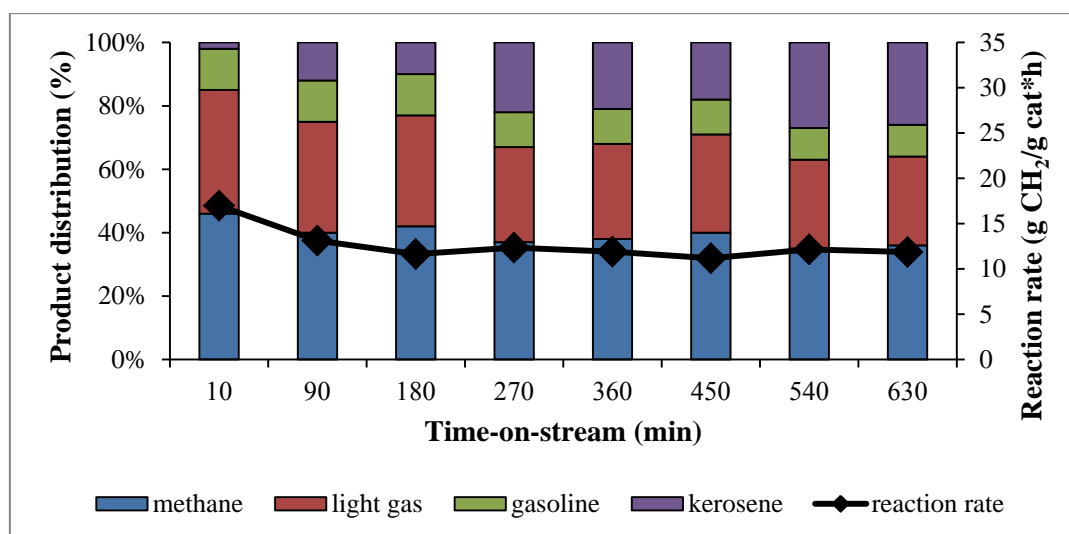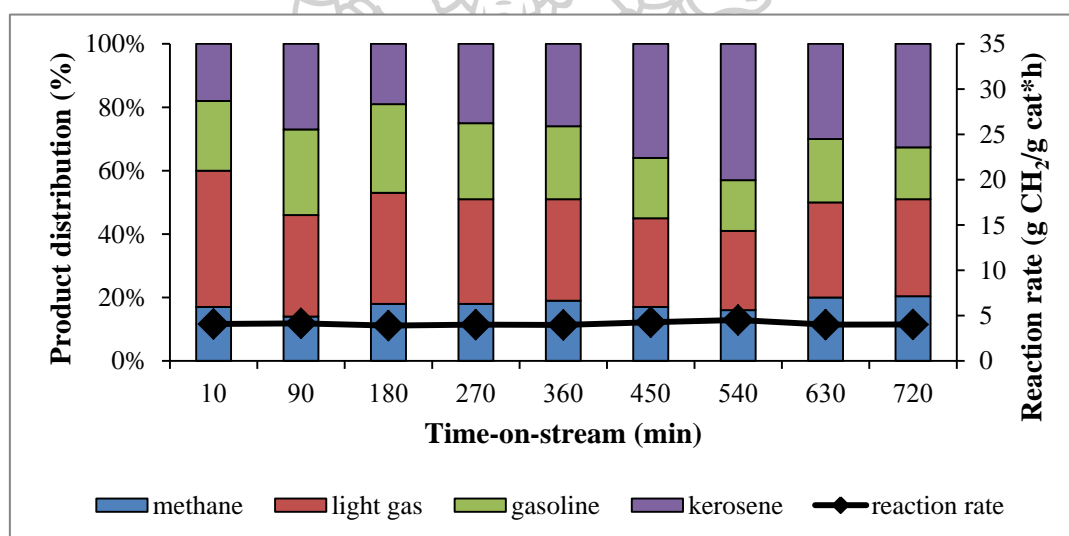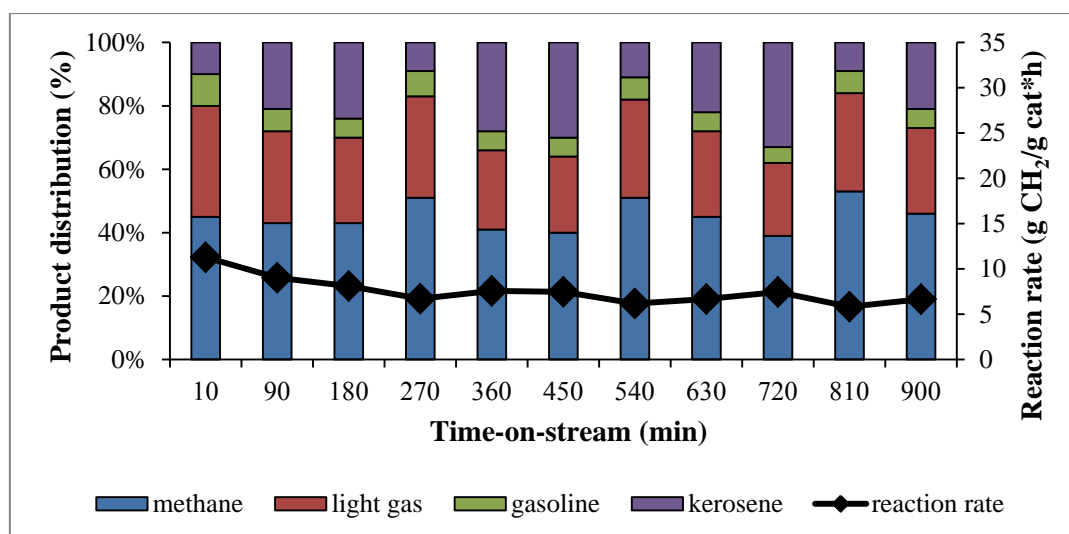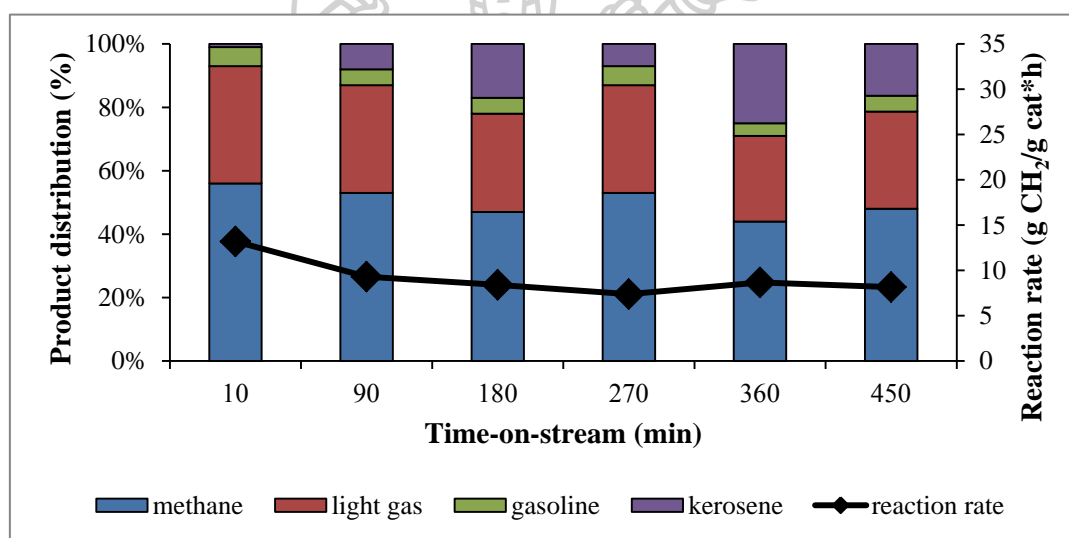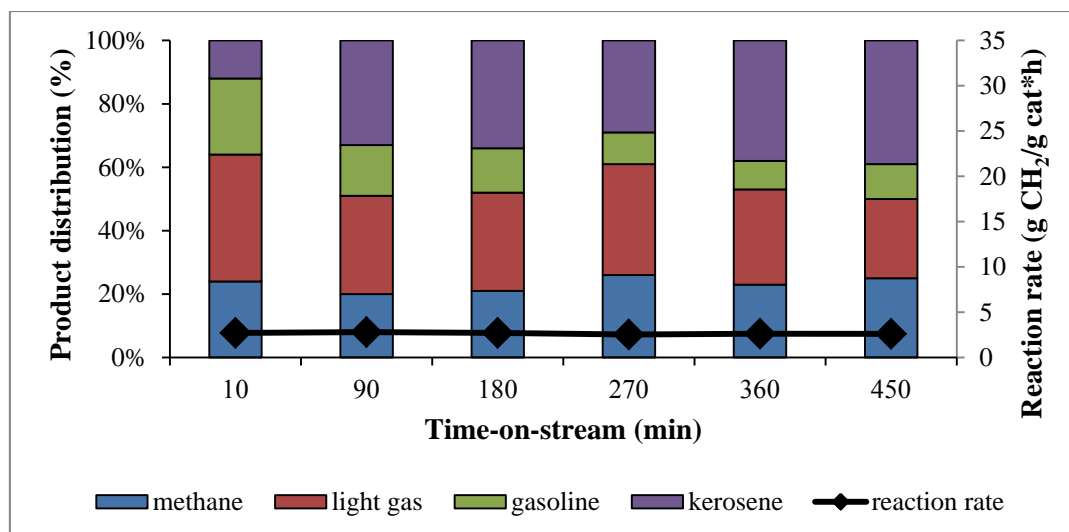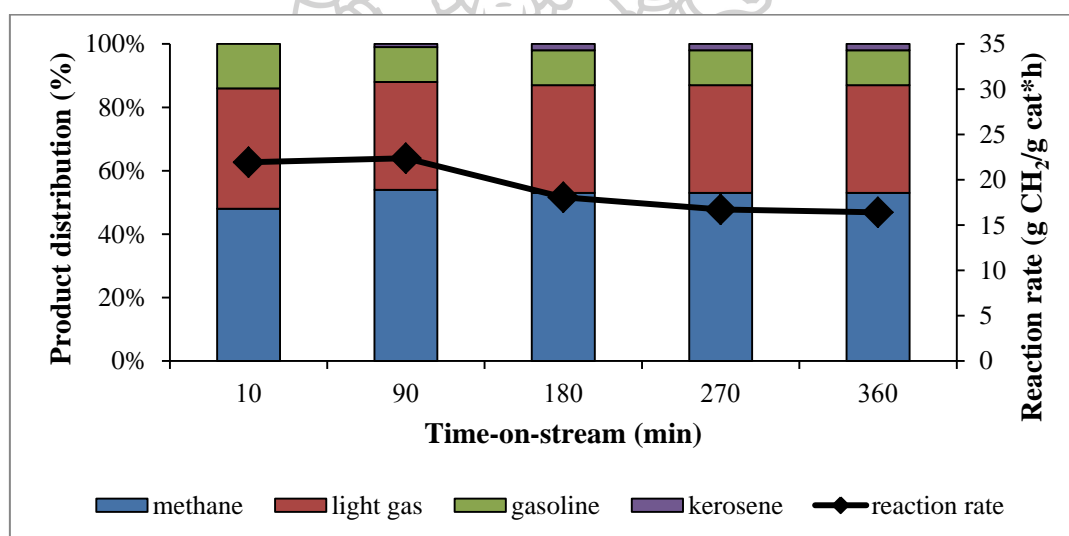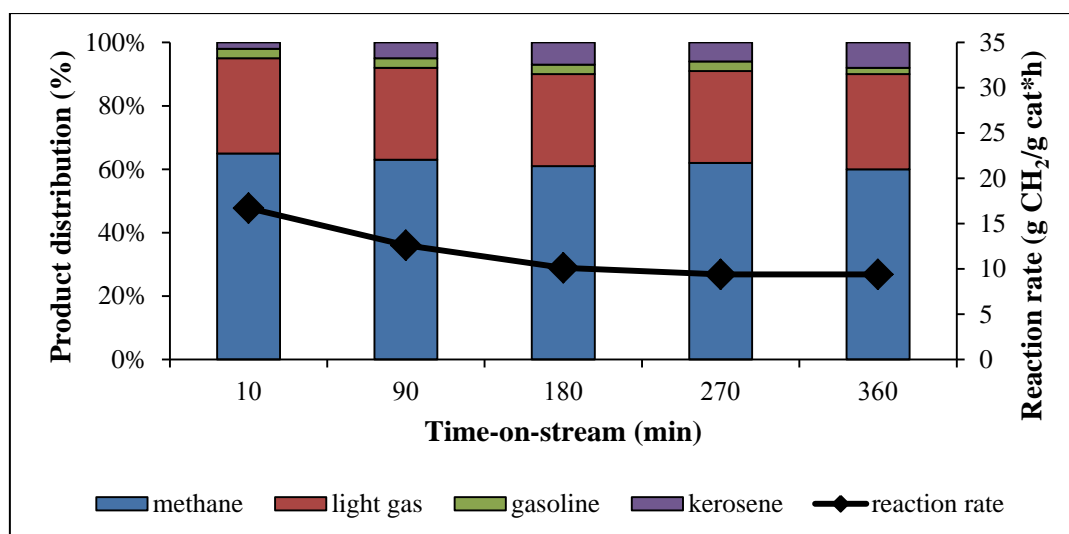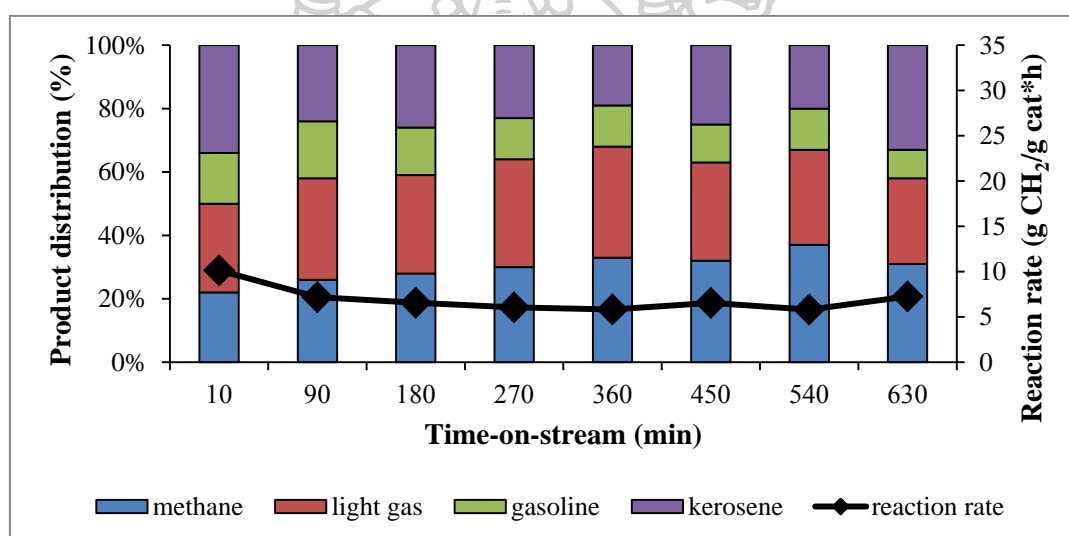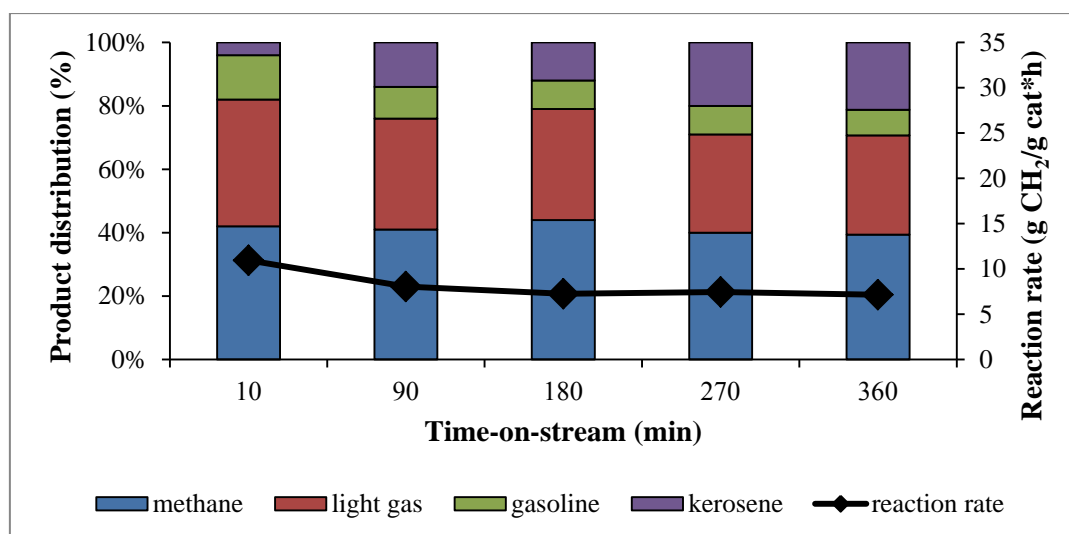
Figure 84 Time-on-stream profile of reaction rate and product distribution over Co/10Co-1Ti:4Zr catalyst
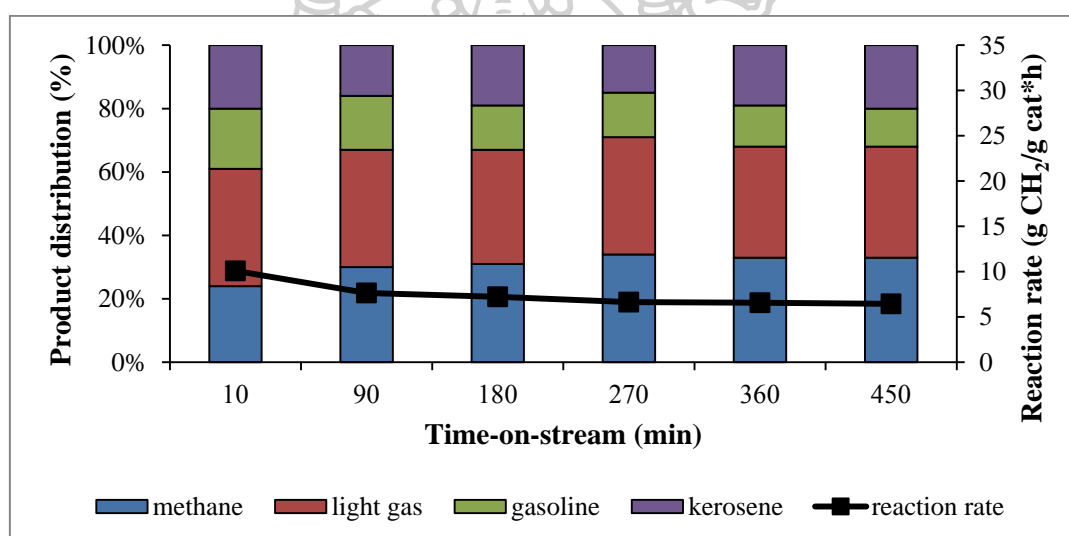

Figure 85 Time-on-stream profile of reaction rate and product distribution over Co/30Co-1Ti:4Zr catalyst

REFERENCES

1. Rahimpour, M.R. and H. Elekaei, A comparative study of combination of Fischer–Tropsch synthesis reactors with hydrogen-permselective membrane in GTL technology. Fuel Processing Technology, 2009. 90(6): p. 747-761.

2. Shimura, K., et al., Fischer–Tropsch synthesis over TiO_2 supported cobalt catalyst: Effect of TiO_2 crystal phase and metal ion loading. Applied Catalysis A: General, 2013. 460–461: p. 8-14.

3. Schulz, H., Short history and present trends of Fischer–Tropsch synthesis. Applied Catalysis A: General, 1999. 186(1): p. 3-12.

4. Khodakov, A.Y., W. Chu, and P. Fongarland, Advances in the Development of Novel Cobalt Fischer−Tropsch Catalysts for Synthesis of Long-Chain Hydrocarbons and Clean Fuels. Chemical Reviews, 2007. 107(5): p. 1692-1744.

5. Moradi, G.R., et al., Promotion of Co/SiO_2 Fischer–Tropsch catalysts with zirconium. Catalysis Communications, 2003. 4(1): p. 27-32.

6. Xiong, H., et al., Catalytic performance of zirconium-modified Co/Al_2O_3 for Fischer–Tropsch synthesis. Journal of Molecular Catalysis A: Chemical, 2005. 231(1–2): p. 145-151.

7. Zhang, J., et al., Chemical treatment of γ-Al_2O_3 and its influence on the properties of Co-based catalysts for Fischer–Tropsch synthesis. Applied Catalysis A: General, 2003. 243(1): p. 121-133.

8. Venezia, A.M., et al., Co/SiO_2 catalysts for Fischer–Tropsch synthesis; effect of Co loading and support modification by TiO_2. Catalysis Today, 2012. 197(1): p. 18-23.

9. Ali, S., et al., Effect of the support on physicochemical properties and catalytic performance of cobalt based nano-catalysts in Fischer-Tropsch reaction. Materials Today Communications, 2017. 10: p. 67-71.

10. Ahn, C.-I. and J.W. Bae, Fischer–Tropsch synthesis on the Al_2O_3-modified ordered mesoporous Co_3O_4 with an enhanced catalytic activity and stability. Catalysis Today, 2016. 265: p. 27-35.

11. Borg, Ø., et al., Fischer–Tropsch synthesis over γ-alumina-supported cobalt catalysts: Effect of support variables. Journal of Catalysis, 2007. 248(1): p. 89-100.

12. Ma, W., et al., Fischer–Tropsch synthesis: Support and cobalt cluster size effects on kinetics over Co/Al_2O_3 and Co/SiO_2 catalysts. Fuel, 2011. 90(2): p. 756-765.

13. Hinchiranan, S., et al., TiO_2 promoted Co/SiO_2 catalysts for Fischer–Tropsch synthesis. Fuel Processing Technology, 2008. 89(4): p. 455-459.

14. Wu, H., et al., Effects of ZrO_2 promoter on physic-chemical properties and activity of Co/TiO_2–SiO_2 Fischer–Tropsch catalysts. Journal of Molecular Catalysis A: Chemical, 2015. 396: p. 108-119.

15. Jalama, K., et al., A comparison of $Au/Co/Al_2O_3$ and $Au/Co/SiO_2$ catalysts in the Fischer–Tropsch reaction. Applied Catalysis A: General, 2011. 395(1–2): p. 1-9.

16. Liu, C., et al., Synthesis of γ-Al_2O_3 nanofibers stabilized Co_3O_4 nanoparticles as highly active and stable Fischer–Tropsch synthesis catalysts. Fuel, 2016. 180: p. 777-784.

17. Riva, R., et al., Metal–support interaction in Co/SiO$_2$ and Co/TiO$_2$. Applied Catalysis A: General, 2000. 196(1): p. 111-123.

18. Ernst, B., et al., Preparation and characterization of Fischer–Tropsch active Co/SiO$_2$ catalysts. Applied Catalysis A: General, 1999. 186(1–2): p. 145-168.

19. Sun, S., N. Tsubaki, and K. Fujimoto, The reaction performances and characterization of Fischer–Tropsch synthesis Co/SiO$_2$ catalysts prepared from mixed cobalt salts. Applied Catalysis A: General, 2000. 202(1): p. 121-131.

20. Jongsomjit, B., T. Wongsalee, and P. Praserthdam, Characteristics and catalytic properties of Co/TiO$_2$ for various rutile:anatase ratios. Catalysis Communications, 2005. 6(11): p. 705-710.

21. Feyzi, M., M.M. Khodaei, and J. Shahmoradi, Effect of preparation and operation conditions on the catalytic performance of cobalt-based catalysts for light olefins production. Fuel Processing Technology, 2012. 93(1): p. 90-98.

22. Li, J. and N.J. Coville, The effect of boron on the catalyst reducibility and activity of Co/TiO$_2$ Fischer–Tropsch catalysts. Applied Catalysis A: General, 1999. 181(1): p. 201-208.

23. Madikizela-Mnqanqeni, N.N. and N.J. Coville, The preparation and study of sol–gel synthesized Co/Zn/TiO$_2$ Fischer–Tropsch catalysts. Applied Catalysis A: General, 2007. 317(2): p. 195-203.

24. Jahangiri, H., et al., A review of advanced catalyst development for Fischer-Tropsch synthesis of hydrocarbons from biomass derived syn-gas. Catalysis Science & Technology, 2014. 4(8): p. 2210-2229.

25. Enache, D.I., M. Roy-Auberger, and R. Revel, Differences in the characteristics and catalytic properties of cobalt-based Fischer–Tropsch catalysts supported on zirconia and alumina. Applied Catalysis A: General, 2004. 268(1–2): p. 51-60.

26. Sinchai, K. and A. Himhoung, Effect of lanthanum on Fischer-Tropsch activity of the FSP-made cobalt based catalyst. 2012, Department of Chemical Engineering,Silpakorn University,.

27. Meetipkij, K. and S. Rattanapanya, Effect of ratio of TiO$_2$ and ZrO$_2$ in the FSP-made Co/TiO$_2$-ZrO$_2$ catalyst on the CO hydrogenation. 2014, Department of Chemical Engineering,Silpakorn University,.

28. Van Berge, P.J., et al., Advances in the cobalt catalyzed Fischer-Tropsch synthesis. Erdoel Erdgas Kohle, 2001. 117(3): p. 138-142.

29. Davis, B.H., Fischer–Tropsch synthesis: current mechanism and futuristic needs. Fuel Processing Technology, 2001. 71(1–3): p. 157-166.

30. Park, S.-J., et al., Effects of titanium impurity on alumina surface for the activity of Co/Ti–Al$_2$O$_3$ Fischer–Tropsch catalyst. Applied Catalysis A: General, 2012. 419–420: p. 148-155.

31. Johnson, G.R. and A.T. Bell, Role of ZrO$_2$ in Promoting the Activity and Selectivity of Co-Based Fischer–Tropsch Synthesis Catalysts. ACS Catalysis, 2016. 6(1): p. 100-114.

32. Koizumi, N., et al., Application of liquid phase deposition method for preparation of Co/ZrO$_x$/SiO$_2$ catalyst with enhanced Fischer–Tropsch synthesis activity: Importance of Co–Zr interaction. Applied Catalysis A: General, 2011. 398(1–2): p. 168-178.

33. Li, Y., et al., Metallic iron nanoparticles: Flame synthesis, characterization and magnetic properties. Particuology, 2013. 11(4): p. 460-467.

34. Bettini, L.G., et al., Mixed-phase nanocrystalline TiO_2 photocatalysts produced by flame spray pyrolysis. Applied Catalysis B: Environmental, 2015. 178: p. 226-232.

35. Boningari, T., R. Koirala, and P.G. Smirniotis, Low-temperature selective catalytic reduction of NO with NH_3 over V/ZrO_2 prepared by flame-assisted spray pyrolysis: Structural and catalytic properties. Applied Catalysis B: Environmental, 2012. 127: p. 255-264.

36. Boningari, T., R. Koirala, and P.G. Smirniotis, Low-temperature catalytic reduction of NO by NH_3 over vanadia-based nanoparticles prepared by flame-assisted spray pyrolysis: Influence of various supports. Applied Catalysis B: Environmental, 2013. 140–141: p. 289-298.

37. Chaisuk, C., et al., Effects of Co dopants and flame conditions on the formation of Co/ZrO_2 nanoparticles by flame spray pyrolysis and their catalytic properties in CO hydrogenation. Catalysis Communications, 2011. 12(10): p. 917-922.

38. Teoh, W.Y., R. Amal, and L. Madler, Flame spray pyrolysis: An enabling technology for nanoparticles design and fabrication. Nanoscale, 2010. 2(8): p. 1324-1347.

39. Liu, G., et al., Catalytic oxidation of benzene over Ce–Mn oxides synthesized by flame spray pyrolysis. Particuology, 2013. 11(4): p. 454-459.

40. Li, Z., et al., Effect of incorporation manner of Zr on the Co/SBA-15 catalyst for the Fischer–Tropsch synthesis. Journal of Molecular Catalysis A: Chemical, 2016. 424: p. 384-392.

41. Askari, M.B., et al., Synthesis of TiO_2 nanoparticles and decorated multi-wall carbon nanotube (MWCNT) with anatase TiO_2 nanoparticles and study of optical properties and structural characterization of TiO_2/MWCNT nanocomposite. Optik - International Journal for Light and Electron Optics, 2017. 149: p. 447-454.

42. Pongthawornsakun, B., et al., Mono- and bi-metallic Au–Pd/TiO_2 catalysts synthesized by one-step flame spray pyrolysis for liquid-phase hydrogenation of 1-heptyne. Applied Catalysis A: General, 2013. 467: p. 132-141.

43. Teoh, W.Y., et al., Flame sprayed visible light-active Fe-TiO_2 for photomineralisation of oxalic acid. Catalysis Today, 2007. 120(2): p. 203-213.

44. Hwang, J.H., et al., A thermogravimetric study of $CoTiO_3$ as oxygen carrier for chemical looping combustion. Catalysis Today, 2018. 303: p. 13-18.

45. Thommes, M., et al., Physisorption of gases, with special reference to the evaluation of surface area and pore size distribution (IUPAC Technical Report). Vol. 87. 2015.

46. Li, Z., et al., Characterizations and product distribution of Co-based Fischer-Tropsch catalysts: A comparison of the incorporation manner. Fuel, 2018. 220: p. 257-263.

47. Khodakov, A.Y., et al., Pore-Size Control of Cobalt Dispersion and Reducibility in Mesoporous Silicas. The Journal of Physical Chemistry B, 2001. 105(40): p. 9805-9811.

48.   Kwon, O.H., et al., Investigation of the electrical conductivity of sintered monoclinic zirconia (ZrO_2). Ceramics International, 2017. 43(11): p. 8236-8245.

49.   Reddy, C.V., et al., Synthesis and characterization of pure tetragonal ZrO_2 nanoparticles with enhanced photocatalytic activity. Ceramics International, 2018. 44(6): p. 6940-6948.

50.   Enache, D.I., et al., In Situ XRD Study of the Influence of Thermal Treatment on the Characteristics and the Catalytic Properties of Cobalt-Based Fischer–Tropsch Catalysts. Journal of Catalysis, 2002. 205(2): p. 346-353.

51.   Troitzsch, U., A.G. Christy, and D.J. Ellis, The crystal structure of disordered $(Zr,Ti)O_2$ solid solution including srilankite: evolution towards tetragonal ZrO_2 with increasing Zr. Physics and Chemistry of Minerals, 2005. 32(7): p. 504-514.

52.   López-López, E., et al., Structural characterization of bulk $ZrTiO_4$ and its potential for thermal shock applications. Journal of the European Ceramic Society, 2012. 32(2): p. 299-306.
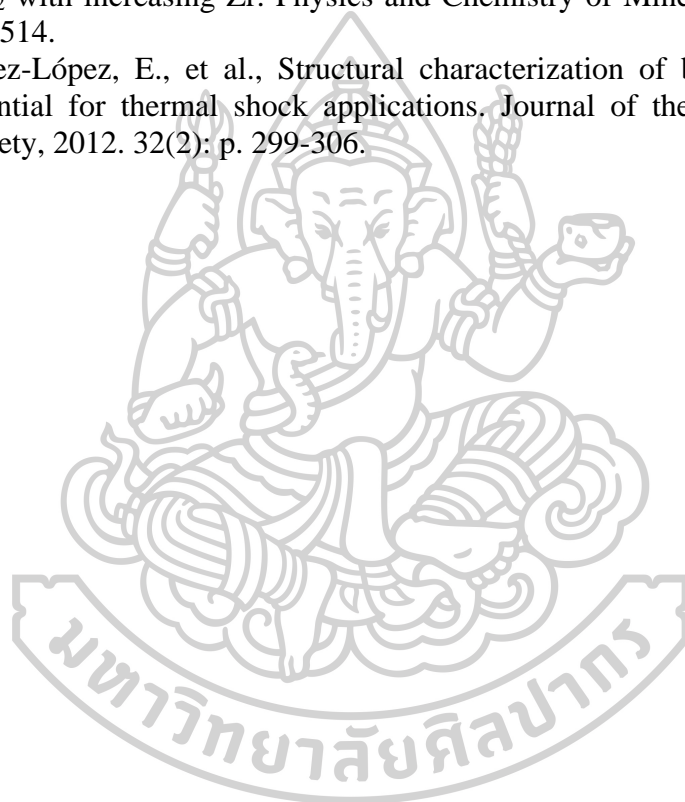
VITA

NAME   Krasanai Sukchoknamchai

DATE OF BIRTH   5 May 1991

PLACE OF BIRTH   Trang

INSTITUTIONS   Silpakorn University
ATTENDED
HOME ADDRESS   99 Khao Chaison sub-district, Khao Chaison district,
                               Phatthalung province, 93130